2 cards
S.L.
Ref.
PUB-433
c1
For Reference
Not to be taken from this room

# μSR NEWSLETTER

Lawrence Berkeley Laboratory, University of California
Meson Science Laboratory, University of Tokyo, Japan

EDITORS:

K. M. Crowe — LBL
A. M. Portis — UC Berkeley
T. Yamazaki — U of Tokyo

CONTRIBUTING EDITORS:

J. H. Brewer — TRIUMF
F. N. Gygax — SIN
V. W. Hughes — Yale
C. Kittel — UC Berkeley
W. J. Kossler — William and Mary
P. M. Platzman — Bell Labs
A. Schenck — SIN

SECRETARY:

S. S. Rosenblum — LBL

DEFINITION OF μSR

*μSR stands for Muon Spin Relaxation, Rotation, Resonance, Research, or what have you. The intention of the mnemonic acronym is to draw attention to the analogy with NMR and ESR, the range of whose applications is well known. Any study of the interactions of the muon spin by virtue of the asymmetric decay is considered μSR, but this definition is not intended to exclude any peripherally related phenomena, especially if relevant to the use of the muon's magnetic moment as a delicate probe of matter.*

RECEIVED
AUG 13 1982
Pub
LBL LIBRARY

No. 27 — July 1, 1982

TABLE OF CONTENTS — Page

Extracting Maximal Information on Positive Muon Diffusion in Metals — 1250
M. Leon

Positive Pi-mesons and Positive Muons as Light Isotopes of Hydrogen — 1255
K. Maier, A. Seeger

Theory of Muon Relaxation due to the Hopping Motion of Positive Muons in Ferromagnets — 1270
Alfred Seeger, Patrizia Monachesi

Diffusion and Trapping of Muons in Niobium — 1321
C. Boekema, R. H. Heffner, R. L. Hutson, M. Leon, M. E. Schillaci, W. J. Kossler, M. Numan, S. A. Dodds

PUB-433 7-82/210 This work was supported by the U.S. Department of Energy under Contract No. DE-AC03-76SF00098
Lawrence Berkeley Laboratory is an Equal Opportunity Employer.

PUB-433

## DISCLAIMER

This document was prepared as an account of work sponsored by the United States Government. While this document is believed to contain correct information, neither the United States Government nor any agency thereof, nor the Regents of the University of California, nor any of their employees, makes any warranty, express or implied, or assumes any legal responsibility for the accuracy, completeness, or usefulness of any information, apparatus, product, or process disclosed, or represents that its use would not infringe privately owned rights. Reference herein to any specific commercial product, process, or service by its trade name, trademark, manufacturer, or otherwise, does not necessarily constitute or imply its endorsement, recommendation, or favoring by the United States Government or any agency thereof, or the Regents of the University of California. The views and opinions of authors expressed herein do not necessarily state or reflect those of the United States Government or any agency thereof or the Regents of the University of California.

TABLE OF CONTENTS

Page

Self-consistant Field Investigation of Location and Hyperfine Interaction of Muonium in Diamond 1343
N. Sahoo, Santosh K. Mishra, K. C. Mishra, A. Coker
T. P. Das, C. K. Mitra, L. C. Snyder, A. Glodanu

Low-temperature Mobility of Positive Muons in Pure Copper 1356
A. Seeger

# EXTRACTING MAXIMAL INFORMATION ON POSITIVE MUON DIFFUSION IN METALS*

M.Leon

Los Alamos National Laboratory
Los Alamos, NM 87545

## ABSTRACT

We discuss how combining zero- and longitudinal-field μSR can give more information on the motion of the $\mu^+$ in the target than zero-field studies alone.

## INTRODUCTION

Transverse-field μSR has been used for several years to provide information of the mobility of the $\mu^+$ in various materials. In nonmagnetic metals, depolarization of the $\mu^+$ is caused by the nuclear magnetic moments surrounding the muon interstitial site; when the muon is hopping from site to site, the depolarization rate is reduced by motional narrowing. Furthermore, in many materials, the depolarization rate is found to be a very complicated function of temperature which has been interpreted in terms of capture and release of the $\mu^+$ by traps.[1] However, since the finding of traps and the release from them can produce the same polarization fuction for transverse-field μSR, significant ambiguity of interpretation remains. Recently, Petzinger pointed out that zero-field μSR can readily resolve these ambiguities, since a muon that is trapped and therefore stationary at long times will have its polarization return to one-third of its initial value, while one that is escaping from traps will have its polarization approach zero at long times.[1]

The purpose of the present paper is to point out how combining zero- and longitudinal-field data can yield more information about the muon's motion at some temperatures than can be extracted from

H = 0 data only. One instance is where the muons are both finding and escaping from a given type of trap, and the escape rate $\varepsilon$ is not smaller than $\Delta$, the Gaussian width of precession frequencies at the trap site. In that case, a family of $(\varepsilon,\nu)$ values--$\nu$ being the trapping rate--all give the same zero-field polarization function. A second instance is where the muons are escaping from one type of trap and finding a second. Then there are families of $(\varepsilon_0,\nu_1)$ values for which the zero-field polarization functions differ only at long times, where the experimental information is poor because of the muon decay. In each case, supplementing the H = 0 measurement by an $H_\parallel$ one can resolve the ambiguity and determine the trapping and escape rates separately. We discuss these situations in detail in the following.

## TRAPPING AND ESCAPE FROM A SINGLE TYPE OF TRAP

The integral equation for the polarization function P(t) (for H = 0, $H_\perp$ or $H_\parallel$) and its solution have been discussed in a recent paper.[2] We assume that depolarization occurs only when the muon is trapped. Typical functions with $\varepsilon$ large enough to produce motional

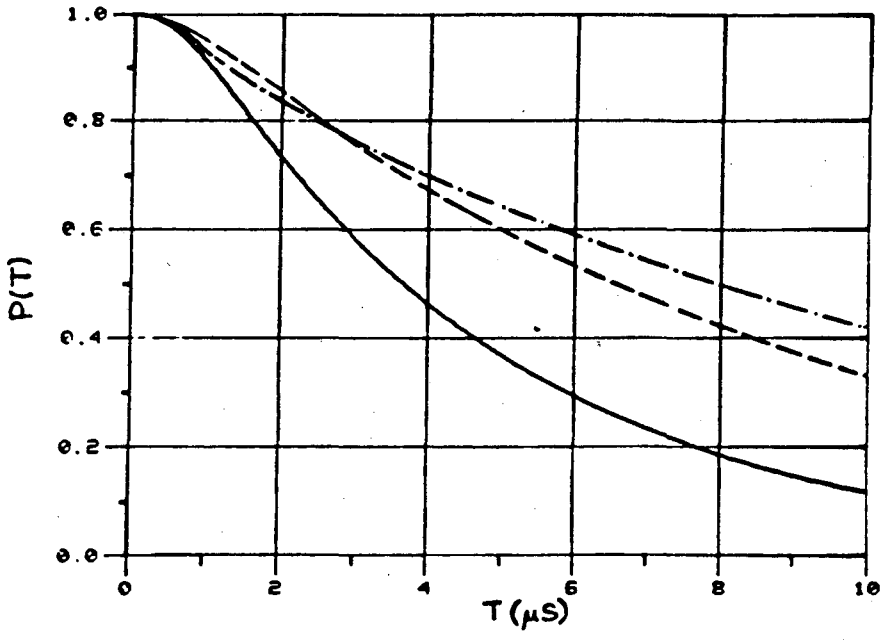


Fig. 1. P(t) for H = 0 (solid curve), $H_\perp$ (dashed curve), and $H_\parallel$ corresponding to muon precession angular frequency $\omega = 2$ (dot-dashed curve). These curves were calculated for $\Delta = 0.5\ \mu s^{-1}$, $\nu = 5\ \mu s^{-1}$, $\varepsilon = 1.45\ \mu s^{-1}$.

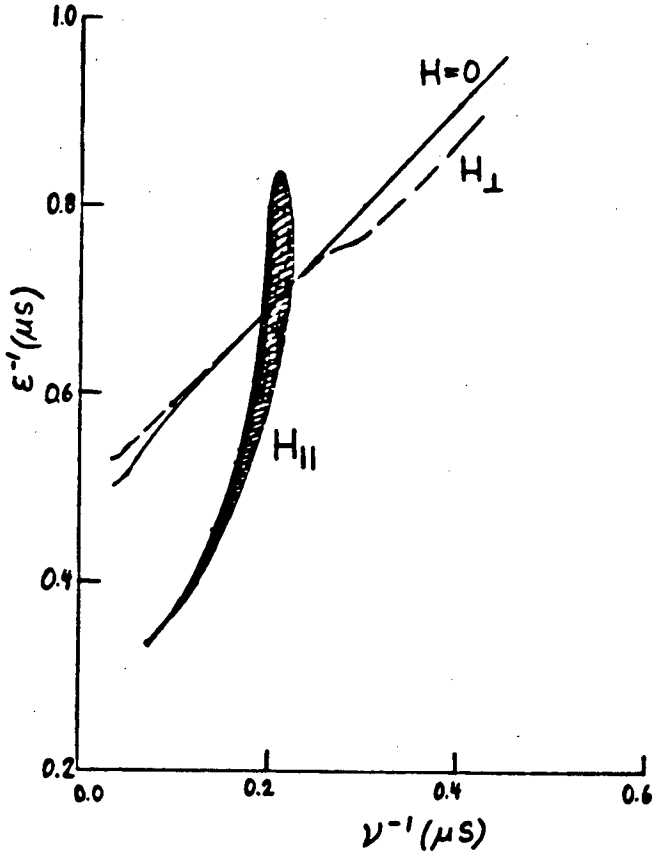


Fig. 2. Points in the $(\nu^{-1},\varepsilon^{-1})$-plane which give rise to P(t) curves essentially identical to those of Fig. 1 ($\Delta,\omega$ fixed at the values of Fig. 1). The H = 0 and $H_\perp$ curves nearly coincide, while the airfoil-shaped area for $H_\parallel$ intersects them at a significant angle.

narrowing are shown in Fig. 1. Essentially identical P(t)'s (over the entire 10 μs range shown!) are generated by families of $(\varepsilon,\nu)$ values in each case. The crucial point is that while the curves of "degeneracy" (i.e., identical P(t)) practically coincide for the H = 0 and $H_\perp$ cases, the area for $H_\parallel$ intersects these at a significant angle; this is shown in Fig. 2 (where for convenience the reciprocals of $\varepsilon$ and $\nu$ are plotted). Thus combining an H = 0 measurement with a properly chosen $H_\parallel$ one will determine <u>both</u> $\varepsilon$ and $\nu$, while an $H_\perp$ experiment does <u>not</u> add information to an H = 0 one.

ESCAPING FROM ONE TYPE OF TRAP AND FINDING A SECOND

Here we suppose that the escape rate $\varepsilon_o$ from trap 1 is not extremely large so that the depolarization in the "free state" (i.e., going from trap to trap of type 1) is not negligible. When the muons are finding the second type of trap, P(t) can be calculated by solving a "hierarchy of integral equations" as discussed in ref. 2. A resulting P(t) for H = 0 is shown in Fig. 3 (solid curve). Also shown is the result neglecting depolarization in the free state, i.e., taking $\varepsilon_o = \infty$, with $\nu_1$ adjusted to make the curves nearly coincide for time t < 5 μs. These two cases would be difficult to distinguish because they differ mainly for t > 5 μs where the data have large error bars.

An analogous pair of curves for $H_{\parallel}$ is shown in Fig. 4. Again the value of $\nu_1$ has been adjusted to make the curves nearly coincide for short times, but now they differ significantly for t > 2 μs. The asymptotic value of P(t), which reflects the static environment of the muon once it is caught in trap 2, is reduced by the depolarization in the free state before it finds trap 2. The presence of $H_{\parallel}$ makes this change of asymptotic value easier to observe by moving it to smaller t. Thus here again combining H = 0 and $H_{\parallel}$ measurements will allow the experimenter to determine two diffusion parameters, now $\varepsilon_o$ and $\nu_1$.

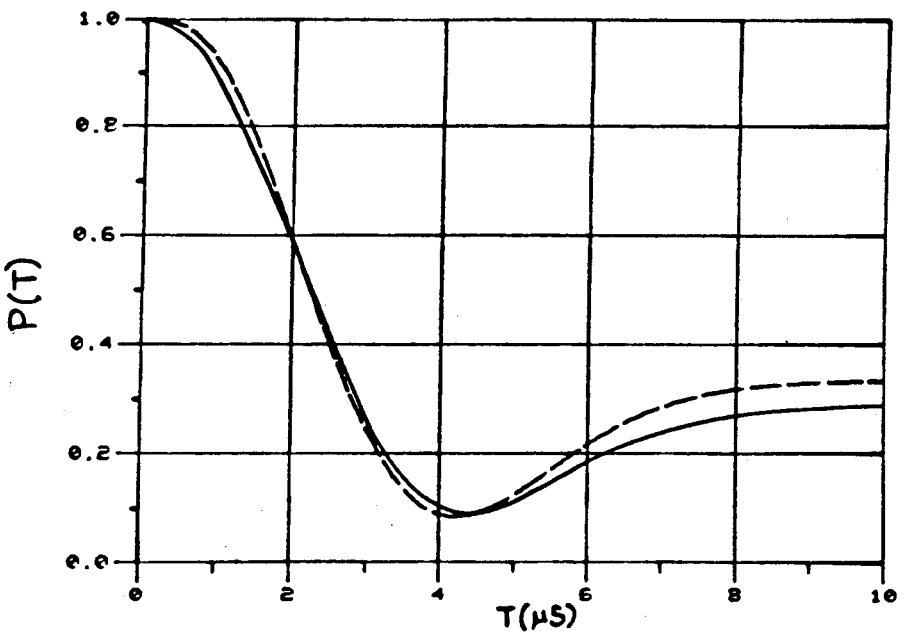


Fig. 3. P(t) for H = 0 and $\Delta_o = \Delta_1 = 0.5\ \mu s^{-1}$. Solid curve: $\varepsilon_o = 2$, $\nu_1 = 1$; dashed curve: $\varepsilon_o = \infty$, $\nu_1 = 1.5$.

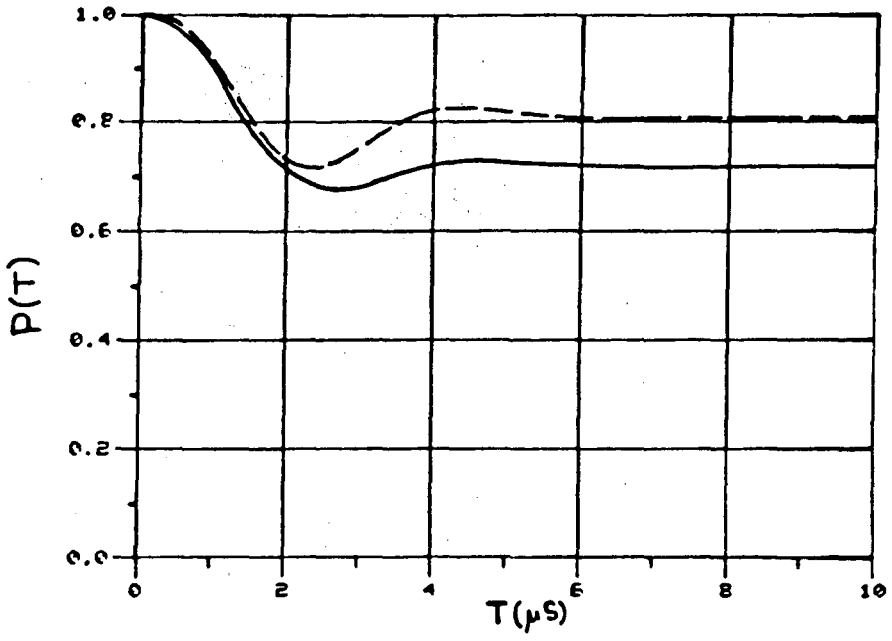


Fig. 4. P(t) for $H_{\parallel}$ such that $\omega = 1.5$, $\Delta_o = \Delta_1 = 0.5\ \mu s^{-1}$. Solid curve: $\varepsilon_o = 2$, $\nu_1 = 1$; dashed curve: $\varepsilon_o = \infty$, $\nu_1 = 2$.

SUMMARY

We have shown how combining longitudinal-field with zero-field μSR experiments can significantly increase the amount of information that can be extracted on the motion of the $\mu^+$ in the target.

REFERENCES

1. K. G. Petzinger, Hyperf. Int. 8 (1981) 639; Phys. Lett. 75A (1980) 225.

2. C. Boekema, R. H. Heffner, R. L. Hutson, M. Leon, M. E. Schillaci, W. J. Kossler, M. Numan, S. A. Dodds; to be published.

*Work supported by the U.S. Department of Energy.

# POSITIVE PI-MESONS AND POSITIVE MUONS AS LIGHT ISOTOPES OF HYDROGEN

K. Maier and A. Seeger

Max-Planck-Institut für Metallforschung, Institut für Physik, and Universität Stuttgart, Institut für theoretische und angewandte Physik, Postfach 800665, D-7000 Stuttgart 80, Germany

## 1. INTRODUCTION

It must be considered as a fortunate coincidence that in a period of great scientific and technological interest in the behaviour of hydrogen in metals and alloys it has become possible to perform experiments on short-lived elementary particles of the same "nuclear charge" as hydrogen. Of these particles positrons ($e^+$) have been employed longest in solid-state physics and chemistry. However, since the positron mass equals the electron mass $m_e$, the dynamic behaviour of a positron in a crystal may be quite different from that of a proton or of a heavier hydrogen nuclide. Therefore, it is often difficult to relate the behaviour of positrons in metals quantitatively to that of protons, particularly when the gap of a factor of 1836 between the proton mass $m_p$ and $m_e$ exists.

In recent years this gap has been partially bridged by investigations using positive muons ($\mu^+$, of mass $m_\mu = 207m_e \approx m_p/9$, lifetime $\tau_\mu = 2.2\cdot10^{-6}$s) and positive pions ($\pi^+$, of mass $m_{\pi\pm} = 273m_e \approx m_p/7$, lifetime $\tau_{\pi\pm} = 2.6\cdot10^{-8}$s). On the one hand, these two "radio-isotopes" of hydrogen are much lighter than the hydrogen nuclides and should therefore exhibit quantum effects more clearly than the latter. On the other hand, they are still heavy compared with the electrons, so that the theoretical treatment of their behaviour in condensed matter may take advantage of the same simplification as that of hydrogen.

Some of the areas in which experimental information useful for the understanding of hydrogen in condensed matter may be obtained with the help of $\mu^+$ and $\pi^+$ are the following:
(i) Quantum theory of diffusion, extension of diffusion measurements

to very low temperatures and isotope effects.
(ii) Lattice sites and vibration amplitudes.
(iii) Interaction with foreign atoms or intrinsic defects.
(iv) Materials with low hydrogen solubility.

By now the use of positive muons as "light isotopes of hydrogen" by means of a variety of so-called $\mu^+$SR (muon spin rotation) techniques may be considered as well established [1,2]. In the present review we confine ourselves to what is presumably the most powerful μSR technique for studying muon diffusion in crystals, namely the measurement of the longitudinal spin relaxation of muons in ferromagnetic single crystals to which a large magnetic field has been applied. In Sect. 3 we shall report on such experiments in progress on α-Fe and on their interpretation.

Compared with muons, the application of positive pions in solid state physics is very young [3,4]. Nevertheless, a number of very promising and encouraging results have been obtained, and a short review of these will be given in Sect. 2. Since pions possess zero spin and are thus without magnetic moments, techniques analogous to $\mu^+$SR are not available. It has recently been realized [3], however, that the behaviour of $\pi^+$ in crystals can be studied very efficiently by means of the lattice steering (channelling) of the positive muons resulting from the decay ($\nu_\mu$ = muon neutrino)

$$\pi^+ \rightarrow \mu^+ + \nu_\mu \quad . \qquad (1)$$

In a sense, positive pions allow us to perform virtually "ideal" channelling experiments, since the decay of muons is monoenergetic with a kinetic energy $E_{kin}$ = 4.12MeV that is convenient for lattice-steering, since the "source" $\pi^+$ decays without leaving any impurities in the crystal, and since the number of implanted $\pi^+$ needed in a given experiment is usually small enough for the accompanying radiation damage to be negligible. Similar experiments can be done on the $\mu^+/e^+$ pair, making use of the muon decay ($\nu_e$ = electron neutrino)

$$\mu^+ \rightarrow e^+ + \bar{\nu}_\mu + \nu_e \qquad (2)$$

and the lattice steering of the relativistic positrons (with energies up to 53 MeV). The feasibility of such experiments has been demonstrated [5]. However, as discussed elsewhere [5], the $\mu^+/e^+$ experiments are much more difficult to perform than the $\pi^+/\mu^+$ lattice-steering experiments, and we shall not consider them further in the present paper.

For a long-range perspective of the application of $\pi^+$ and $\mu^+$ to solid-state problems the reader is referred to a recent conference report [6], for further background information on lattice steering to the review literature [7,8].

## 2. CRYSTAL PHYSICS USING $\pi^+/\mu^+$ LATTICE STEERING

### 2.1. Introductory Remarks

Fast $\pi^+$ and $\mu^+$ injected into crystals are slowed down to thermal energy ("thermalized") within about $10^{-12}$s, i.e., in times that are very short compared with their lifetimes. Subsequently they either occupy interstitial sites in the crystal or, in the presence of impurities or other crystal defects, special trapping sites. Information on the implanted particles is obtained through the charged particles ($\mu^+$ or $e^+$) in the decays (1) or (2). The emission probability of $\mu^+$ in the decay (1) is isotropic, but the probability for the muons to leave the crystal is not (Fig. 1). This is due to the fact that the trajectories of $\mu^+$ emitted in directions close to one of the major crystallographic directions are subject to lattice-steering effects. Lindhard's critical angle $\Psi_{cr}$ [ 9] for the existence of lattice-steering phenomena depends on the atomic number Z and the lattice spacing d in the crystallographic direction. For muons with $E^{\mu}_{kin}$ = 4.12 MeV we obtain

$$\Psi_{cr} = 0.15(Z/d)^{1/2} \quad (\Psi_{cr} \text{ in degrees, d in Å}) . \qquad (3)$$

The $\Psi_{cr}$ are of the order of magnitude of a few tenth of a degree (Ta <111> : 0.8°; Ge <110> : 0.4°). The muon flux distributions around the lattice-steering directions contain detailed information on the behaviour of pions in the crystal.

On the material side the only requirement is the need for fairly large and perfect single crystals with a mosaic spread that is small compared with the critical angles. The growth of such crystals does not present serious problems for valence crystals and for the majority of the metals. With the help of carefully aligning small crystals to a reasonable large 'quasi-single crystal', a technique which has been developed for neutron scattering experiments, $\pi^+/\mu^+$ measurements on

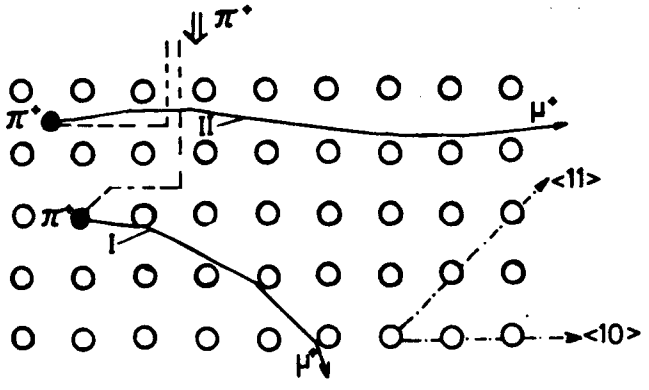


Fig. 1.

Lattice steering of decay muons (I) from a pion located on a lattice site and (II) from a pion located in an interstice.

nearly all crystalline solids are possible.

## 2.1. Experimental [10]

The experimental set-up has to satisfy the following requirements:

(i) In order to resolve the muon intensity profiles the angular resolution of the detecting apparatus has to be better than about $0.2^{\circ}$. For a crystal size of about $2\times2cm^2$ this implies a minimum distance crystal–detector of D = 6m. A crystal size of not less than about $2\times2cm^2$ is highly desirable for intensity reasons, since at the Swiss Institute of Nuclear Research (SIN), at which all experiments discussed in this review have been carried out, the incident $\mu^+$ flux of about $10^8\pi^+s^{-1}$ is distributed over a cross-section of about that magnitude.

(ii) In order to reduce the counting time and to eliminate the effects of fluctuations in the primary $\mu^+$ intensity, the entire angular distribution of the emitted muons has to be measured at the same time and cannot be determined by angular scans as is commonly done in channelling experiments. Thus a two-dimensional position-sensitive detector capable of accepting an angular range of about $4\Psi_{cr}$ is required.

(iii) The channelled decay muons undergo dechannelling when penetrating the crystal. According to an estimate by Van Vliet [11] the mean multiple-scattering angle $\Delta\Psi$ after a penetration length of 10μm at room temperature amounts to $0.18^{\circ}$ (Ta) or $0.12^{\circ}$ (Au) for best-channelled muons in a <100> channel, and to $0.58^{\circ}$ (Ta) or $0.53^{\circ}$ (Au) for muons with high transverse energy (directional straggling). A comparison with the expected critical angles shows that only muons coming from depths of not more than 20μm should be counted. In order to deposit as many $\pi^+$ as possible within a layer of this thickness from the entrance surface, the pion beam (typically with a kinetic energy of 65 MeV, corresponding to a momentum p = 150 MeV/c) has to be moderated (Fig. 2).

The maximum stopping density in the surface layer is obtained if the thickness of the moderator approximately corresponds to the pion range. However, on account of the fluctuations of the energy there is a fluctuation in the range of the individual pions ("range straggling"). The width of this range-straggling distribution is too large for the directional straggling of the majority of the muons reaching the surface to be tolerated. Since for a given small-angle scattering mechanism the square of the scattering angle is proportional to the energy loss, we may eliminate undesirable muons by monitoring their energy loss. This requires the detector to resolve the muon energy with a resolution better than 400 keV (corresponding to a depth of about 15μm in Ta). By a proper choice of the detector thickness, the large flux of background positrons (mainly from the $\mu^+$-decays in the crystal) can be discriminated by using the detector in an dE/dx arrangement for positrons.

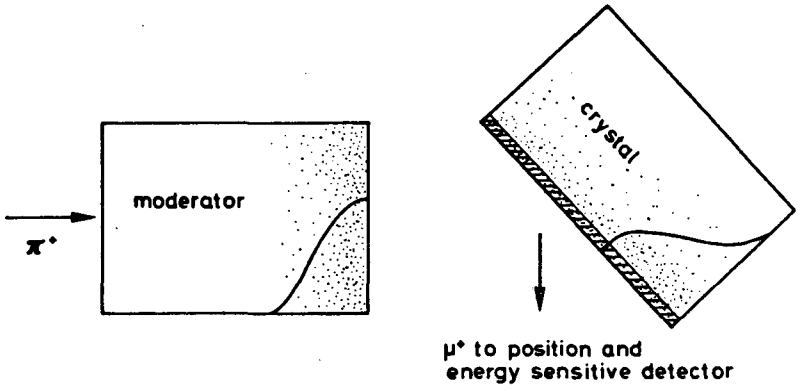


Fig. 2. Range straggling of 150 MeV/c $\pi^+$ in the moderator and the crystal. The full lines and the dots represent the density of deposited pions. Only about 1% of the $\pi^+$ are stopped within the volume on which the measurements are performed (hatched area); the decay muons coming from this volume are identified by measuring their kinetic energy.

The crystal is mounted on a goniometer allowing angular tilts in two directions by about $3^o$ and rotations by about $45^o$. The samples are preoriented by standard X-ray techniques and mounted in such a way that the crystallographic direction to be investigated points (within $0.1^o$) in the direction of the detector. Because of the relatively low kinetic energy of the muons of about 4 MeV the entire muon path (from crystal to detector) of about 8 m length has to be in vacuum, since even a helium-gas atmosphere would lead to considerable small-angle scattering of the muons. The scattering chamber is shielded in such a way that only muons from the crystal can reach the detector. Rutherford scattering of the pions gives only a small uniform background. The majority of the scattered pions decay in flight within the first two meters; therefore their "blocking structure" is completely averaged out.

The muon intensity profiles are measured with a windowless position-sensitive scintillation detector (1.5mm thick) with a counting area of 300mm in diameter divided into four sectors. About 70% of the scintillation light is collected in four photomultiplier tubes. The coordinates X, Y of an event are determined by

$$X = x_1/(x_1+x_2) \quad , \qquad Y = y_1/(y_1+y_2) \quad , \qquad (4)$$

where $x_1$, $x_2$, $y_1$, and $y_2$ denote the pulse heights of the four tubes. The division according to (4) is done on-line with analogue dividers. The spatial resolution of the detector is better than 2cm, its energy resolution for 4 MeV muons corresponds to FWHM = 300 keV. In front of and behind the scintillators are anti-counter tubes in order to

reduce the background due to high-energy positrons crossing the detector under small angles (thus having a prolonged path length and giving rise to scintillation light similar to that of 4 MeV muons). For a pion momentum of 150 MeV/c and a sample area of $4cm^2$ a signal-to-background ratio of 15 : 1 has been obtained.

## 2.3. Results

There are many potential applications of the technique. We give here a number of examples; further results are expected in near future. The results to be desribed below were obtained with a crystal-detector distance of 8.15m.

a) Pion sites

The pion lifetime is short enough for pions in "pure" materials not to be affected by the impurities present, so that, disregarding the isotope effect for the time being, we can gain information on the hydrogen sites, irrespective of the hydrogen solubility. Fig. 3 shows the $\mu^+$ intensity profiles along <100> and <111> directions of a tantalum crystal. Heights and widths of the two profiles are compatible with tetrahedral interstices, in agreement with the determination of deuteron sites [12]. The muon flux distribution is sensitive to the vibrations (thermal or quantum mechanical) of the pions. This allows us to study the potential in the neighbourhood of the pion sites and thus to gain further information relevant for the understanding of hydrogen in condensed matter.

From the measured profiles in Fig. 3 we may conclude that in Ta the vibration amplitudes of the pion are rather small (< 0.2 Å at 200 K).

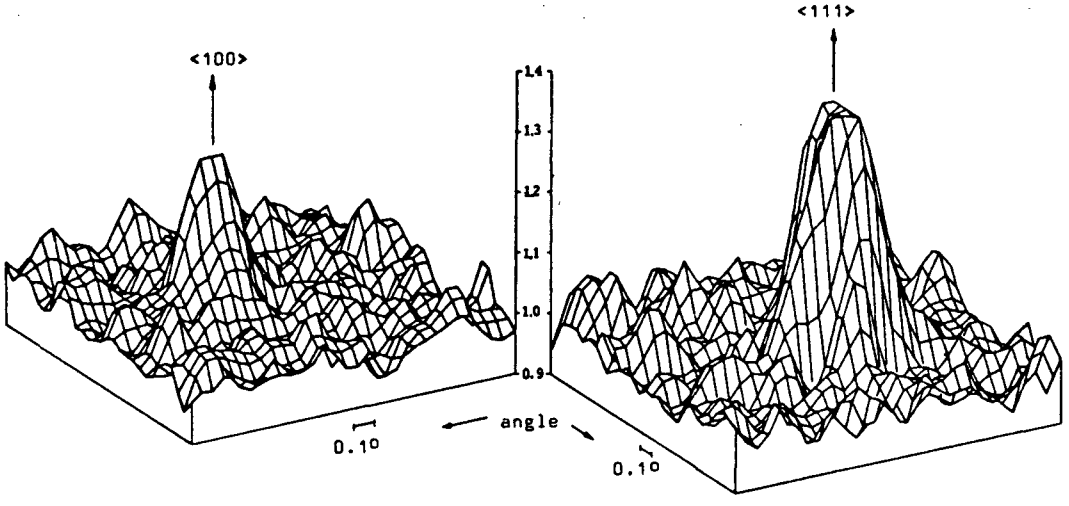


Fig. 3. Normalized intensity of decay muons from positive pions stopped in a Ta single crystal at 200 K along <100> and <111> directions.

Similar $\mu^+$ profiles were found in Au <110>, Ge <110>, and Mo <100>. Here measurements in other directions have yet to be performed in order to determine the occupied sites with certainty.

b) Temperature dependence of energy loss

The dependence of the flux distribution on the energy of the emerging muons (i.e., on the energy loss during the channelling) gives us information on the dechannelling by phonon scattering.

Fig. 4 shows the temperature dependence of the number of muons within the half-width of the <100> channelling peak of Ta (normalized with respect to the same solid angle in a random direction) for the first or second energy window of the detector. In the first energy window there is very little interference of phonon scattering up to 350 K. This suggests that if the measurements are limited to muons with very small energy losses we can carry out the $\pi^+/\mu^+$ lattice steering experiments even at very high temperatures.

c) Trapping of $\pi^+$ at oxygen dissolved in tantalum

From $\mu^+$SR experiments we know that in many crystals positive muons are highly mobile even down to very low temperatures. We may expect a qualitatively similar behaviour for positive pions. This means that in spite of their short lifetime $\pi^+$ may be used to "decorate" lattice defects present in sufficiently high concentrations. In most cases the trapping affects the channelling pattern rather strongly, so that pions constitute probes for studying defects in crystals in much the same way as has been demonstrated for positive muons [13,14,15].

Fig. 5 shows that at room temperature the muon profile of a tantalum crystal containing 0.17 at % oxygen is very similar to that of a pure crystal, but at lower temperatures the width of the profile increases and the height decreases. These experiments indicate that

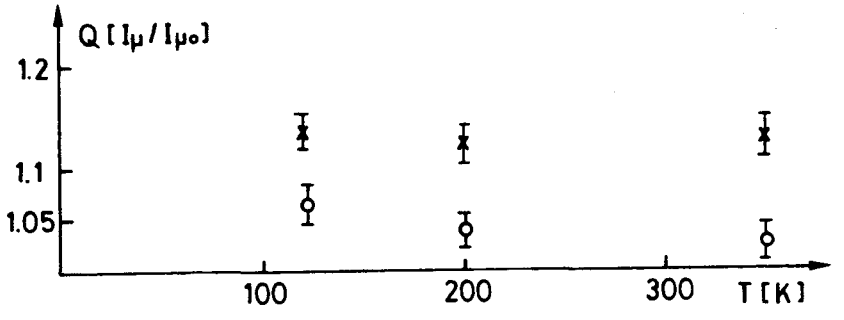


Fig. 4. Normalized muon intensity (within FWHM) in Ta <100> as a function of temperature. X: Muons with 0-0.5 MeV energy loss. O: Muons with 0.5-1 MeV energy loss. With larger energy losses channelling profiles could not be observed.

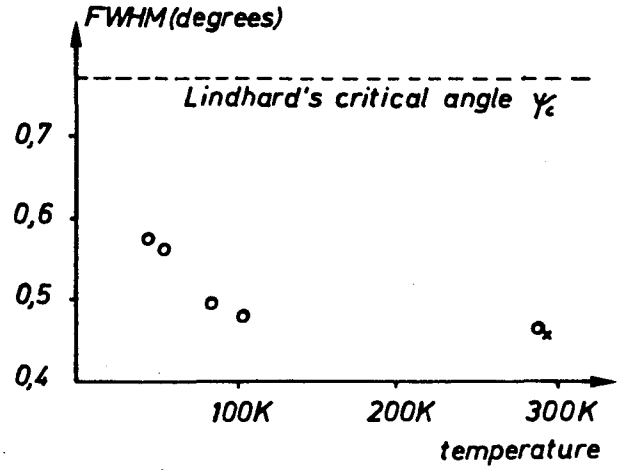


Fig. 5.

Trapping of $\pi^+$ at oxygen impurities in Ta. X: Pure crystal.

the pions may get trapped at the oxygen atoms at sites that are displaced from the pion sites in a perfect environment. The free enthalpy of binding between pions and oxygen atoms is such that at low temperatures the pions stay most of their lifetime in the traps, whereas at room temperature they are virtually free and thus spend most of the time at their "normal" sites.

d) Germanium

From the $\mu^+$SR studies on Si and Ge it is known that in these materials at low temperatures muonium atoms (Mu) are formed [16]. In spite of intensive research the mechanism of muonium formation and the lattice sites involved have remained unclear [17]. In ultra-high-purity Ge crystals a maximum of the muon intensity has been observed in the <110> directions. Below 80 K this channelling peak broadens markedly over a quite narrow temperature interval (Fig. 6). We suspect that this is a consequence of pionium Pi = ($\pi^+e^-$) formation and the establishment of a Pi—Ge bond which draws the pion closer to one of the lattice rows forming the channel. If this interpretation is confirmed these experiments constitute the first observation of the new "element" pionium Pi.

## 2.4. Time-differential lattice steering

Making use of the time structure of the SIN pion beam it is possible to measure the lattice-steering pattern as a function of the "pion age" (i.e., the time a pion has spent in the crystal before decaying), provided the cyclotron is operated in the 17 MHz mode or, even better, in a 10 MHz mode.

The pulse widths of the beams SIN/πE1 and SIN/πE3 are about $1.10^{-9}$s. The time of flight of the decay muons between the crystal and the muon detector is known from the muon energy. The time resolution of the scintillation detector employed is better than $2\cdot10^{-9}$s; its energy resolution better than 8%. This means that we are able to

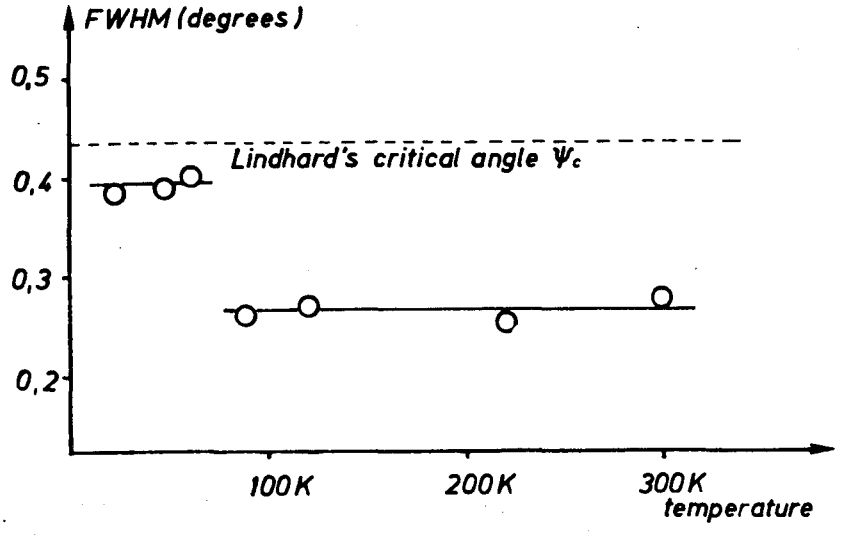


Fig. 6.

Full width at half maximum of lattice steering peak along <110> in ultra-high purity germanium as a function of temperature.

measure the time the pion stays in the crystal with a precision of at least $5 \cdot 10^{-9}$s.

The application of the technique to time-differential lattice steering is planned for the near future. It should be possible to detect the kinetics of trapping of $\pi^+$ at crystal defects or of pionium formation (e.g., in valence crystals) on the time scale $5 \cdot 10^{-9}$s to $6 \cdot 10^{-8}$s (for the 17 MHz mode of SIN).

## 3. LONGITUDINAL MUON-SPIN RELAXATION IN α-IRON IN HIGH MAGNETIC FIELDS

### 3.1. Introductory Remarks

The ideal method to study diffusion and localization of positive muons in metals is the measurement of the decay of muon-spin polarization in longitudinal magnetic fields (i.e. fields parallel or antiparallel to the direction of initial polarization of the muon beam). The longitudinal relaxation rates $\Gamma_1$ are far less sensitive to impurities or lattice imperfections than the spin-phase relaxation rates $\Gamma_2$ obtained from transverse-field experiments. This is due to the fact that as long as no exterior alternating fields act on the muon magnetic moments, only mobile muons give rise to a longitudinal relaxation rate. By contrast, immobilized muons (e.g., muons trapped by impurities) do contribute to the spin relaxation rate $\Gamma_2$ in transverse fields.

Due to the strong variation of local magnetic fields between interstitial sites in ferromagnetic α-iron the longitudinal relaxation rates may be measured over a very wide temperature range

extending from about room temperature down to well below liquid-helium temperature. This offers the possibility to study quantum-mechanical effects on the diffusion of light positively charged particles in metals.

## 3.2. Theory

The magnetic field acting on the muon magnetic moments is given by

$$\underline{B}_\mu = \underline{\bar{B}}_\mu + \underline{B}_{dip} \quad , \tag{5}$$

where

$$\underline{\bar{B}}_\mu = \underline{B}_{appl} + \underline{B}_{Lorentz} + \underline{B}_{Fermi} \tag{5a}$$

comprises the applied field $\underline{B}_{appl}$, the demagnetizing field $\underline{B}_{demag}$, the Lorentz field $\underline{B}_{Lorentz}$, and the Fermi field $\underline{B}_{Fermi}$, which is due to the contact interaction of the muon spins with the spin polarization of the conduction electrons at the muon sites. Via the last term $\underline{\bar{B}}_\mu$ depends on the type of muon site (octahedral or tetrahedral); it is, however, independent of the tetragonality axes of these sites. The last-mentioned property of $\underline{\bar{B}}_\mu$ is not shared by the dipolar field $\underline{B}_{dip}$, which depends on both the interstitial site and on the direction of its tetragonality axis with respect to the magnetization. We characterize $\underline{B}_{dip}$ by the field $\underline{B}^{\parallel}_{dip}$ at interstitial sites with tetragonal axes parallel to the magnetization direction <100>. By symmetry $\underline{B}^{\parallel}_{dip}$ must be parallel or antiparallel to the magnetization direction. The field at the interstices with tetragonality axes perpendicular to the <100> magnetization direction are given by $-\frac{1}{2}\underline{B}^{\parallel}_{dip}$. The longitudinal relaxation rate $\Gamma_1$ depends strongly on the crystallographic directions of $\underline{\bar{B}}_\mu$ [1,18]. (Since we shall consider only $\underline{B}_{appl}$ large enough to saturate the sample magnetically we need not to distinguish between the direction of $\underline{\bar{B}}_\mu$ and of the magnetization). If we confine ourselves to $\underline{\bar{B}}_\mu$ lying in $(0\bar{1}\bar{1})$ planes and characterize the direction of $\underline{\bar{B}}_\mu$ by the angle $\theta$ with respect to <100>, we have for muon sites with tetragonal symmetry

$$\Gamma_1^{(\theta)} = \frac{3}{4}\sin^2\theta\,(1+3\cos^2\theta)\Gamma_1^{<111>} . \tag{6}$$

For $\underline{\bar{B}}_\mu$ parallel to <100> it follows from elementary considerations that $\Gamma_1^{<100>} \equiv 0$.

$\Gamma_1$ assumes its maximum value for $\underline{\bar{B}}_\mu$ parallel to <111> since in this case the dipolar fields at the interstitial site lie in $<2\bar{1}\bar{1}>$ directions perpendicular to the magnetization direction and thus exert the maximum torque on the muon moment in a longitudinal-polarization arrangement. Under the assumption that the muon motion may be described by a correlation time $\tau_c$ we find [1]

$$\Gamma_1^{<111>} = \frac{1}{2}(\gamma_\mu B_{dip}^{//})^2 \frac{\tau_c}{1+\omega_\mu^2\tau_c^2} , \qquad (7)$$

where $\gamma_\mu = 8.52 \cdot 10^8 T^{-1} s^{-1}$ denotes the gyromagnetic ratio of the muons and $\omega_\mu = \gamma_\mu \bar{B}_\mu$ the precession frequency of the muon spins. According to (7), $\Gamma_1$ exhibits a maximum at $\omega_\mu \tau_c = 1$. From the dependence of this maximum on $\underline{B}_{appl}$ we may determine $\underline{B}_{dip}^{//}$ and hence the <u>site</u> of the $\mu^+$. The temperature dependence of $\Gamma_1$ at fixed $\underline{B}_{appl}$ provides us with the temperature dependence of the muon <u>mobility</u>. Most transverse relaxation measurements in iron have been carried out in zero applied fields. In this case $\bar{\underline{B}}_\mu = \underline{B}_{Lorentz} + \underline{B}_{Fermi}$ is parallel to <100> and the transverse relaxation rate is given by

$$\Gamma_2^{<100>} = \frac{1}{2}(\gamma_\mu B_{dip}^{//})^2 \tau_c , \qquad (8)$$

which coincides with the longitudinal relaxation rate $\Gamma_1^{<111>}$ for $\omega_\mu \tau_c << 1$.) In the present model the muon diffusion coefficient is given by

$$D = \alpha a_o^2/\tau_c , \qquad (9)$$

where $a_o$ = edge length of the elementary cube and $\alpha = 1/36$ for octahedral interstices and $\alpha = 1/72$ for tetrahedral interstices.

## 3.3. Experiment [19]

A schematic view of the apparatus designed for the use of surface muons is shown in Fig. 7. The superconducting magnet for fields up

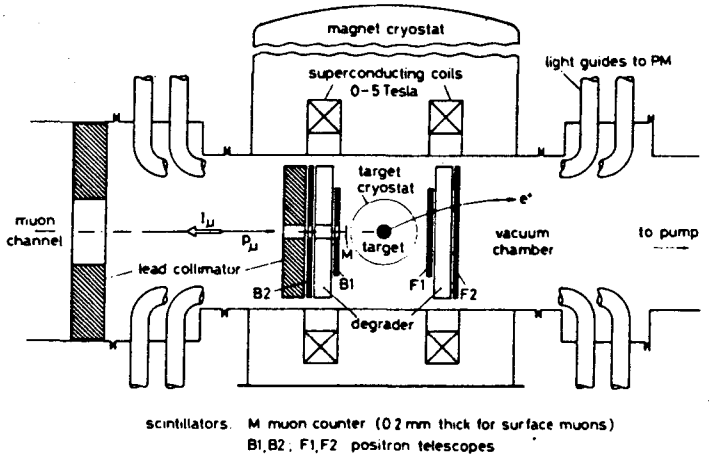


Fig. 7.

Schematic view of the apparatus for the measurement of longitudinal muon-spin relaxation in high magnetic fiels.

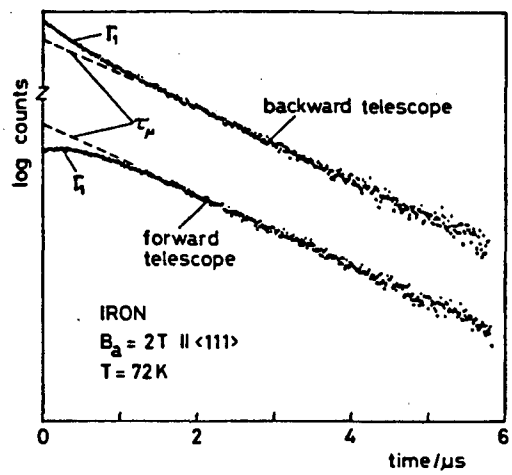


Fig. 8. Muon decay spectra of an α-iron single crystal at 52 K. Applied magnetic field 2 T parallel to the muon polarization and to a <111> crystallographic direction.

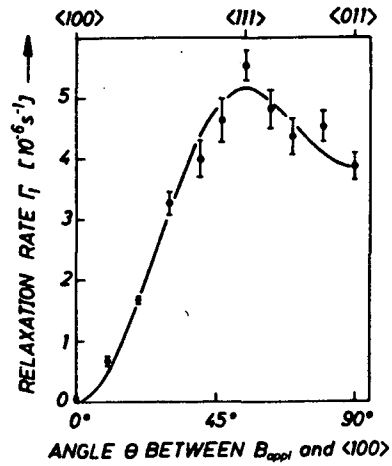


Fig. 9. Dependence of the longitudinal relaxation rate $\Gamma_1$ of α-Fe on the angle θ between <100> and an applied field in a (001) plane at 52 K [21]. $B_{appl}$ = 2 T. Solid curve: prediction (6) for muon sites of tetragonal symmetry.

to 5 T consists of a pair of coils in Helmholtz geometry (homogeneity $\Delta B_{appl}/B_{appl} < 10^{-4}$ within a sphere of 3cm diameter). The helium-evaporation cryostat with 25μm thick titanium windows allows measurements between 3 K and 300 K. The target, a single crystal of α-iron 9mm in diameter [20], was mounted on a rotatable holder with a <110> direction parallel to the rotation axis in order to measure the dependence of $\Gamma_1$ on the crystallographic direction of $\underline{B}_{appl}$.

Timing signals are given by the scintillators M (0.2mm thick) for incoming muons and F1 or B1 (5mm) for "forward" or "backward" decay positrons. The degrades (1cm of Cu) between the positron telescopes F1F2 and B1B2 absorb low energy positrons in order to enhance the analyzing power for the measurement of the forward-backward asymmetry of the $\mu^+$ decay. Fig. 8 shows (on a semilogarithmic scale) spectra measured at 72 K with $B_{appl}$ = 2 T. At times $t > 2 \cdot 10^{-6}$s they are entirely determined by the muon lifetime $\tau_\mu = 2.2 \cdot 10^{-6}$s; the deviation from a straight line at shorter times is due to the longitudinal relaxation of the $\mu^+$-spin polarization.

## 3.4. Results

Fig. 9 gives an example of the dependence of $\Gamma_1$ on the crystallographic direction of $\underline{B}_{appl}$ [21]. The agreement between experiment and theory (cf. (6) and solid line) is good. This was confirmed at different temperatures and different applied fields. From these results we conclude that the muons in α-iron occupy sites of tetragonal symmetry

i.e., tetrahedral or/and octahedral interstices .

Fig. 10 shows an Arrhenius plot of $\Gamma_1^{<111>}$ as a function of temperature. The comparison with zero-applied-field relaxation rates $\Gamma_2^{<100>}$ [22] demonstrates the sensitivity of transverse-field μSR to impurities and the superiority of longitudinal field experiments: the deviation of $\Gamma_2^{<100>}$ from the longitudinal relaxation rate $\Gamma_1$ above ~70 K is due to lattice imperfections.

At temperatures above 20 K the longitudinal relaxation rates show no significant dependence on the strength of $\underline{B}_{appl}$, indicating that we are in the regime $\omega_\mu \tau_c << 1$. Therefore, the maximum in $\Gamma_1$ at 40 K cannot be the maximum at $\omega_\mu \tau_c = 1$ predicted by (7) but has to be explained in terms of a change in the intrinsic diffusion mechanism.

Yagi et al. [21] have suggested that at low temperatures (below about 20 K) positive muons in α-Fe occupy preferentially tetrahedral interstices, whereas at higher temperatures there is an equipartition between octahedral and tetrahedral interstices (which both possess tetragonal symmetry and, therefore, give both rise to the orientation dependence (6) ). All the experiments carried out since have supported this hypothesis.

Fig. 10 shows that below 20 K there is a definite dependence of the longitudinal relaxation rate $\Gamma_1^{<111>}$ on the strength of the applied field but that not even at the largest applied fields a maximum in the temperature dependence of the relaxation rate has been found down to 4 K, the lowest temperature employed so far. Measurements down to 0.3 K with the help of a $^3$He-cryostat are being prepared and should clarify the situation.

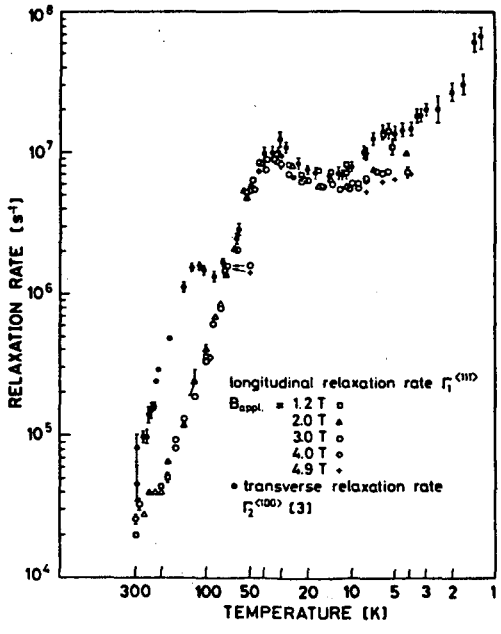


Fig. 10.

Temperatures dependence of the longitudinal relaxation rate $\Gamma_1^{<111>}$ at applied fields $B_{appl}$ ranging from 1.2 to 4.9 T. For comparison, recent zero-applied-field relaxation measurements [22] are included. The deviation of these data from $\Gamma_1$ at temperatures > 70 K demonstrates the sensitivity of transverse relaxation rates to impurities.

If more than one type of interstices is occupied the theory outlined in Sect. 3.2. does no longer suffice. Seeger and Monachesi [18] have recently given a detailed general theory, covering in particular the case of transitions between octahedral and tetrahedral interstices. The general treatment shows that at high temperatures the simple theory of Sect. 3.2. remains valid provided $(B^{\parallel}_{dip})^2$ is treated as an adjustable parameter. For temperatures above 60 K one may fit the $\Gamma_1^{<111>}$ data of Fig. 10 by assuming that the muon diffusion coefficient D varies with temperature either according to the classical law

$$D \sim \exp(-H^M/kT) \qquad (10)$$

with the migration enthalpy $H^M = (0.033 \pm 0.001)$ eV or according to the multi-phonon incoherent tunnelling law [23]

$$D \sim T^{-1/2} \exp(-H_a/kT) \qquad (11)$$

with the lattice-activation enthalpy $H_a = (0.038 \pm 0.001)$ eV.

According to Teichler and Seeger [24], at low temperatures (11) has to be replaced by the one-phonon law

$$D \sim T \quad . \qquad (12)$$

The available experiments are in agreement with (12) (which predicts $\Gamma_2^{<100>} \sim T^{-1}$) but a final test has to await the outcome of the above-mentioned experiments in the $^3$He cryostat.

Acknowledgement

The authors gratefully acknowledge the help of G. Jünemann, G. Flik, D. Herlach, and H.-D. Carstanjen, who collaborated on the channelling work. The measurements on Ge were performed on ultra-high-purity crystals kindly provided by E. Haller (Berkeley). The work reported in Sect. 3 is part of the Stuttgart–Heidelberg $\mu^+$SR collaboration programme with the participation of T. Aurenz, H. Bossy, K.P. Döring, M. Gladisch, N. Haas, D. Herlach, W. Jacobs, M. Krauth, M. Krenke, H. Matsui, P. Monachesi, H. Orth, G. zu Putlitz, J. Vetter, and E. Yagi. We are further indebted to G. Wiederoder, R. Henes, P. Keppler, and W. Maisch for their technical assistance, to Miss L. Holland Miss H. Schweyer for preparing the typescript, and to Prof. W. Frank for critically reading the manuscript. The experiments were made possible by the financial support of the Bundesministerium für Forschung und Technologie, Bonn, through the programme "Mittelenergiephysik" and, last not least, by the excellent experimental conditions at SIN.

REFERENCES

[1] A. Seeger, Hydrogen in Metals I (eds. G. Alefeld and J. Völkl) p. 349, Springer, Berlin–Heidelberg–New York 1978

[ 2] H. Orth, K.P. Döring, M. Gladisch, D. Herlach, W. Maysenhölder, H. Metz, G. zu Putlitz, A. Seeger, J. Vetter, W. Wahl, M. Wigand, and E. Yagi, Hydrogen in Metals—Münster 1979, p. 631, Akademische Verlagsgesellschaft, Wiesbaden 1979; see also Z.Phys.Chemie, N.F., 116, 241 (1979)

[ 3] K. Maier, Nuclear Physics Methods in Materials Research (eds. K. Bethge, H. Baumann, H. Jex, and F. Rauch) p. 264, Vieweg, Braunschweig 1980

[ 4] K. Maier, G. Flik, D. Herlach, G. Jünemann, H. Rempp, A. Seeger, and H.-D. Carstanjen, Phys. Letters 83A, 341 (1981)

[ 5] K. Maier, G. Flik, D. Herlach, G. Jünemann, A. Seeger, and H.-D. Carstanjen, Phys. Letters 86A, 126 (1981)

[ 6] A. Seeger, Proceedings of the 5th Meeting of the International Collaboration on Advanced Neutron Sources (ICANS-V) (eds. G. S. Bauer and D. Filges), Jül-Conf. 45, 1981, p. 113

[ 7] D.S. Gemmell, Rev. Mod. Phys. 46, 129 (1974)

[ 8] R. Sizmann and C. Varelas, Festkörperprobleme XVII (ed. J. Treusch) p. 261, Vieweg, Braunschweig 1977

[ 9] J. Lindhard, K. Dan, Vid. Selsk, Mat.-Fys. Medd. 34 (1965) no. 4

[10] K. Maier, G. Flik. A. Seeger, D. Herlach, H. Rempp, G. Jünemann, and H.-D. Carstanjen, Nucl. Instr. and Meth., in the press (Proc. 9th Intern. Conf. on Atomic Collisions in Solids, Lyon 1981)

[11] D. Van Vliet, AERE Report 6395, Harwell 1970

[12] H.-D. Carstanjen, phys.stat.sol. (a) 59, 11 (1980)

[13] A. Seeger, Positron Annihilation (eds. R.R. Hasiguti and K. Fujiwara) p. 771 (The Japan Institute of Metals, Sendai 1980)

[14] D. Herlach, Recent Developments in Condensed Matter Physics, Vol. 1 (ed. J.T. Devreese) p. 93 Plenum Publishing Corp., New York 1981

[15] A. Seeger, Proceedings 5th Intern. Symposium on High-Purity Materials in Science and Technology (eds. J. Morgenthal and H. Oppermann) Vol. II, p. 253, Akademie der Wissenschaften der DDR, Dresden 1980

[16] P.F. Meier, Exotic Atoms '79 (ed. by K. Crowe, J. Duclos, G. Fiorentini, and G. Torelli) p. 331, Plenum Press, New York and London 1980

[17] B.D. Patterson, Hyperfine Interact. 6. 155 (1979)

[18] A. Seeger and P. Monachesi, Phil. Mag., in the press

[19] T. Aurenz, H. Bossy, M. Gladisch, N. Haas, D. Herlach, W. Jacobs, M. Krauth, M. Krenke, H. Matsui, P. Monachesi, H. Orth, G. zu Putlitz, A. Seeger, J. Vetter, E. Yagi, and K.P. Döring, SIN Newsletter Nr. 14 (1982)

[20] K. Lubitz and G. Göltz, Appl. Phys. 19, 237 (1979)

[21] E. Yagi, H. Bossy, K.P. Döring, M. Gladisch, D. Herlach, H. Matsui, H. Orth, G. zu Putlitz, A. Seeger, and J. Vetter, Hyperfine Interact. 8, 553 (1981)

[22] H. Graf, G. Balzer, E. Recknagel, A. Weidinger, and R.I. Grynszpan, Phys. Rev. Letters 44, 133 (1980)

[23] C.P. Flynn and A.M. Stoneham, Phys. Rev. B 1, 3966 (1970)

[24] H. Teichler and A. Seeger, Phys. Letters 82A, 91 (1981)

# Theory of Muon Spin Relaxation due to the Hopping Motion of Positive Muons in Ferromagnets

By ALFRED SEEGER and PATRIZIA MONACHESI†
Max-Planck-Institut für Metallforschung, Institut für Physik, and Universität Stuttgart, Institut für theoretische und angewandte Physik, Postfach 800665, D-7000 Stuttgart-80, Germany

## ABSTRACT

The interaction of the magnetic moments of spin-polarized positive muons with the magnetic fields at the interstices in ferromagnetic (or ferrimagnetic) materials may be used to study the localization and the hopping motion of thermalized muons by observing the relaxation of the longitudinal or transverse spin polarization or the shift of the muon spin precession frequency as a function of the orientation of a strong applied magnetic field. The general theory is developed and applied to the special cases of muon diffusion between two types of interstices of tetragonal symmetry in body-centred cubic metals ($\alpha$-Fe) or of cubic symmetry in face-centred cubic metals (Ni). It is shown that by a suitable choice of the strength and the crystallographic direction of the applied magnetic field quite detailed information on the quantum diffusion of positively charged light particles in crystals may be obtained.

† Present address: Université de Lausanne, Institut de Physique théorique, Dorigny, CH-1015 Lausanne

## § 1. Introduction and Overview.

The diffusion of particles that are much lighter than the host atoms but nevertheless heavy compared with the electrons forms a challenging field of both experimental and theoretical condensed-matter physics. The outstanding problem in this area, of great technological importance in a wide variety of materials, is the diffusion of hydrogen (or its isotopes, in particular tritium). However, it is not easy to obtain reliable experimental data on hydrogen diffusion in condensed matter at low temperatures, where the diffusivity is small and trapping by impurities or other imperfections (dislocations, grain or phase boundaries) may be very important.*)

On the theoretical side, at low temperatures quantum effects (e.g., tunneling of the diffusing particles through potential barriers) play an important rôle. The field is therefore also known as "quantum diffusion" (Flynn and Stoneham 1977, Kagan and Klinger 1974, Stoneham 1980, Teichler 1980, 1981, Teichler and Seeger 1981). In crystalline materials it may be subdivided into the regimes of "coherent" and of "incoherent" diffusion. The first may be treated with the help of many-particle Bloch states formed by the wavefunctions of the diffusing particles and the lattice distorsions surrounding them. Thermally excited phonons or static imperfections (e.g., impurities) induce scattering transitions between these states that on a macroscopic scale may be described in terms of a particle diffusivity D.

*) For a survey of the behaviour of hydrogen in metals and alloys the reader should consult several contributions to Alefeld and Völkl (1978a, b).

The second regime is that of "hopping" motion. An appropriate physical picture is that the diffusing particles and their "displacement clouds" are localized, usually in interstices, and that they move by thermally assisted jumps from one site to the next. This regime comprises both classical "over-barrier" jumps and incoherent tunnelling jumps, in which the phonon occupation numbers undergo changes beyond what would be required by a pure translation from one lattice cell to another.

As hinted above, the distinction between the coherent and the incoherent diffusion regimes and the establishing of the temperature dependence of the diffusivity D in each of them is not an easy task for the experimentalist. It is therefore most welcome that in recent years diffusion experiments on positive muons ($\mu^+$) and positive Pi-mesons ($\pi^+$) implanted into crystals have become feasible. These particles possess masses $m_\mu \approx m_p/9$ and $m_{\pi^\pm} \approx m_p/7$ that are much smaller than the proton mass $m_p$. Their electrical charge, however, is the same as that of the hydrogen nuclides, so that for the purpose of diffusion studies we may consider $\mu^+$ and $\pi^+$ as "light isotopes" of hydrogen (Seeger 1978,1979).

The present paper deals with what according to our present knowledge constitutes the most powerful technique for studying the diffusion of $\mu^+$ in crystalline materials, viz., the investigation of muon spin relaxation in ferromagnetic (or, more generally, ferrimagnetic) crystals of suitable crystal structures. In the meson factories longitudinally spin-polarized muons are obtained from the decay

$$\pi^+ \rightarrow \mu^+ + \nu_\mu \quad , \qquad (1.1)$$

where $\nu_\mu$ denotes muon neutrinos. When implanted into metals the $\mu^+$ are thermalized without appreciable loss of their polarization in times that are many orders of magnitudes shorter than their mean lifetime $\tau_\mu = 2.2\ \mu s$. The interaction of their magnetic moments with the magnetic fields at the muon sites may lead to a precession of the muon spins and to a gradual loss of the spin polarization. Both phenomena can be quantitatively followed with the help of the muon decay reaction

$$\mu^+ \rightarrow e^+ + \bar{\nu}_\mu + \nu_e , \qquad (1.2)$$

since due to parity non-conservation the probability of emission of the positrons ($e^+$) is asymmetric with respect to the direction of the muon spin.

The theory to be worked out in detail in the present paper pertains to the case of <u>hopping motion</u>*). The basic ideas have been communicated earlier (Seeger 1978) and have in the meantime been verified experimentally (Yagi et al. 1981). Since on account of the generality of the present treatment the results are somewhat involved, we give in the following a short overview in terms of simple physical arguments. There is a close relationship to the study of diffusion by means of nuclear magnetic resonance (Bloembergen, Purcell, and Pound 1948, Slichter 1980, Wolf 1981).

We consider an ensemble of polarized $\mu^+$ implanted and thermalized at time t = 0. When a $\mu^+$ diffuses through a ferromagnetic crystal it experiences in general a time-dependent magnetic field

*) For the case of bandlike motion of the $\mu^+$ see Fujii ( 1979 ).

$$\underset{\sim}{B}_\mu(t) = \underset{\sim}{\bar{\bar{B}}}_\mu + \underset{\sim}{\tilde{B}}(t) \quad , \qquad (1.3)$$

where $\underset{\sim}{\bar{\bar{B}}}_\mu$ denotes the <u>time-independent</u> ensemble average of $\underset{\sim}{B}_\mu(t)$. The time-dependent contribution $\underset{\sim}{\tilde{B}}(t)$ arises from the fact that even in perfect crystals the magnetic field at different interstices will in general be different. (This may be due to the dipolar field $\underset{\sim}{B}_{dip}$ and/or the Fermi field $\underset{\sim}{B}_{FERMI}$ to be discussed below.) Since $\underset{\sim}{\tilde{B}}(t)$ for a given muon depends on all its jumps up to time t, $\underset{\sim}{\tilde{B}}(t)$ is a stochastic field which must be treated by taking the appropriate ensemble averages (§4).

The direction of $\underset{\sim}{\bar{\bar{B}}}_\mu$ defines the longitudinal and transverse components of the muon spin polarization $\underset{\sim}{P}$. If $\underset{\sim}{\tilde{B}}(t) \equiv 0$, the longitudinal polarization component $P_1$ stays constant, whereas the transverse component (of modulus $P_2$) rotates perpendicular to $\underset{\sim}{\bar{\bar{B}}}_\mu$ with the angular velocity

$$\omega_\mu = \gamma_\mu \underset{\sim}{\bar{\bar{B}}}_\mu \quad , \qquad (1.4)$$

where $\gamma_\mu = 8.5161 \cdot 10^8 s^{-1} T^{-1}$ denotes the gyromagnetic ratio of the muons.

In discussing the effect of a non-vanishing $\underset{\sim}{\tilde{B}}(t)$, it is convenient to treat the cases of longitudinal ($P_1 \neq 0$, $P_2 = 0$) and transverse ($P_1 = 0$, $P_2 \neq 0$) polarization separately. In either case the muon spin polarization is affected only by the $\underset{\sim}{\tilde{B}}$ components perpendicular to the direction of $\underset{\sim}{P}$. In the <u>longitudinal</u> case these components introduce transitions between the

Zeeman levels of the muon spins and thus cause the longitudinal polarization $P_1$ to relax towards its equilibrium value. The relaxation rate, in the following called longitudinal relaxation rate $\Gamma_1$, will be large when the Fourier spectrum of $\tilde{\underset{\sim}{B}}(t)$ contains strong components near the Zeeman frequency $\omega_\mu$ (also given by (1.4)). This means that as a function of the muon jump frequency, which may be varied by varying the temperature, $\Gamma_1$ exhibits a maximum when the "correlation time" $\tau_c$ associated with the jumps (see § 4.1) satisfies the condition $\tau_c \omega_\mu \approx 1$. If $\omega_\mu$ is known from measurement of the precession frequency, an absolute scale for the muon jump frequencies may be established in this way.

Due to their stochastic nature non-vanishing transverse components of $\tilde{\underset{\sim}{B}}(t)$ cause the individual spins to precess at slightly different angular frequencies. This leads to a gradual reduction to zero of the transverse polarization $P_2$ at a rate proportional to the square of the amplitude of the transverse component of $\tilde{\underset{\sim}{B}}$. If this component has the same direction as $\tilde{\underset{\sim}{B}}_\mu$, the low-frequency Fourier components are clearly more effective in relaxing the transverse polarization than high-frequency contributions, so that one expects the transverse relaxation rate $\Gamma_2$ to be proportional to the reciprocal of the muon jump frequency. This means that in this case $\Gamma_2$ does not show a maximum as a function of the muon jump frequency, in contrast to the longitudinal relaxation rate $\Gamma_1$. In the special case that $\tilde{\underset{\sim}{B}}$ and $\tilde{\underset{\sim}{B}}_\mu$ are parallel or antiparallel it is hence not possible to separate experimentally the square of the amplitude of the time-dependent magnetic field $\tilde{\underset{\sim}{B}}(t)$ from the muon jump frequency.

Compared with $\Gamma_1$ measurements, the study of muon spin diffusion by means of $\Gamma_2$ measurements has another important drawback. Positive muons may easily be trapped by impurities or other crystal imperfections. In the trapped locations the magnetic field $\underset{\sim}{B}_\mu$ acting on the muons will in general be different from $\bar{\bar{\underset{\sim}{B}}}_\mu$. Hence the spins of trapped muons precess at angular velocities that are different from those of muons at "ideal sites". Particularly when the jump frequency and hence the diffusion path of the muons is large, the trapping effects may be so pronounced as to make the deduction of diffusivities from $\Gamma_2$ measurements virtually impossible. By contrast, $\Gamma_1$ measurements are much less sensitive against trapping. It is true that repeated trapping and detrapping may give contributions to the longitudinal relaxation as well but these come usually from a frequency range that is so different from that involved in bulk diffusion that for sufficiently "diluted" traps there should be no practical problems.

On the other hand, measurements in transverse geometry are extremely helpful in determining the spin precessing frequency $\omega_\mu$ and hence the field $\bar{\bar{B}}_\mu$. In ferromagnets $\bar{\bar{B}}_\mu$ contains contributions which are not a priori known and which must be determined experimentally before one can deduce absolute values of the muon jump frequencies.

In perfect crystals $\tilde{\underset{\sim}{B}}(t)$ and hence the depolarization rate is clearly zero if the muons reside only on sites that are crystallographically and magnetically equivalent and if (as we shall assume throughout the paper) the time

spent by the muons during their jumps are too short to lead to any appreciable depolarization. Examples for $\tilde{\underset{\sim}{B}}(t) \equiv 0$ are provided by muons that occupy only octahedral interstices of face-centred cubic (fcc; e.g., Ni or β-Co) or hexagonal close-packed (e.g., α-Co or Gd) crystals.

The situation is quite different in body-centred cubic (bcc) crystals, e.g. in α-Fe. There are no interstices with cubic symmetry in this crystal structure. Let us illustrate the situation by considering muons located in tetrahedral interstices (open circles in Fig. 1), which possess tetragonal point symmetry.

In the demagnetized state the magnetic dipole moments $\underset{\sim}{\mu}_{ion}$ of the Fe ions and also the spontaneous magnetization $\underset{\sim}{M}_{sp}$ are parallel to one of the cubic axes, in the example of Fig. 1(a) to the 3-axis. For reasons of symmetry, the magnetic field produced by the magnetic moments of the Fe ions at the interstitial sites, $\underset{\sim}{B}^{dip}$, is parallel (or antiparallel) to this axis. Lorentz's (1909 ) theorem demands that the vectorial average $\bar{\underset{\sim}{B}}_{dip}$ over tetrahedral interstices with tetragonal axes parallel to the three cubic axes (briefly called, 1-, 2-, 3-sites) must be zero (comp. Seeger 1978). From symmetry it follows that $\underset{\sim}{B}_{dip}$ at the 1- and 2-sites must be opposite in direction to and of half the modulus of $\underset{\sim}{B}_{dip}$ at 3-sites. Under these circumstances, muons jumping between sites of different tetragonalities experience a stochastic field $\tilde{\underset{\sim}{B}}(t)$ with values alternating between $B^{\parallel}_{dip}/2$ and $-B^{\parallel}_{dip}$, where $B^{\parallel}_{dip}$

denotes the dipolar field (with the sign convention at the end of § 3.1) at those interstitial sites whose tetragonality axes are parallel to the magnetization direction [comp.(3.9)]. If the muon polarization is perpendicular to the magnetization, $\tilde{\underset{\sim}{B}}(t)$ is perpendicular to $\underset{\sim}{P}$ and hence gives rise to a transverse depolarization. However, if $\underset{\sim}{P}$ is parallel to $\bar{\bar{\underset{\sim}{B}}}_{\mu}$, i.e. in the case of longitudinal polarization, $\underset{\sim}{B}_{dip}$ does not exert a torque on the muon magnetic moments, hence $\Gamma_1 \equiv 0$ in the demagnetized state.

In order to obtain a non-vanishing longitudinal relaxation rate we have to arrange for $\underset{\sim}{B}_{dip}$ to have components perpendicular to $\bar{\bar{\underset{\sim}{B}}}_{\mu}$. This can be done by saturating the magnetization by means of a large enough external field $\underset{\sim}{B}_{appl}$ in a direction different from <100>. The extreme and at the same time simplest case is that of saturation in a <111> direction (Fig. 1b).

If the magnetic moments of the Fe ions point in the direction of one of the cube diagonals, symmetry arguments (Seeger 1978) show that the dipolar contributions $\underset{\sim}{B}^{(i)}_{dip}$ at the three types of interstitial sites (i = 1, 2, 3) must lie in the three <211> directions of the {111} planes perpendicular to $\underset{\sim}{\mu}_{ion}$ and hence to $\bar{\bar{\underset{\sim}{B}}}_{\mu}$. This leads indeed to a finite longitudinal relaxation with the characteristics discussed above. In this special case $\underset{\sim}{B}_{dip}$ does not have a component parallel to $\bar{\bar{\underset{\sim}{B}}}_{\mu}$, but since there is nevertheless always a $\underset{\sim}{B}_{dip}$ component perpendicular to $\underset{\sim}{P}$ we obtain a finite transverse relaxation rate $\Gamma_2$ with the

same dependence on the muon jump frequency as $\Gamma_1$. Symmetry arguments show that $\Gamma_2^{<111>} = \Gamma_1^{<111>}/2$ as long as the only contributions to $\tilde{\underset{\sim}{B}}_\mu$ come from $\underset{\sim}{B}^{dip}$ (Seeger 1978).

From the preceding discussion it is obvious that in order to make use of the full potential of muon spin relaxation in ferromagnets for the study of quantum diffusion we have to treat the dependence of the relaxation rate on the direction of the applied magnetic field $\underset{\sim}{B}_{appl}$. On the one hand this requires a detailed study of the various magnetic fields involved (§3). On the other hand it gives us two fringe benefits: (i) the symmetry of the muon sites may be explored and (ii) in the regime of high relaxation rates the experimental conditions for the accurate determination of relaxation rates may be optimized by choosing the crystallographic orientation of $\tilde{\underset{\sim}{B}}_\mu$ appropriately. Moreover, as we shall see in § 5.3, there is an orientation dependence of the muon spin precession frequency that contains further information on the correlation time $\tau_c$.

The comparison of the present theory with available experiments (Yagi et al. 1981) demonstrates unambigously that in α-Fe the muons reside in interstices of tetragonal symmetry. Since in the bcc structure there are two types of such interstices [octahedral (O) and tetrahedral (T)] and since it is not a priori clear how the muons move between them, we have to treat a fairly elaborate diffusion model (§2) in order to provide a sufficiently general framework within which the experimental data may be discussed. In the calculation of the relaxation rates on the basis of this model (§4) we confine ourselves to the hopping regime of muon diffusion. We do avoid, however, the usual assumption that the correlation times are large compared to the muon lifetime $\tau_\mu$ and derive correction terms for situations in which this assumption does not apply.

As a special case our general treatment covers the case of interstices with cubic point symmetry, e.g. octahedral and tetrahedral interstices in fcc metals. From the preceding discussion it is obvious that in this case the mechanisms so far considered (all based on non-vanishing $B_{dip}$) do not give rise to a finite relaxation rate. The hyperfine ("contact") interactions with the spin-polarized conduction electrons at the muon site, expressed in terms of the so-called Fermi field $\underset{\sim}{B}_{FERMI}$, are in general different at the octahedral and the tetrahedral sites. If the muons jump between the two types of sites a spin relaxation may arise. The usual assumption is that $\underset{\sim}{B}_{FERMI}$ is always parallel (or antiparallel) to the magnetization. This means that we may obtain a transverse but not a longitudinal relaxation rate. In § 5.2 we apply these ideas to Ni and show that they might indeed account for the transverse relaxation rate observed in the ferromagnetic state of Ni. The same mechanism may also contribute to the transverse relaxation in α-Fe if there are jumps between tetrahedral and octahedral interstices.

## § 2. The Diffusion Model

The two most spacious interstices in the bcc lattice are the octahedral interstices O at positions $(\frac{1}{2}, \frac{1}{2}, 0)$ in the cubic elementary cell and the tetrahedral interstices T at positions $(\frac{1}{2}, \frac{1}{4}, 0)$, both of them with tetragonal point symmetry. We make the assumption that these are the only types of interstices to be taken into account. This is supported by the experiments in so far as the experimental data show that the interstices occupied by positive muons in α-Fe possess tetragonal or higher (i.e.,cubic) symmetry (Yagi et al. 1981) and as there are no interstices of cubic symmetry in this crystal structure.

It is not a priori clear whether the O or the T sites are energetically more favourable,nor is it evident what will be the most probable diffusion path in either case. We shall therefore treat a quite general model,which is likely to include all important possibilities. Fig.2 indicates the notation used.

The frequency of direct jumps between nearest-neighbour T sites is denoted by $\nu_{TT}$, that of direct jumps between nearest-neighbour O sites by $\nu_{OO}$, and that between next-nearest-neighbour O sites by $\nu'_{OO}$. The frequencies of jumps between an octahedral site and one of its nearest-neighbour or next-nearest-neighbour T sites are denoted by $\nu_{OT}$ or $\nu'_{OT}$, respectively,those of the reverse jumps by $\nu_{TO}$ or $\nu'_{TO}$, respectively. In this "six frequency model" [one of the jump frequencies may be expressed in terms of the others by taking into account detailed balancing—see (2.10)] the only jumps not changing the tetragonality of the occupied sites are those associated with the frequencies $\nu'_{OT}$ and $\nu'_{TO}$.

If we denote by $p_T$ or $p_O$ the probabilities that an octahedral or tetrahedral

site is occupied and by $b_{TT}$, $b_{OO}$, $b'_{OO}$, $b_{TO} = b_{OT}$, $b'_{TO} = b'_{OT}$, the jump distances associated with the various jumps, the present model gives us for the muon diffusion coefficient

$$D = \frac{1}{6}\{p_T(g_{TT}\nu_{TT}b_{TT}^2 + g_{TO}\nu_{TO}b_{OO}^2 + g'_{TO}\nu'_{TO}b_{TO}^2) + p_O(g_{OO}\nu_{OO}b_{OO}^2 + g'_{OO}\nu'_{OO}b'^2_{OO} + g_{OT}\nu_{OT}b_{TO}^2 + g'_{OT}\nu'_{OT}b'^2_{OT})\} \quad . \tag{2.1}$$

The geometrical factors $g_{TT}=4$, $g_{OO}=4$, $g'_{OO}=8$, $g_{TO}=2$, $g'_{TO}=4$, $g_{OT}=4$, $g'_{OT}=8$ represent the number of crystallographically equivalent sites that may be reached from a given interstice by the various types of jumps. In terms of the length $a_o$ of the elementary cube edge the squares of the jump distances are given by $b_{TT}^2=a_o^2/8$, $b_{OO}^2=a_o^2/4$, $b'^2_{OO}=a_o^2/2$, $b_{TO}^2=a_o^2/16$, $b'^2_{TO}=5a_o^2/16$.

Since there are twice as many T sites as O sites, in thermal equilibrium we have

$$2p_O^{eq} = p_T^{eq}\exp(-\frac{\Delta H}{kT}) \ , \tag{2.2}$$

where $\Delta H$ is the difference in the enthalpy of a muon at an O site and at a T site. Together with

$$p_T + p_O = 1 \ , \tag{2.3}$$

(2.2) gives us

$$p_T^{eq} = \frac{2}{2+\exp(-\frac{\Delta H}{kT})} \ , \qquad p_O^{eq} = \frac{\exp(-\frac{\Delta H}{kT})}{2+\exp(-\frac{\Delta H}{kT})} \ , \tag{2.4}$$

where kT denotes Boltzmann's constant times the absolute temperature. Inserting the geometrical factors given above into (2.1) results in the following expression for the muon diffusion coefficient:

$$D = \frac{a_o^2}{6}\{(\frac{1}{2}\nu_{TT} + \frac{1}{8}\nu_{TO} + \frac{5}{4}\nu'_{TO})p_T^{eq} + (\nu_{OO} + 4\nu'_{OO} + \frac{1}{4}\nu_{OT} + \frac{5}{2}\nu'_{OT})p_O^{eq}\} \cdot \tag{2.5}$$

For later use we shall distinguish not only T and O sites but also the three different tetragonality axes. We denote the T sites with axes parallel to [100] ,

[010] , or [001] by subscripts 1,2,3, and the corresponding O sites by subscripts 4,5,6. We may then write for the time variation of the occupation probabilities $p_j(t)$ of these sites

$$\partial p_j / \partial t = \sum_{k=1}^{6} (w_{kj} p_k - w_{jk} p_j) \quad , \qquad j=1,\ldots 6 \quad , \qquad (2.6)$$

The transition rates $w_{jk}$ are related to the jump frequencies introduced above according to

$$\begin{aligned}
w_{12} = w_{21} = w_{23} = w_{32} = w_{31} = w_{13} &= 2\,\nu_{TT} \\
w_{45} = w_{54} = w_{56} = w_{65} = w_{64} = w_{46} &= 2\,\nu_{OO} + 4\,\nu'_{OO} \\
w_{14} = w_{25} = w_{36} &= 4\,\nu'_{TO} \\
w_{41} = w_{52} = w_{63} &= 8\,\nu'_{OT} \\
w_{15} = w_{16} = w_{24} = w_{26} = w_{34} = w_{35} &= \nu_{TO} \\
w_{51} = w_{61} = w_{42} = w_{62} = w_{43} = w_{53} &= 2\,\nu_{OT} \quad .
\end{aligned} \qquad (2.7)$$

Under conditions of thermal equilibrium the left-hand sides of (2.6) vanish (detailed balancing), giving us

$$\sum_{k=1}^{6} (w_{kj} p_k^{eq} - w_{jk} p_j^{eq}) = 0 \quad , \qquad j=1,\ldots 6 \qquad (2.8)$$

where

$$p_1^{eq} = p_2^{eq} = p_3^{eq} = \frac{1}{3}\, p_T^{eq} \qquad (2.9a)$$

and

$$p_4^{eq} = p_5^{eq} = p_6^{eq} = \frac{1}{3}\, p_O^{eq} \quad . \qquad (2.9b)$$

From (2.8) and (2.9) it follows

$$(2\, w_{15} + w_{14}) p_T^{eq} = (2\, w_{51} + w_{41}) p_O^{eq} \qquad (2.10a)$$

or, with (2.4) and (2.7),

$$(\nu_{TO} + 2\,\nu'_{TO}) = (\nu_{OT} + 2\,\nu'_{OT}) \exp(-\frac{\Delta H}{kT}) \quad . \qquad (2.10b)$$

We find finally for the diffusion coefficient

$$D = \frac{a_o^2}{6} \{\tfrac{1}{2}\nu_{TT}p_T^{eq} + (\nu_{OO}+4\nu'_{OO})p_O^{eq} +$$

$$\tfrac{1}{4}(\nu_{TO}+2\nu'_{TO}) \left[ 1+4\left(\frac{\nu'_{TO}}{\nu_{TO}+2\nu'_{TO}} + \frac{\nu'_{OT}}{\nu_{OT}+2\nu'_{OT}}\right)\right] p_T^{eq}\} \quad . \tag{2.11}$$

Well known special cases of (2.11) are

$$D= \frac{a_o^2}{12} \nu_{TT} \tag{2.12a}$$

[$\Delta H>0$ (T sites energetically favoured), $\Delta H >> kT$ (low temperatures)]

and

$$D= \frac{a_o^2}{6} (\nu_{OO} + 4\nu'_{OO}) \tag{2.12b}$$

[$\Delta H<0$ (O sites energetically favoured) , $|\Delta H| >> kT$] .

In the high-temperature limit ($|\Delta H| << kT$) we have $p_T^{eq}= 2/3$, $p_O^{eq}= 1/3$,

hence

$$D= \frac{a_o^2}{18} (\nu_{TT}+\nu_{OO} + 4\nu'_{OO} + \frac{1}{2} \nu_{TO} + 3\nu'_{TO} + 2\nu'_{OT}) \quad . \tag{2.13}$$

## § 3. The Magnetic Fields

### 3.1 Classification and definitions.

Muon diffusion and the magnetic fields at the interstices determine together the "magnetic history" of positive muons in metals (in which so far there is no evidence for muonium formation). In ferromagnetic metals we may distinguish three different classes of magnetic fields acting on the muon magnetic moments, viz.,

(i) macroscopic fields which may be considered constant on an atomic scale,

(ii) fields which are different for different types of interstices (e.g. tetrahedral or octahedral) but independent of the crystallographic orientation of interstices of lower than cubic point symmetry,

(iii) fields which depend not only on the type of the interstices but, in the case of point symmetry lower than cubic, also on their crystallographic orientation.

Class (i) comprises the applied field $\underset{\sim}{B}_{appl}$, the demagnetizing field $\underset{\sim}{B}_{demag}$, and the Lorentz field $\underset{\sim}{B}_{LORENTZ}$. The demagnetizing field is determined by the magnetization of the sample, $\underset{\sim}{M}_{sample}$, and the demagnetization tensor $\underset{=}{N}$ according to

$$\underset{\sim}{B}_{demag} = -\underset{=}{N} \cdot \mu_o \underset{\sim}{M}_{sample} \quad , \tag{3.1}$$

where $\mu_o$ is the permeability of the vacuum. If the applied field is homogeneous and the sample is of ellipsoidal shape, $\underset{\sim}{B}_{demag}$ is uniform in the sample.

The Lorentz field is the field created by the electronic magnetic moments at the atomic sites lying <u>outside</u> the so-called Lorentz sphere (a sphere around the muon location with radius large compared with the interatomic distance but small compared with the size of the ferromagnetic domains). The Lorentz field is given by

$$\underset{\sim}{B}_{LORENTZ} = \frac{\mu_o}{3} \underset{\sim}{M}_{domain} \quad , \tag{3.2}$$

where $\underset{\sim}{M}_{domain}$ is the magnetization of the domain in which the Lorentz sphere is located. $M_{domain}$ varies between the spontaneous magnetization $M_{sp}$ in the limit of a demagnetized sample (in the absence of hysteretic effects equivalent to $B_{appl}=0$) and the saturation magnetization $M_{sat}$ in the limit of very large applied fields.

The fields created by the magnetic moments of the electrons <u>inside</u> the Lorentz sphere contribute to the classes (ii) and (iii). From a phenomenological point of view the <u>averages</u> of the fields associated with different crystallographic orientations of a given type of interstitial site give us the fields of class (ii), whereas the <u>deviations</u> from these averages lead to the fields of class (iii).

In cubic crystals the preceding phenomenological distinction between classes (ii) and (iii) practically coincides with the subdivision of the electronic magnetic moments into those of the conduction electrons, resulting in the Fermi <u>contact interaction</u> at the muon location, and those of the core electrons, giving rise to <u>magnetic dipole moments</u> (and possibly higher moments as well) located at the atom sites.

According to our present knowledge, which is mainly based on neutron diffraction experiments (Shull 1968), the effective magnetic field describing the contact interaction, $\underset{\sim}{B}_{FERMI}$, is parallel or antiparallel to the direction of the magnetization and hence independent of the crystallographic orientation of interstitial sites of lower than cubic point symmetry. It does vary, however, between different types of interstices, e.g. tetrahedral and octahedral interstices.

We denote by $\underset{\sim}{B}_{dip}$ the magnetic fields at the muon sites created by the magnetic moments of the ion cores and by $\overline{\underset{\sim}{B}}_{dip}$ their vectorial average over the different crystallographic orientation of a given type of sites. It follows from magnetostatics that in cubic crystals $\overline{B}_{dip} = 0$. This means that in <u>cubic</u> crystals $\underset{\sim}{B}_{dip}$ does not contribute to classes (i) or (ii). By contrast, in <u>non-cubic</u> crystals $\underset{\sim}{B}_{dip}$ does in general give a contribution to the fields of class (ii).

At any given moment the field $\underset{\sim}{B}_{\mu}(t)$ felt by a muon is given by

$$\underset{\sim}{B}_{\mu}(t) = \underset{\sim}{B}_{appl} + \underset{\sim}{B}_{demag} + \underset{\sim}{B}_{LORENTZ} + \underset{\sim}{B}_{FERMI}(t) + \underset{\sim}{B}_{dip}(t), \qquad (3.3)$$

where $\underset{\sim}{B}_{FERMI}(t)$ and $\underset{\sim}{B}_{dip}(t)$ refer to the site occupied by the muon at time t. If positive muons occupy only <u>one</u> type of interstitial sites and if they jump sufficiently rapidly between these sites, the spin precession frequency or the Zeeman frequency (depending on whether $\overline{\underset{\sim}{B}}_{\mu}$ is transverse or longitudinal to the muon polarization $\underset{\sim}{P}$) is given by

$$\omega_{\mu} = \gamma_{\mu} \overline{B}_{\mu} \quad , \qquad (3.4)$$

where

$$\overline{\underset{\sim}{B}}_{\mu} = \underset{\sim}{B}_{appl} + \underset{\sim}{B}_{demag} + \underset{\sim}{B}_{LORENTZ} + \underset{\sim}{B}_{FERMI} + \overline{\underset{\sim}{B}}_{dip} \quad . \qquad (3.5)$$

If the muons occupy, say, <u>two</u> different types of interstitial sites and if the jumps between these sites are sufficiently fast, (3.4) has to be generalized to

$$\omega_{\mu} = \gamma_{\mu} \overline{\overline{B}}_{\mu} \qquad (3.6)$$

where

$$\overline{\overline{\underset{\sim}{B}}}_{\mu} = \underset{\sim}{B}_{appl} + \underset{\sim}{B}_{demag} + \underset{\sim}{B}_{LORENTZ} + p_T^{eq} \underset{\sim}{B}_{FERMI}^{T} + p_O^{eq} \underset{\sim}{B}_{FERMI}^{O} \quad . \qquad (3.7)$$

In (3.7) the two types of interstices are distinguished by the suffixes T and O ; furthermore, we have confined ourselves to cubic crystals by putting $\bar{\underset{\sim}{B}}_{dip} = 0$.

Of particular interest are cases in which all the fields in (3.5) or (3.7) are either parallel or antiparallel. Then these equations may be written as scalar equations with the following sign conventions: Fields parallel to the magnetization are counted as positive, antiparallel fields are given a negative sign. With this convention $B_{appl}$ is non-negative, $B_{LORENTZ}$ is positive, $B_{demag}$ is non-positive, whereas $B_{FERMI}$ may have either sign. In ideal crystals sign and magnitude of $B_{FERMI}$ are known from neutron diffraction experiments (Shull 1968). However, the presence of a positive muon in an interstice may modify these values profoundly (Kanamori 1981), so that $B^T_{FERMI}$ and $B^O_{FERMI}$ must be considered as parameters to be deduced from experiment.

## 3.2 The dipolar field.

For reasons of symmetry, at an interstitial site with tetragonal point symmetry the dipolar field $\underset{\sim}{B}_{dip}$ must be either parallel or antiparallel to the magnetization $\underset{\sim}{M}$ if this has the same direction as the tetragonal axis of the site. In this case we may write

$$\underset{\sim}{B}_{dip} = B^{\parallel}_{dip} \frac{\underset{\sim}{M}}{M} \qquad (3.8)$$

and characterize the dipolar field by the scalar $B^{\parallel}_{dip}$. In cubic crystals the dipolar fields at the interstices with tetragonal axes perpendicular to $\underset{\sim}{M}$ are given by

$$B^{\perp}_{dip} = -\frac{1}{2} B^{\parallel}_{dip}. \qquad (3.9)$$

In the following we shall denote $B^{\parallel}_{dip}$ by $B^T_{dip}$ or $B^O_{dip}$ for tetrahedral or octahedral interstices, respectively.

The general expression for $\underset{\sim}{B}_{dip}$ reads

$$\underset{\sim}{B}_{dip} = \frac{\mu_o}{4\pi} \sum_j \frac{3\underset{\sim}{r}_j(\underset{\sim}{r}_j \cdot \underset{\sim}{\mu}^j_{ion}) - (\underset{\sim}{r}_j \cdot \underset{\sim}{r}_j)\underset{\sim}{\mu}^j_{ion}}{\underset{\sim}{r}_j^5} , \qquad (3.10)$$

where the sum extends over the magnetic dipole moments inside the Lorentz sphere and where $\underset{\sim}{\mu}^j_{ion}$ denotes the magnetic moment of the $\underset{\sim}{j}^{th}$ ion and $\underset{\sim}{r}_j$ the vectors from the interstitial site under consideration to the positions of the magnetic dipole moments.

Since an interstitial muon displaces the neighbouring ions and since it also may affect the magnitude and directions of their magnetic moments, the precise value of $\underset{\sim}{B}_{dip}$ must at present be treated as an adjustable parameter. Nevertheless, if the lattice distortion around a muon does not destroy the tetragonal point symmetry of the interstices, (3.8) and (3.9) remain valid. An estimate of $B''_{dip}$ may be obtained by neglecting the distortion of the crystal by the muons and by attributing the entire magnetization to the magnetic moments of the ions. This gives us for bcc structures (Kronmüller et al. 1979)

$$B^O_{dip} = 21.33 \frac{\mu_o}{8\pi} M_{domain} , \qquad (3.11a)$$

$$B^T_{dip} = 6 \frac{\mu_o}{8\pi} M'_{domain} . \qquad (3.11b)$$

For use in §4, we introduce the distinction between the 'magnetic' ($x_i$=x,y,z) Cartesian coordinate system and the crystallographic ($x'_i$=x',y',z') coordinate system. In cubic crystals the ($x'_i$)-axes coincide with the cubic axes.*) The z axis is chosen parallel to $\underset{\sim}{\bar{\bar{B}}}_\mu$, the x axis parallel to the direction of the transverse component of the initial muon polarization $\underset{\sim}{P}(0)$. ( If the initial polarization does not possess a component transverse to $\underset{\sim}{\bar{\bar{B}}}_\mu$, the choice of the x and y axes is immaterial.) Eqs. (3.8,9) may be generalized to the case of any arbitrary direction of $\underset{\sim}{M}$ as follows.

*) The reader will note that this notation differs slightly from that used in § 1.

If $\beta_1$, $\beta_2$, $\beta_3$ are the direction cosines of $\underset{\sim}{M}$ with respect to the cubic axes and if n labels the symmetry of the 4-fold tetragonal axes of the interstices (see §2), then in the $(x_i')$-system $B_{dip}'^{(n)}$ is given by

$$\underset{\sim}{B}_{dip}'^{(x')} = \frac{B_{dip}^{\parallel}}{2}(-2\beta_1, \beta_2, \beta_3)$$
$$\underset{\sim}{B}_{dip}'^{(y')} = \frac{B_{dip}^{\parallel}}{2}(\beta_1, -2\beta_2, \beta_3) \qquad (3.12)$$
$$\underset{\sim}{B}_{dip}'^{(z')} = \frac{B_{dip}^{\parallel}}{2}(\beta_1, \beta_2, -2\beta_3) \quad .$$

The components of the dipole fields in the 'magnetic' coordinate system may be found by the usual transformation involving the nine direction cosines $\alpha_{qp}$ between the 'magnetic' (q=x,y,z) and the cubic (p=x', y', z') axes:

$$B_{dip,q}^{(n)} = \sum_{p=1}^{3} \alpha_{qp} B_{dip,p}'^{(n)} \quad . \qquad (3.13)$$

By their nature, $\underset{\sim}{B}_{FERMI}$ and the fields belonging to category (i) are already expressed in the 'magnetic' reference system.

From the preceding results it follows that in a bcc lattice with muons occupying tetrahedral and/or octahedral interstices and a general direction of $\underset{\sim}{M}$, $\underset{\sim}{B}_{dip}$ contributes to both the longitudinal and the transverse muon spin relaxation but not to the spin precession frequency, whereas $\underset{\sim}{B}_{FERMI}$ contributes to the transverse spin relaxation and to the precession frequency but not to the longitudinal spin relaxation (for details see § 4.2).

## §4. Relaxation and Correlation Functions

### 4.1 General theory

As mentioned in § 1, in calculating the spin relaxation of positive muons in ferromagnets we consider only the interaction of the muon magnetic moment with the magnetic fields of electronic origin. In the 'magnetic' coordinate system introduced in § 3 we may write the muon spin Hamiltonian as

$$H(t) = H_0 + \tilde{H}(t) \quad , \qquad (4.1)$$

where

$$H_o = -\hbar\gamma_\mu \bar{\bar{B}}_\mu I_z \tag{4.2}$$

and

$$\mathcal{H}(t) = -\hbar\,\gamma_\mu \sum_q \tilde{B}_q(t)\, I_q \,. \tag{4.3}$$

In (4.2) the $I_q$ represent the components of the muon spin operator and $\hbar$ denotes, as usual, Planck's constant divided by $2\pi$. In (4.2,3) the magnetic field felt by by the muons $B_\mu(t)$, has been subdivided according to (1.3) into the time-dependent part $B(t)$ and the time-independent average value $\bar{\bar{B}}_\mu(t)$. In the following we shall assume that the magnetic moments of the muons interact with $B_\mu(t)$ only while the muons are situated in a cubic crystal on at most two different types of sites (in § 3 denoted by T and O). Then $\bar{\bar{B}}_\mu$ is given by (3.7).

The field $\tilde{B}_\mu(t)$ reflects the 'magnetic history' of positive muons thermalized at time t=0 and is responsible for the relaxation of the muon spin polarization. The time scale of this "magnetic history" may be characterized by a 'correlation time' $\tau_c$, which is a measure of the time required for a diffusing muon to feel a magnetic field $B_\mu(\tau_c)$ substantially different from $B_\mu(0)$. Unless the muons jump only between sites at which the local magnetic fields are the same, $\tau_c$ is of the order of magnitude of the mean time of residence at a site. We are primarily interested in situations where $\tau_c \ll \tau_\mu$. In such situations the appropriate mathematical tool for calculating the spin relaxation is the density matrix formalism, a perturbation theory approach valid for times $t > \tau_c$ well known from NMR theory (Slichter 1980, Wolf 1979).

By a generalization of the procedure described in detail by Slichter (1980) one obtains for the <u>transverse polarization</u>

$$P_x(t) = P_x(0)\, R_2(t) \cos\left[\omega_\mu t + \Omega(t)\right] \,, \tag{4.4a}$$

where the <u>transverse relaxation function</u> is given by

$$R_2(t) = \exp\{-\int_0^t (t-t')\left[G_{zz}(t') + G_{xx}(t')\cos(\omega_\mu t')\right]dt'\} \,, \tag{4.4b}$$

and where

$$\Omega(t) = \int_0^t (t-t')\, G_{xx}(t')\sin(\omega_\mu t')\,dt' \,. \tag{4.4c}$$

(Note that due to the choice of the (x,y,z) coordinate system at the end of § 3 we have $P_y(0) = 0$.)

The time variation of the longitudinal polarization may be written as

$$P_z(t) = P_z(0)\, R_1(t) \tag{4.5a}$$

with the longitudinal relaxation function

$$R_1(t) = \exp\{-\int_0^t (t-t')\left[G_{xx}(t')+G_{yy}(t')\right]\}\cos(\omega_\mu t')dt' \quad . \tag{4.5b}$$

In the preceding equations the quantities $G_{qq}$ denote the correlation functions of the time-dependent part $\tilde{\underset{\sim}{B}}(t)$ of the magnetic field felt by the diffusing muons. They are defined as

$$G_{qq} = \gamma_\mu^2 \langle \tilde{B}_q(0)\cdot\tilde{B}_q(t)\rangle \qquad (q=x,y,z) \;, \tag{4.6}$$

where the averaging (< >) is over an ensemble of thermalized muons. The frequency $\omega_\mu$ appearing in (4.4) and (4.5) is given by (3.6) and denotes the muon spin precession frequency in the case $G_{xx} \equiv 0$. We see from (4.4c) that for sufficiently strong relaxation the spin precession frequency may differ from $\omega_\mu$; details will be discussed below.

Baryshevskii and Kuten' (1976), who were apparently the first to state (4.4,5), emphasized that, due to the finite lifetime of the muons, in the case of strong relaxation the muon spin relaxation rates are often determined at times t after the thermalization of the muons that are comparable with or less than one order of magnitude larger than $\tau_c$. In such cases it is not permissible to extend the upper limit of integration in (4.4) and (4.5) to infinity, as is usually done in NMR theory. If we do go to the limit $t\to\infty$ the familiar results of the Bloch–Wangsness–Redfield theory [for references see Wolf (1979)] are obtained, namely

$$\Gamma_1(\omega_\mu\tau_c) \equiv -\frac{d\ln R_1(t)}{dt} = \int_0^\infty \left[G_{xx}(t')+G_{yy}(t')\right]\cos(\omega_\mu t')dt' \tag{4.7a}$$

for the longitudinal relaxation rate; and

$$\Gamma_2(\omega_\mu\tau_c) \equiv -\frac{d\ln R_2(t)}{dt} = \int_0^\infty \left[G_{zz}(t')+G_{xx}(t')\cos(\omega_\mu t')\right]dt' \tag{4.7b}$$

for the transverse relaxation rate. In (4.7) $\tau_c$ denotes the correlation time introduced above; it determines the time scale of the correlation functions (4.6).

## 4.2 Calculation of the correlation functions

Since in the present model the field $\underset{\sim}{B}_\mu(t)$ felt by a muon is completely determined by the interstice it occupies at time t, the calculation of the correlation function (4.6) may be reduced to the solution of the 'master equation' (2.6) for the occupancy of the various interstitial sites. Let us denote by $p_j^i(t)$ the probability that a muon occupies at time t the site j under the condition that it was at site i at time t=0, and let us furthermore denote the q component of $\tilde{\underset{\sim}{B}}$ at site j by $\tilde{B}_q^j$. We may then define the 'partial' correlation functions

$$G_{qq}^i(t) \equiv \gamma^2 \tilde{B}_q^i \sum_{j=1}^{6} \tilde{B}_q^j \, p_j^i(t) \qquad (q=x,y,z) \quad . \qquad (4.8)$$

The functions $p_j^i(t)$ are the solutions of (2.6) under the initial condition $p_j^i(0) = \delta_{ij}$ (i,j=1,...6) and are given in the Appendix. From (4.8) the correlation functions (4.6) are obtained by taking the average over the initial distribution of the thermalized muons, to wit

$$G_{qq}(t) = \sum_{i=1}^{6} G_{qq}^i \, p_i^{eq} \quad . \qquad (4.9)$$

Solving (1.3) for $\tilde{\underset{\sim}{B}}(t)$ by means of (3.3) and (3.7) gives us

$$\tilde{\underset{\sim}{B}}(t) = \underset{\sim}{B}_{dip}(t) + \underset{\sim}{B}_{FERMI}(t) - (p_T^{eq} \underset{\sim}{B}_{FERMI}^T + p_0^{eq} \underset{\sim}{B}_{FERMI}^0) \; , \qquad (4.10)$$

where $\underset{\sim}{B}_{dip}(t)$ and $\underset{\sim}{B}_{FERMI}(t)$ refer to the site occupied at time t.

If we insert (4.10) and (A.8) into (4.8), we see that the correlation functions (4.9) have the form

$$G_{qq}(t) = \sum_{p=1}^{3} A_q^p \exp(-t/\tau_p) \quad , \qquad (4.11)$$

with $\tau_p$ given by

$$\tau_1 = (u-v)^{-1} \quad , \quad \tau_2 = (u+v)^{-1} \quad , \qquad (4.11a)$$

$$\tau_3 = (2w_{15} + w_{14})^{-1} p_0^{eq} = (2w_{51} + w_{41})^{-1} \, p_T^{eq} \; . \qquad (4.11b)$$

In (4.11a) the quantities u and v are combinations of the $w_{ij}$'s; their expressions

may be found in the Appendix. The coefficients $A_q^p$ are given by

$$A_q^p = \frac{\gamma_\mu^2 F_q}{4v} \{p_T^{eq} [v - (-1)^p (u - 3w_{12} - 2w_{15} - w_{14})] (B_{dip}^T)^2 +$$

$$+ p_O^{eq} [v - (-1)^p (u - 3w_{45} - 2w_{51} - w_{41})] (B_{dip}^O)^2 -$$

$$- (-1)^p [p_T^{eq} (w_{14} - w_{15}) + p_O^{eq} (w_{41} - w_{51})] 2B_{dip}^T B_{dip}^O \}$$

$$p=1,2; \quad q=x,y,z \tag{4.12a}$$

with the orientation factors

$$F_q = \frac{1}{2} \sum_{r=1}^{3} [3\beta_r^2 \alpha_{qr}^2 - \beta_r \alpha_{qr} \sum_{s=1}^{3} \beta_s \alpha_{qs}] , \qquad q=x,y,z \tag{4.12b}$$

and

$$A_{x,y}^3 = 0 \tag{4.12c}$$

$$A_z^3 = \gamma_\mu^2 p_T^{eq} p_O^{eq} (B_{FERMI}^T - B_{FERMI}^O)^2 \quad . \tag{4.12d}$$

Making use of $\beta_r = \alpha_{3r}$ and the orthonormality relationships between the $\alpha_{qr}$ we may simplify (4.12b) to

$$F_q = \frac{3}{2} \sum_{r=1}^{3} \alpha_{3r}^2 \alpha_{qr}^2 \quad , \qquad q=x,y \tag{4.13a}$$

$$F_z = \frac{1}{2} (3 \sum_{r=1}^{3} \alpha_{3r}^4 - 1) = \frac{1}{2} \sum_{r=1}^{3} \alpha_{3r}^2 (3\alpha_{3r}^2 - 1) \quad . \tag{4.13b}$$

From (4.13) we see that

$$F_x + F_y + F_z = 1 \tag{4.14a}$$

and, with (4.12a,c,d,), that

$$A_x^p + A_y^p + A_z^p = A^p \quad , \qquad p=1,2,3, \tag{4.14b}$$

where $A^p$ is independent of the orientation of $\underset{\sim}{\overline{\overline{B}}}_\mu$ (comp. 4.27).

We note further that for $\underset{\sim}{\bar{\bar{B}}}_\mu$ parallel to <100> we have $F_x = F_y = 0$, $F_z = 1$, and for $\underset{\sim}{\bar{\bar{B}}}_\mu$ parallel to <111> we have $F_x = F_y = 1/2$, $F_z = 0$.

## 4.3 Calculation of the relaxation functions

Insertion of (4.10) into (4.6), (4.4), and (4.5) gives us

$$\ln R_1(t) = -\Gamma_1 t + \sum_{p=1}^{2} (A_x^p + A_y^p) \frac{\tau_p^2}{(1+\omega_\mu^2 \tau_p^2)^2} \{ (1-\omega^2 \tau_p^2) [\exp(-t/\tau_p)\cos(\omega_\mu t) - 1]$$

$$- 2\omega_\mu \tau_p \exp(-t/\tau_p) \sin(\omega_\mu t)\} \qquad (4.15a)$$

with

$$\Gamma_1 = \sum_{p=1}^{2} (A_x^p + A_y^p) \frac{\tau_p}{(1+\omega_\mu^2 \tau_p^2)} \quad , \qquad (4.15b)$$

$$\ln R_2(t) = -\Gamma_2 t + \sum_{p=1}^{3} \{ A_z^p \tau_p^2 [\exp(-t/\tau_p) - 1] + A_x^p \frac{\tau_p^2}{(1+\omega_\mu^2 \tau_p^2)^2} (1-\omega^2 \tau_p^2) \cdot$$

$$\cdot [\exp(-t/\tau_p)\cos(\omega_\mu t) - 1] - 2\omega_\mu \tau_p \exp(-t/\tau_p) \sin(\omega_\mu t)\} \qquad (4.16a)$$

with

$$\Gamma_2 = \sum_{p=1}^{3} (A_z^p \tau_p + A_x^p \frac{\tau_p}{1+\omega_\mu^2 \tau_p^2}) \quad , \qquad (4.16b)$$

and

$$\Omega(t) = \Delta\omega t - \delta + \sum_{p=1}^{2} A_x^p \frac{\tau_p^2}{(1+\omega_\mu^2 \tau_p^2)^2} [(1-\omega_\mu^2 \tau_p^2)\sin(\omega_\mu t) + 2\omega_\mu \tau_p \cos(\omega_\mu t)] \cdot$$

$$\cdot \exp(-t/\tau_p) \qquad (4.17a)$$

with

$$\Delta\omega = \sum_{p=1}^{2} A_x^p \frac{\omega_\mu \tau_p^2}{1+\omega_\mu^2 \tau_p^2} \qquad (4.17b)$$

and

$$\delta = \sum_{p=1}^{2} A_x^p \frac{2\omega_\mu \tau_p^3}{(1+\omega_\mu^2 \tau_p^2)^2} \quad . \tag{4.17c}$$

The present approach gives reliable results only for $t>\tau_c$ (comp. § 4.1). We may thus neglect the terms containing $\exp(-t/\tau_p)$; they may be used to estimate the range of applicability of the final equations.

The final expressions for $t>\tau_p$ read

$$\ln R_1(t) = -\Gamma_1 t - \sum_{p=1}^{2} (A_x^p + A_y^p) \frac{(1-\omega_\mu^2\tau_p^2)\tau_p^2}{(1+\omega_\mu^2\tau_p^2)^2} \tag{4.18a}$$

$$\ln R_2(t) = -\Gamma_2 t - \sum_{p=1}^{3} \left[ A_z^p \tau_p^2 + A_x^p \frac{(1-\omega_\mu^2\tau_p^2)\tau_p^2}{(1+\omega_\mu^2\tau_p^2)^2} \right] \tag{4.18b}$$

$$\Omega(t) = \Delta\omega t - \delta = \sum_{p=1}^{2} A_x^p \frac{\omega_\mu \tau_p^2}{1+\omega_\mu^2\tau_p^2} \left[ t - \frac{2\,\tau_p}{1+\omega_\mu^2\tau_p^2} \right]. \tag{4.18c}$$

We see that the generalization of the Bloch-Wangsness-Redfield theoryto a finite upper limit in the t' integration gives the same time dependence as the 'classical' theory (in the present case characterized by time-independent relaxation rates $\Gamma_1$ and $\Gamma_2$) plus additional terms which simulate a 'fast' relaxation process and which become the more important the larger $t/\tau_p$, in accordance with our expectations. In addition there may be a change in the spin precession frequency and in the precession phase, but only if the correlation function $G_{xx}$ does not vanish identically.

## 4.4 Dependence on the crystallographic direction of $\underset{\sim}{\bar{\bar{B}}}_\mu$

Since $A_z^3$ is independent of the orientation of $\underset{\sim}{\bar{\bar{B}}}_\mu$ and $A_{x,y}^3 \equiv 0$, the entire orientation dependence may be expressed in terms of two functions only. For these we choose

$$F \equiv F_x + F_y = 1 - F_z \tag{4.19a}$$

which is independent of the direction of the muon polarization, and $F_x$, which depends on the directions of both $\bar{\bar{\underset{\sim}{B}}}_\mu$ and $\underset{\sim}{P}(0)$. If we denote the crystallographic direction of $\bar{\bar{\underset{\sim}{B}}}_\mu$ by a superscript, we have

$$\Gamma_1^{(\theta)} = F\ \Gamma_1^{<111>} \quad , \tag{4.20}$$

$$\Gamma_2^{(\theta)} = (1-F)\Gamma_2^{<100>} + F_x\ \Gamma_1^{<111>} + F\ A_z^3\ \tau_3 \quad , \tag{4.21}$$

$$\Delta\omega^{(\theta)} = 2\ F_x\ \Delta\omega^{<111>} \quad . \tag{4.22}$$

The orientation dependence (4.20-22) is characteristic for the tetragonal symmetry of the muon sites. Eq.(4.20) has been used by Yagi at al. (1981) to test this feature of the model on α-Fe. Eq. (4.22) may also be used for this purpose. In measurements on a given specimen, with the help of (4.21) we may investigate wether $\Gamma_2$ contains appreciable contributions from muon trapping (see § 1). If this is not the case we may determine the term $A_z^3\ \tau_3$ from the relationship

$$\Gamma_2^{<111>} = \frac{1}{2}\ \Gamma_1^{<111>} + A_z^3\ \tau_3 \quad , \tag{4.23}$$

to which (4.21) reduces in the special case of θ=<111>. As will be discussed in more detail in § 5.1, the term $A_z^3\hat{\tau}_3$ contains only muon jump frequencies pertaining to the exchange between sites with different Fermi fields. Its experimental determination is therefore particularly important for studying this aspect of the model.

With the information given at the end of §4.2 we obtain easily the longitudinal and transverse relaxation rates for $\bar{\bar{\underset{\sim}{B}}}_\mu$ parallel to <100> and <111> [for $\Gamma_2^{<111>}$ see (4.23)]:

$$\Gamma_1^{<100>} \equiv 0 \quad , \tag{4.24}$$

$$\Gamma_2^{<100>} = \sum_{p=1}^{3} A^p \tau_p \tag{4.25}$$

$$\Gamma_1^{<111>} = \frac{A^1\tau_1}{1+\omega_\mu^2\tau_1^2} + \frac{A^2\tau_2}{1+\omega_\mu^2\tau_2^2} \tag{4.26}$$

$$= \frac{A^1\tau_1+A^2\tau_2+\omega_\mu{}^2\tau_1\tau_2(A^1\tau_2+A^2\tau_1)}{1+\omega_\mu^2(\tau_1^2+\tau_2^2)+\omega_\mu^4\tau_1^2\tau_2^2}$$

with

$$A^p = \frac{\gamma_\mu^2}{4} \{ p_T^{eq}[v-(-1)^p(u-3w_{12}-2w_{15}-w_{14})](B_{dip}^T)^2 + \tag{4.27 a}$$

$$+ p_0^{eq}[v-(-1)^p(u-3w_{45}-2w_{51}-w_{41})](B_{dip}^0)^2 -$$

$$- (-1)^p[p_T^{eq}(w_{14}-w_{15})+p_0^{eq}(w_{41}-w_{51})]2B_{dip}^T B_{dip}^0, \; p=1,2 \; .$$

and

$$A^3 = A_z^3 \tag{4.27 b}$$

The preceding results exhibit indeed the features derived by physical arguments in §1. For $\omega_\mu\tau_p \ll 1$ the following relationship holds in addition to (4.23):

$$\Gamma_2^{<100>} = \Gamma_1^{<111>} + A_z^3\tau_3 + O(\omega_\mu\tau_c) \tag{4.28}$$

The comparison of the $\Gamma_1^{<111>}$ measurements of Yag al. (1981) with the $\Gamma_2^{<100>}$ data of Graf at al. (1980) indicate the existence of a finite contribution $A_z^3\tau_3$ between about 8 K and 35 K. This observation supports the interpretation of Yagi et al.(1981), according to which in this temperature interval $p_0^{eq}$ increases from very small values to 1/3.

## 5. Discussion

### 5.1 Critique of the model

Within the framework of the generalized Bloch-Wangsness-Redfield theory the present paper gives an exact solution of a well-defined and fairly elaborate model for the behaviour of positive muons and muon spins in ferromagnetic metals. We list here the principal assumptions of this model and discuss their merits and limitations.

(i) Positive muons injected into metals are thermalized in times extremely short compared with their lifetime and do not form muonium Mu = $(\mu^+e^-)$. The evidence on both items comes entirely from negative results. (a) So far it has not been possible to detect in metals any effects of non-thermalization of $\mu^+$. This is not surprising, since from theory and available evidence on positrons the thermalization time is expected to be of the order of magnitude of $10^{-12}$s or smaller, at least at temperatures not lower than liquid-helium temperatures. (b) In metals there is no evidence for a fast polarization process that might be due to Mu formation. Formation of $Mu^-=(\mu^+e^-e^-)$ cannot be excluded on the basis of the existing experiments but would leave the conclusions of the present paper unchanged.

(ii) The $\mu^+$ or $(Mu^-)$ are located in well-defined interstices of the host structures and are able to move between these by jumps characterized by (temperature-dependent) jump frequencies. This assumption excludes the possibility that muons are in so-called tunnelling states (analogous to the band-states familiar from the one-electron theory of crystals) and move by coherent tunnelling (i.e., with no change of the phonon occupation numbers other than those associated with the translational motion). The present theory covers both 'classical' motion (i.e., jumps of the diffusion particle over the potential barriers in the theory of "small-polaron" motion known as 'hopping' or phonon-assisted tunnelling (Holstein 1959,a,b, Flynn and Stoneham 1970, Kagan and Klinger 1974, Teichler and Seeger 1981.)

The theory of muon spin relaxation in α-iron associated with coherent tunnelling has been treated by Fuji (1979 ). Whether in α-iron coherent tunnelling has been seen experimentally is controversal. While Grynspan et al. (1979) and Graf et al. (1980) attribute (different) features of their measurements of the transverse spin relaxation rate in α-Fe to coherent tunnelling, on the basis of measurements of the longitudinal spin relaxation Yagi et al. (1981) maintain that down to liquid-helium temperatures there is no evidence for coherent $\mu^+$ tunnelling in this metal. It is one of the main purposes of the present paper to work out the theory of muon spin relaxation in α-Fe in such details that the hypothesis of $\mu^+$ diffusion by hopping can be critically tested.

(iii) The time of residence of the muons at the interstices is assumed to be so long compared with the time it takes them to carry out a jump that the only magnetic fields that have to be taken into account are those at the interstitial sites, if necessary suitably averaged to allow for the finite extension of the muon wavefunction at the interstices.

As long as the muons move by 'hopping', the preceding assumption is the better fulfilled the lower the temperature, since the time of residence increases with decreasing temperature. In α-Fe it may become doubtful as the Curie temperature is approached. However, at these temperatures the muon spin relaxation rate in perfect crystals (with which the present paper is concerned) will be so small that it cannot be detected with the available experimental techniques.

(iv) It is assumed that apart from the applied field the magnetic fields interacting with the muon magnetic moments are entirely of electronic origin.

In Fe, Ni and Gd the abundance of nuclides with non-vanishing spin is so small that this assumption is justified. By contrast $^{59}$Co, which possesses a fairly high nuclear magnetic moment, has an abundance of 100%. In Co the dipole—dipole interaction between nuclear magnetic moments and muon moments may indeed give the main contribution to the transverse relaxation rate at low temperatures. Since on account of the high hyperfine field at the nuclear sites the precession frequency of the nuclear spins

exceeds that of the muons, the nuclear contribution to the muon spin relaxation rate of ferromagnetic cobalt requires a special treatment which goes beyond the scope of this paper (Seeger 1978).

(v) That part of the magnetic field acting on the muon magnetic moments that depends on the type of interstices occupied by the muons is assumed to consist of two contributions, viz. the Fermi field $\underset{\sim}{B}_{FERMI}$ due to the hyperfine interaction with the spin-polarized conduction electrons, and the dipolar field $\underset{\sim}{B}_{dip}$ coming from the magnetic moments of the d- (or f-) electrons. Contributions from higher multipoles located at the atomic sites are neglected compared with the two contributions just mentioned, an assumption which is certainly well justified. It follows from magnetostatics that $\underset{\sim}{B}_{dip}=0$ at interstices of cubic symmetry (Lorentz 1909) and that at interstices of lower-than-cubic symmetry in cubic crystals $\overline{\underset{\sim}{B}}_{dip}=0$, where $\overline{\underset{\sim}{B}}_{dip}$ denotes the average over crystallographically equivalent sites (e.g., in bcc structures over the three possible orientations of the tetragonal axes of octahedral or tetrahedral interstices).

As already mentioned (§3), the usual assumption has been made that $\underset{\sim}{B}_{FERMI}$ is either parallel or antiparallel to the magnetization, i.e., that it does not show the phenomenon of crystal anisotropy. This has the consequence that in the case of hopping between interstices with different Fermi fields (e.g., octahedral and tetrahedral interstices) $\underset{\sim}{B}_{FERMI}$ will contribute to the transverse but not to the longitudinal relaxation. Under suitable conditions this assumption may be tested experimentally by comparing transverse and longitudinal relaxation rates at different crystallographic orientations of the magnetization.

$B_{FERMI}$ and $B_{dip}$ have to be treated as adjustable parameters. Estimates may be obtained in the case of $B_{FERMI}$ from electron theory (Katayama 1979, Kanamori 1981), in the case of $B_{dip}$ from magnetostatics with the help of the assumption that the presence of a muon changes $\underset{\sim}{B}_{dip}$ only little.

The model employed in the present paper is designed to be rather general and to cover a wide variety of physical situations. A number of simple predictions of the model have already been discussed qualitatively in §1. For a quantitative comparison with experiment and accurate determination of the parameters of the model explicit expressions for special cases of practical importance are required. The most important of these will be treated in § 5.2. § 5.3 will be devoted to specific problems connected with the measurement and the analysis of the muon spin precession frequency.

5.2 Special cases.

(i) Vanishing dipolar fields. If $\underset{\sim}{B}_{dip} \equiv 0$, the only non-vanishing $A_q^p$ is $A_z^3$. This means that the longitudinal relaxation rate is zero and that in the approximation (4.18b) the transverse relaxation function becomes

$$\ln R_2(t) = -A_z^3 \tau_3 (t + \tau_3) \quad , \tag{5.1}$$

where $A_z^3$ and $\tau_3$ are given by (4.12d) and A.10b). We see that a finite relaxation rate is possible only if neither $p_T^{eq}$ nor $p_0^{eq}$ is unity, i.e. if in thermal equilibrium the muons occupy more than one type of sites.

As already remarked in §1, the theory of muon spin relaxation developed in this paper includes as a special case fcc metals in which the muons occupy octahedral and/or tetrahedral interstices. Since in fcc structures both types of interstices have cubic point symmetry, the dipolar fields $\underset{\sim}{B}_{dip}$ are zero. In perfect fcc crystals muon spin relaxation can therefore only be obtained if jumps between O and T sites do occur and if the Fermi fields at the two sites are different. In bcc metals the term $A_z^3 \tau_3$ may be determined experimentally from a comparison of $\Gamma_1^{<111>}$ and $\Gamma_2^{<111>}$ according to (4.23) and analyzed in a manner similar to that described presently.

In the following we treat a simple model in which the diffusion of muons in fcc metals takes place between nearest-neighbour interstices in O-T-O-T-O sequences. The relationships between the equilibrium occupation

probabilities $p_O^{eq}$ and $p_T^{eq}$, the transition rates $w_{jk}$, the jump frequencies $\nu_{Ig}$, and the enthalpy difference $\Delta H$ between muons in O and T interstices derived in § 2 remain valid if we put all jump frequencies equal to zero with the exception of $\nu'_{OT}$ and $\nu'_{TO}$ and if we attribute these to jumps between adjacent interstices. The expression for the muon diffusion coefficient D in terms of these quantities changes, however. It is now given by

$$D = \frac{a_o^2}{8}\{2\, p_O^{eq}\, \nu'_{OT} + p_T^{eq}\, \nu'_{TO}\} = \frac{a_o^2}{4}\, \frac{\nu'_{OT}}{2\exp(\Delta H/kT) + 1} \quad , \tag{5.2}$$

where we have made use of (2.4) and (2.10b). We have written the right-hand side of (5.2) in a way that is convenient for the case $\Delta H < 0$ (octahedral sites energetically favoured over tetrahedral sites).

As will be discussed presently, in Ni the relaxation process that might be attributed to O-T-O jumps becomes strongly temperature dependent only above the Debye temperature. This suggests that we may write

$$\nu'_{OT} = \nu^o \exp\,[(\Delta H - H_{TO})/kT] \quad , \tag{5.3}$$

where we have assumed that $\Delta H < 0$ and where $H_{TO}$ is the effective barrier for jumps from T to O sites. The frequency $\nu^o$ denotes an effective pre-exponential factor that may be weakly temperature dependent (e.g., $\propto T^{-1/2}$). Insertion of (5.3) into (4.11b) and (5.1,2) gives us for the muon diffusion coefficient

$$D = \frac{a_o^2}{4}\nu^o \frac{\exp[(\Delta H - H_{TO})/kT]}{2\exp(\Delta H/kT) + 1} \quad . \tag{5.4}$$

and for the transverse relaxation function

$$\ln R_2(t) = -\frac{\gamma_\mu^2}{2\nu^o}\,(B^T_{FERMI} - B^O_{FERMI})^2\, \frac{\exp\left[(\Delta H + H_{TO}/kT\right]}{\left[2\exp\,(\Delta H/kT) + 1\right]^3}\,(t + \tau_3) \quad . \tag{5.5}$$

For $|\Delta H| \gg kT$ (low temperatures) Eqs.(5.4) and (5.5) reduce to

$$D = \frac{a_o^2}{4} \nu^o \exp\left[-(|\Delta H| + H_{TO})/kT\right] \tag{5.6}$$

and

$$\ln R_2(t) = -\frac{\gamma_\mu^2}{2\nu^o} (B^T_{FERMI} - B^O_{FERMI})^2 \exp\left[(\Delta H + H_{TO})/kT\right] (t + \tau_3), \tag{5.7}$$

for $|\Delta H| \ll kT$ (high temperatures) to

$$D = \frac{a_o^2}{12} \nu^o \exp\left[-(|\Delta H| + H_{TO})/kT\right] \tag{5.8}$$

and

$$\ln R_2(t) = -\frac{\gamma_\mu^2}{54\nu^o} (B^T_{FERMI} - B^O_{FERMI})^2 \exp\left[(\Delta H + H_{TO})/kT\right] (t+\tau_3). \tag{5.9}$$

It is remarkable that in both regimes the same laws hold for the temperature dependences, though with different pre-exponential factors.

Let us compare the preceding results with the experimental data on Ni (Denison et al. 1979). Up to about 350 K the transverse relaxation rate $\Gamma_2$ is approximately temperature independent and has a value of about $0.8 \cdot 10^6$s. At higher temperatures $\Gamma_2$ drops rapidly with increasing temperatures. The low-temperature value is usually attributed to imperfections, the drop at higher temperatures to motional narrowing (Denison et al. 1979). However, in pure Ni the low-temperature relaxation rate and the temperature interval of the drop appear to be fairly reproducible, so that an explanation in terms of intrinsic properties is more likely. In the following we shall investigate the question whether the relaxation rate of ferromagnetic Ni may be understood by assuming that at low temperatures $\mu^+$ occupy preferentially O sites*), whereas at high temperatures we have $p_O^{eq}=p_T^{eq}/2=1/3$.

*) It is easily verified that the opposite assumption cannot explain the available data.

In order to account for the approximate temperature independence of $\Gamma_2$ below 350 K, we have to assume that $(B^T_{FERMI} - B^0_{FERMI})^2 \exp[(\Delta H + H_{TO})/kT](\nu^o)^{-1}$ is virtually temperature independent. This is feasible if $\Delta H \simeq - H_{TO}$ and if the temperature dependences of the three factors just mentioned are such that they compensate each other approximately, at least over the temperature range over which (5.7) may be expected to hold. For the purpose of obtaining an order-of-magnitude estimate of $\Delta H$ we make the stronger assumption that each of the three factors is separately temperature independent. We obtain then for the temperature dependence of the relaxation time

$$\frac{0.81 \times 10^{-6}\ s^{-1}}{\Gamma_2(T)} = [2 \exp(\Delta H/kT) + 1]^3 \quad . \qquad (5.10)$$

If the $\Gamma_2$ values observed close to the Curie point are attributed to inhomogeneities and thus disregarded, (5.9) gives satisfactory fits to the data of Denison et al. (1979) for $-\Delta H$ of about 0.07 eV to 0.09 eV. Since the non-exponential factors in (5.5) and (5.7) are likely to have a positive temperature dependence, the lower value for $|\Delta H|$ might be more appropriate.

If we adopt $\Delta H = -0.07$ eV, $p^{eq}_T$ varies between 0.05 at 220 K and 0.35 at the Curie temperature of 631 K. The low-temperature contact field in Ni is $B_{FERMI} = -0.07$ T and should, according to present interpretation, be identified with $B^0_{FERMI}$. When normalized at low temperatures, $-B_{FERMI}$ deviates from $M_{sp}$ by about 10 % over the temperature range in which $\Gamma_2$ drops. This deviation presumably constitutes an upper limit for the admixture of $B^T_{FERMI}$ and suggests that at low temperatures $|B^0_{FERMI} - B^T_{FERMI}| \approx 10^{-2}$ T. If we assume further $\Delta H + H_{TO} = 0$, according to (5.7) the experimental low-temperature value of $\Gamma_2$ requires $\nu^o = 4.5 \cdot 10^7 s^{-1}$. This is a reasonable order of magnitude for phonon-assisted tunnelling (hopping) between adjacent sites. The hypothesis that the transverse muon spin relaxation in Ni is due

to hopping between octahedral and tetrahedral interstices with different Fermi fields is thus in reasonable agreement with the experimental facts.

The "Fermi-field" relaxation just discussed is an example of $\tilde{\underset{\sim}{B}}(t)$ parallel to $\bar{\bar{\underset{\sim}{B}}}_{\mu}$. As expected from the discussion in § 1, in such a case it is not possible to determine the field factor $(B^{O}_{FERMI} - B^{T}_{FERMI})^2$ and the muon jump frequency separately from measurements of $\Gamma_2$. However, as we have seen in §4, the relaxation rate is completely described by $\Gamma_2$ only if the correlation time $\tau_c = \tau_3$ is not too large. This condition will be violated at sufficiently low temperatures, and it should hence be possible to detect deviations from the exponential time dependence of the transverse relaxation function. If we extrapolate $\tau_3$ to low temperature by means of (5.3), we estimate that in Ni $\tau_3 \approx 10^{-6}$s (where detectable deviations are expected) should be reached at about 170 K.

(ii) $\bar{\bar{B}}_\mu$ lying in the (110) plane. This special case is particularly important for the comparison with experiments, since the (110) plane contains the three symmetry axes [001], [1$\bar{1}$1], and [1$\bar{1}$0]. If we denote the angle between $\bar{\bar{\underset{\sim}{B}}}_\mu$ and the [001] direction by $\theta$, we obtain

$$F(\theta) = \frac{3}{4}(\sin^2\theta + \frac{3}{4}\sin^2 2\theta). \qquad (5.11)$$

$F_x(\theta)$ depends on the direction of the initial muon polarization $\underset{\sim}{P}(0)$. If $\underset{\sim}{P}(0)$ is parallel to [110] we have

$$F_x(\theta) = \frac{3}{4}\sin^2\theta \qquad , \qquad (5.12)$$

if it lies in the (110) plane we have

$$F_x(\theta) = \frac{9}{16}\sin^2 2\theta \qquad . \qquad (5.13)$$

It is a consequence of the definition of F (Eq. 4.19) that (5.12) and (5.13) add to give (5.11). The functions (5.11 -13) are shown in Fig. 3.

(iii) Only one type of interstitial sites involved. If the temperature is lowered to values $T \ll |\Delta H|/k$, only one type of interstitial sites is occupied. Unless the exceptional situation discussed in Sect. 5.1 obtains, we may disregard all jump frequencies with the exception of $w_{12}$ in the case of $\Delta H > 0$ (T sites energetically favoured) or of $w_{45}$ in the case $\Delta H < 0$ (O sites energetically favoured). In the first case we have $u = v = 3\, w_{12}/2$, hence $\tau_1^{-1} = 0$, $\tau_2^{-1} = 3w_{12}$, $\tau_3^{-1} = 0$, in the second case $u = v = 3\, w_{45}/2$, hence $\tau_1^{-1} = 0$, $\tau_2^{-1} = 3\, w_{45}$, $\tau_3^{-1} = 0$.

If we denote by $\tau_c$ that one of the $\tau_p$ that remains finite, we obtain

$$\Gamma_2^{<100>} = \frac{1}{2}(\gamma_\mu B_{dip}^{\parallel})^2 \tau_c \tag{5.14}$$

$$\Gamma_1^{<111>} = 2\Gamma_2^{<111>} = \frac{1}{2}(\gamma_\mu B_{dip}^{\parallel})^2 \frac{\tau_c}{1+\omega_\mu^2\tau_c^2} \tag{5.15}$$

$$\Delta\omega^{<111>} = \frac{1}{2}(\gamma_\mu B_{dip}^{\parallel})^2 \; \omega_\mu\tau_c \; \frac{\tau_c}{1+\omega_\mu^2\tau_c^2} \tag{5.16}$$

Eqs. (5.14,15) agree with the results reported earlier (Seeger 1978). As we expect from the discussion in § 1, $\Gamma_2^{<111>}$ is proportional to the product $(B_{dip}^{\parallel})^2\tau_c$, so that the determination of $\tau_c$ from $\Gamma_2^{<111>}$ requires a knowledge of $B_{dip}^{\parallel}$. Considered as a function of $\tau_c$ (5.15) shows a maximum at $\omega_\mu\tau_c = 1$. The relaxation rate at this maximum is given by $\hat{\Gamma}_1^{<111>} = (\gamma_\mu B_{dip}^{\parallel})^2\tau_c/4$, so that with a knwowledge of $\omega_\mu$ we may determine $(B_{dip}^{\parallel})^2$ and $\tau_c$ separately. In the absence of muons we have $(B_{dip}^{O}/B_{dip}^{T})^2 = 12.74$. This suggests that in the presence of muons the ratio of $(B_{dip}^{O})^2$ to $(B_{dip}^{T})^2$ is large, too, and that from experimental determination of $(B_{dip}^{\parallel})^2$ at low temperatures we may find out wheter tetrahedral or octahedral interstices are preferentially occupied.

There is an alternative way of the determining $\omega_\mu\tau_c$ and $(B_{dip}^{\parallel})^2$ separately. Dividing (5.16) by (5.15) gives us

$$\Delta\omega^{<111>}/\Gamma_1^{<111>} = \omega_\mu\tau_c \tag{5.17}$$

Compared with the determination of $\omega_\mu\tau_c$ from (5.15) the determination from (5.17) has the attractive feature that it can also be used if $\omega_\mu\tau_c$ cannot be made comparable with or larger than

unity , e.g. because sufficiently large magnetic fields are not available. In such cases particularly accurate determinations of the muon spin precession frequency are required. A way of measuring $\Delta\omega^{<111>}$ with high precision will be indicated in § 5.3.

(iv) Small precession frequencies and high temperatures. By small precession frequencies we mean that $\omega_\mu \tau_p$ (p=1,2) may be neglected compared with unity. In the high-temperature case we may in addition put

$$p_T^{eq} = 2/3, \; p_O^{eq} = 1/3 \tag{5.18a}$$

and, on account of detailed balancing,

$$2w_{15}+w_{14} = w_{51}+w_{41}/2 \tag{5.18b}$$

or

$$\nu_{TO}+2\nu'_{TO} = \nu_{OT}+2\nu'_{OT} \tag{5.18c}$$

According to (4.21) and (4.28), for the calculation of the relaxation rates it suffices to consider $A_z^3\tau_3$ and

$$\Gamma_1^{<111>} = A^1\tau_1+A^2\tau_2 \quad . \tag{5.19}$$

From (4.27) and (A.10b) we obtain

$$\Gamma_1^{<111>} = \frac{\gamma_\mu^2}{2(u^2-v^2)} \Big\{ p_T^{eq}(B_{dip}^T)^2(3w_{45}+2w_{51}+w_{14})+p_O^{eq}(B_{dip}^O)^2(3w_{12}+2w_{15}+w_{14})+ 2B_{dip}^T\, B_{dip}^O[p_T^{eq}(w_{14}-w_{15})+p_O^{eq}(w_{15}-w_{51})]\Big\} \tag{5.20}$$

with $(u^2-v^2)$ being given by (A.12).

We see that not even in the high-temperature case (5.18) is there a simple relationship between relaxation rates and muon diffusion coefficient (2.13) unless we make assumptions on the

relative magnitudes of the jump frequencies. A simple but nevertheless physically interesting assumption is that all jump frequencies may be disregarded compared with $\nu_{OT}$ and $\nu_{TO}$, i.e., that the muon migration proceeds entirely by O-T-O sequences. This gives us

$$\Gamma_1^{<111>} = \frac{\gamma_\mu^2}{3\nu_{TO}p_T^{eq}} \left\{p_O^{eq}\, B_{dip}^O - p_T^{eq}\, B_{dip}^T\right\}^2 = \frac{\gamma_\mu^2}{18}\frac{a_o^2}{D}\left\{p_O^{eq}\, B_{dip}^O - p_T^{eq}\, B_{dip}^T\right\}^2 . \tag{5.21}$$

If for comparison with the cases of octahedral or tetrahedral occupancy we assume (5.18a) to be valid and $B_{dip}^O/B_{dip}^T = -3.569$ as in an ideal crystal (Seeger 1978), we may write (5.21) as

$$\Gamma_1^{<111>} = \alpha\frac{\gamma_\mu^2}{144}\frac{a_o^2}{D}(B_{dip}^T)^2 . \tag{5.22}$$

Then $\alpha = 1$ for tetrahedral occupancy, $\alpha = 25.4$ for octahedral occupancy and $\alpha = 30.9$ for the O-T-O jump mechanism leading to (5.21). The assumption on the order of magnitude of the factor $\alpha$ made in the interpretation of their $\Gamma_1^{<111>}$ measurements by Yagi et al. (1981) is thus confirmed by the above estimate.

Under the same assumption as above we obtain

$$A_z^3\tau_3 = \frac{\gamma_\mu^2}{12}\frac{a_o^2}{D}\left\{p_T^{eq}\, p_O^{eq}\,(B_{FERMI}^T - B_{Fermi}^O)\right\}^2 \tag{5.23}$$

or, with (5.18a),

$$A_z^3\tau_3 = \frac{\gamma_\mu^2}{243}\frac{a_o^2}{D}(B_{FERMI}^T - B_{FERMI}^O)^2 . \tag{5.24}$$

Since in $\alpha$-Fe $|B_{FERMI}^T - B^O{}_{FERMI}|$ does presumably not exceed $|B_{dip}^T|$ significantly, in the comparison of high-temperature values of $\Gamma_2^{<100>}$ and $\Gamma_1^{<111>}$ [comp. (4.28)] we may neglect the $A_z^3\tau_3$ term , again in agreement with the discussion of Yagi et. al (1981).

5.3 Accurate determination of the spin precession frequency. Accurate determinationsof the muon spin precession frequencies as well as of the transverse relaxation rate require that the spatial variation of $\bar{\bar{\underset{\sim}{B}}}_\mu$ in the sample is very small. This can always be achieved in two limiting cases, namely that of (a) a fully demagnetized sample in zero applied field, and (b) in magnetically saturated specimens, i.e., in large applied fields.

(a) We have $B_{appl} = 0$, $B_{demag} = 0$, hence

$$\bar{\bar{B}}_\mu(0) = B_{LORENTZ} + B_{FERMI} \quad . \tag{5.25}$$

In the demagnetized state $B_{LORENZ}$ is given by $M_{sp}/3$, where $M_{sp}$ is the spontaneous magnetization. In $\alpha$-Fe $B_{FERMI}$ is negative (Gurevich et al.1976); its modulus is smaller than $B_{LORENTZ}$. Hence the Fermi field is given by

$$B_{Fermi} = p_T^{eq} B_{FERMI}^T + p_O^{eq} B_{FERMI}^T = |\bar{\bar{B}}_\mu(0)| + B_{LORENTZ} \quad . \tag{5.19}$$

From sufficiently accurate measurements of the temperature dependence of $M_{sp}$ and of $\bar{\bar{B}}_\mu(0)$ in the demagnetized state one may therefore obtain information on the temperature dependence of $p_T^{eq}$ and $p_O^{eq}$ and thus on $\Delta H$ [comp. (2.3)]

(b) In a finite applied field a homogeneous magnetization can only be achieved in specimens of ellipsoidal shape. For simplicity we consider here specimens of spherical shape. If the applied field is large enough to achieve saturation, in such specimens the demagnetizing and the Lorentz field cancel each other, so that we have

$$\bar{\bar{B}}_\mu = B_{appl} + B_{FERMI} \tag{5.20}$$

As in case (a) one may deduce information on $p_T^{eq}$ and $p_0^{eq}$ from measurements of the temperature dependence of the precession frequency.

It follows from § 4 that the muon spin precession frequency is given by $\bar{\bar{B}}_\mu/\gamma$ if $\underset{\sim}{B}_{appl}$ is parallel to <100>, but that it differs from this value for any other direction of $\underset{\sim}{B}_{appl}$. The maximum deviation $3\Delta\omega^{<111>}/2$ occurs if $\underset{\sim}{\bar{\bar{B}}}_\mu$ lies in the $[1\bar{1}0]$ direction and if the initial muon polarization is parallel to the [001] direction.

Particularly accurate determinations of $\Delta\omega^{<111>}$, as required for the experimental determination of $\omega_\mu\tau_c$ discussed in § 5.2 (iii) or its generalization to more than one $\tau_p$, should be carried out at constant $\underset{\sim}{\bar{\bar{B}}}_\mu$ in order to eliminate any possible systematic errors in the interpretation of the measurements, e.g. due to a possible dependence of $B_{FERMI}$ on the direction of magnetization. This can be done as follows. Apply a sufficiently large external field in the $[1\bar{1}0]$ direction [$\theta=\pi/2$ in (5.12,13)] and rotate the crystal around this axis in such a way that the direction of the initial polarization $\underset{\sim}{P}(0)$ changes from the [001] to the [110] direction. According to (5.13) and (5.12) this is equivalent to going from $F_x=(9/16)\sin^2\pi = 0$ to $F_x = 3/4$, hence according to (4.22) $\Delta\omega$ varies from $\Delta\omega = 0$ to $\Delta\omega = 3\Delta\omega^{<111>}/2$. Since relative changes of the spin precession frequency can be measured very precisely and since near [001] and

[110] the precession frequency is insensitive against small uncertainties in the crystallographic direction of $\underset{\sim}{P}(0)$*, $\Delta\omega^{<111>}$ may be obtained with high occurrency.

## APPENDIX

### Solution of the Master Equation

The system of equation (2.6) may be written as

$$dp_j/dt = \sum_{k=1}^{6} w_{kj}\, p_k \quad , \qquad (j = 1,\ldots,6) \qquad (A.1)$$

where the non-diagonal elements of the 6x6 matrix $\underline{\underline{w}}$ are given by (2.7) and the diagonal elements by

$$\begin{aligned} w_{11} &= w_{22} = w_{33} = -(2w_{12}+2w_{15}+w_{14}) \\ w_{44} &= w_{55} = w_{66} = -(2w_{45}+2w_{51}+w_{41}) \quad . \end{aligned} \qquad (A.2)$$

Since (A.1) is a linear differential equation with constant coefficients, barring certain degeneracies its general solution may be written as a linear combination of exponential functions $\exp(-t/\tau_p)$ with decay times $\tau_p$ to be found by solving an eigenvalue problem. In the present case the solution of this problem is simplified considerably by the particular structure of $\underline{\underline{w}}$, which reflects the fact that we are dealing with transitions within and between two groups of sites with tetragonal symmetry.

* If $\Psi$ denotes the angle between $\underset{\sim}{P}(0)$ and [001], the angular variation of $\Delta\omega$ is given by $F_x(\Psi) = (3/4)\sin^2\Psi$.

Nowick (1970) has shown that the matrix transformation

$$\underline{\underline{p}}^* = \underline{\underline{\Omega}}\,\underline{\underline{p}} \tag{A.3}$$

transforms (A.1) into

$$d\underline{\underline{p}}^*/dt = \underline{\underline{w}}^*\underline{\underline{p}}^*(t) \quad , \tag{A.3a}$$

with

$$\underline{\underline{w}}^* = \underline{\underline{\Omega}}\,\underline{\underline{w}}\,\underline{\underline{\Omega}}^+ \quad , \qquad (\underline{\underline{\Omega}}\,\underline{\underline{\Omega}}^+ = 1) \tag{A.3b}$$

where $\underline{\underline{\Omega}}$ is the block matrix

$$\underline{\underline{\Omega}} = \begin{pmatrix} \underline{\underline{\Omega}}_T & 0 \\ 0 & \underline{\underline{\Omega}}_0 \end{pmatrix} \tag{A.4a}$$

with the 3 x 3 submatrices

$$\underline{\underline{\Omega}}_{T,0} = \begin{pmatrix} 3^{-1/2} & 3^{-1/2} & 3^{-1/2} \\ 2\cdot 6^{-1/2} & -6^{-1/2} & -6^{-1/2} \\ 0 & 2^{-1/2} & -2^{-1/2} \end{pmatrix} \tag{A.4b}$$

According to (A.3b) $\underline{\underline{w}}^*$ may now be written as a block matrix

$$\underline{\underline{w}}^* = \begin{pmatrix} \underline{\underline{w}}_3^* & 0 & 0 \\ 0 & \underline{\underline{w}}_1^* & 0 \\ 0 & 0 & \underline{\underline{w}}_1^* \end{pmatrix} \tag{A.5}$$

with the 2 x 2 submatrices

$$\underline{\underline{w}}_1^* = \begin{pmatrix} -(3w_{12}+2w_{15}+w_{14}) & w_{41}-w_{51} \\ w_{14}-w_{15} & -(3w_{45}+2w_{51}+w_{21}) \end{pmatrix} \tag{A.6a}$$

$$\underline{\underline{w}}_3^* = \begin{pmatrix} -(2w_{15}+w_{14}) & (2w_{51}+w_{41}) \\ (2w_{15}+w_{14}) & -(2w_{51}+w_{41}) \end{pmatrix} \tag{A.6b}$$

The eigenvalues of $\underline{\underline{w}}^*$ are those of the submatrices(A.6) and the solution

of (A.3a) becomes

$$p^*(t) = p^*(0)\exp(w^*t) \quad , \tag{A.7}$$

where $\exp(w^*t)$ is a matrix function containing the eigenvalues of $w^*$ and $p^*(0)$ is the matrix of the initial values following from (A.3) and the initial conditions for the $p_j$, viz. $p_j^i(0) = \delta_{ij}$.

Performing the inverse transformation of (A.3), $p(t) = \Omega^+ p^*(t)$, one obtains finally

$$\begin{aligned}
&p_1^1=p_2^2=p_3^3 = (\pi_1-2\pi_2)/3 \\
&p_2^1=p_3^1=p_1^2=p_3^2=p_1^3=p_2^3= (\pi_1+\pi_2)/3 \\
&p_4^1=p_5^2= p_6^3 = (\pi_3+2\pi_4)/3 \\
&p_5^1=p_6^1= p_4^2=p_6^2=p_4^3=p_5^3 = (\pi_3-\pi_4)/3 \\
&p_4^4=p_5^5=p_6^6 = (\tilde{\pi}_1-2\tilde{\pi}_2)/3 \\
&p_5^4=p_6^4=p_4^5=p_6^5=p_4^6=p_5^6= (\tilde{\pi}_1+\tilde{\pi}_2)/3 \\
&p_1^4=p_2^5=p_3^6 = (\tilde{\pi}_3+2\tilde{\pi}_4)/3 \\
&p_2^4=p_3^4=p_1^5=p_3^5=p_1^6=p_2^6 = (\tilde{\pi}_3-\tilde{\pi}_4)/3
\end{aligned} \tag{A.8}$$

The functions $\pi_s$ are given by

$$\pi_1 = \tau_3[(2w_{15}+w_{41}) + (2w_{15}+w_{14})\exp(-t/\tau_3)]$$

$$\pi_2 = \frac{\tau_1\tau_2}{\tau_1-\tau_2}\left\{(3w_{12}+2w_{15}+w_{14})[\exp(-t/\tau_1)-\exp(-t/\tau_2)] - [\frac{\exp(-t/\tau_1)}{\tau_2} - \frac{\exp(-t/\tau_2)}{\tau_1}]\right\}$$

$$\pi_3 = \tau_3(2w_{15}+w_{14})\ [1-\exp(-t/\tau_3)] \qquad (A.9)$$

$$\tilde{\pi}_4 = \frac{\tau_1\tau_2}{\tau_2-\tau_1}\ 2(w_{14}-w_{15})\ [\exp(-t/\tau_1)-\exp(-t/\tau_2)]$$

The $\tilde{\pi}_s$ are obtained from the $\pi_s$ by replacing $w_{ij}$ by $w_{ji}$, with the exception that $w_{12}$ is to be replaced by $w_{45}$. The decay times $\tau_p$

$$\tau_1^{-1} = u-v \quad , \quad \tau_2^{-1} = u+v \qquad (A.10a)$$

are the eigenvalues associated with (A.6a) and

$$\tau_3^{-1} = 2w_{15}+w_{14}+2w_{51}+w_{41} = (2w_{15}+w_{14})p_0^{eq} = (2w_{51}+w_{41})\ p_T^{eq} \qquad (A.10b)$$

is the nonvanishing eigenvalue associated with (A.6b).

In (A.10a) the abbrevations

$$2u = 3(w_{12}+w_{45})+2(w_{15}+w_{51})+(w_{14}+w_{41}) \quad , \qquad (A.11a)$$

$$4v^2 = [3(w_{12}-w_{45})+2(w_{15}+w_{51}) + (w_{14}-w_{41})]^2 + 4(w_{14}-w_{15})(w_{41}-w_{51}), \qquad (A.11b)$$

in (A.10b) detailed balancing (2.10d) have been used.

For use in the main text we record

$$u^2-v^2 = (3w_{12}+2w_{15}+w_{14})(3w_{45}+2w_{51}+w_{41})-(w_{15}-w_{14})(w_{51}-w_{41}). \qquad (A.12)$$

REFERENCES

Alefeld, G., and Völkl, J. (eds.), 1978a, Hydrogen in Metals I, Basic Properties, Springer, Berlin-Heidelberg-New York; 1978 b, Hydrogen in Metals II, Application-Oriented Properties, Springer, Berlin-Heidelberg-New York

Baryshevskiĭ, V.G., and Kuten', S.A., 1976, Sov. Phys.-Solid State 18, 1677

Bloembergen, N., Purcell, E.M., and Pound, R.V., 1948, Phys. Rev. 73, 679

Denison, A.B., Graf, H., Kündig, W.,and Meier, P.F., 1979, Helv. Phys. Acta 52, 460

Flynn, C.P., and Stoneham, A.M., 1970, Phys. Rev. B 1, 3966

Fujii, S., 1979, J. Phys. Soc. Japan 46, 1843

Graf, H., Balzer, G., Recknagel,E., Weidinger, A., and Grynszpan, R.I., 1980, Phys. Rev. Letters 44, 1333

Grynszpan, R.I., Nishida, N., Nagamine, K., Hayano, R. S., Yamazaki, T., Brewer, J.H., and Fleming, D.G., 1979, Solid State Comm. 29, 143

Gurevich, I.I., Klimov, A.I., Maĭorov, V.N., Meleshko, E.A., Nikolskiĭ, B.A., Selivanov, V.I., and Suetin, V.A., 1976, Soviet Phys. - JETP 42, 222

Holstein, T., 1959 a, Ann. Phys. (N.Y) 8, 325; 1959 b, Ann. Phys. (N.Y.) 8, 343

Kagan, Yu., and Klinger, M.J., 1974, J. Phys. C : Solid State Phys. 7, 2791

Kanamori, J., Yoshida, H.K., and Terakura, K. 1981, Hyperfine Interact. 8, 573

Katayama, H., Terakura, K., and J. Kanamori, 1979, Solid State Commun. 29, 431

Kronmüller, H., Hilzinger, H.R., Monachesi, P., and Seeger, A., 1979, Appl. Phys. 18, 183

Lorentz, H.A., 1909, The Theory of Electrons, B.G.Teubner, Leipzig

Nowick, A.S., 1970, Phys. Chem. Solids 31, 1819

Seeger, A., 1978, Hydrogen in Metals I (ed. by G. Alefeld and J. Völkl), p. 349,Springer, Berlin-Heidelberg-New York

Seeger, A., 1979, Proc. Fifth Intern. Conf. Positron Annihilation (ed. by R.R. Hasiguti and K. Fujiwara), p. 771, The Japan Institute of Metals, Sendai

Slichter, C.P., 1980, Principles of Magnetic Resonance, 2nd ed., Springer, Berlin-Heidelberg-New York

Shull, C.G., 1969, Magnetic and Inelastic Scattering of Neutrons by Metals (ed. by T.J. Rowland and P.A. Beck) p. 15, Gordon and Breach, New York

Stoneham, A.M., 1980, Exotic Atoms '79 (ed. by K. Crowe, J. Duclos, G. Fiorentini, and G. Torelli) p. 209, Plenum Press, New York

Teichler, H., 1980, Exotic Atoms '79 (ed. by K. Crowe, J. Duclos, G. Fiorentini, and G. Torelli) p. 283, Plenum Press, New York; 1981, Hyperfine Interact. 8, 505

Teichler, H., Seeger, A., 1981 , Phys. Letters 82A, 91

Wolf, D., 1979, Spin Temperature and Nuclear-Spin Relaxation in Matter, Clarendon Press, Oxford

Yagi, E., Bossy, H., Döring, K.-P., Gladisch, M., Herlach, D., Matsui, H., Orth, H., zu Putlitz, G., Seeger, A., and Vetter, J., 1981 , Hyperfine Interact. 8, 553

## FIGURE CAPTIONS

Fig. 1: Dipolar magnetic fields at tetrahedral interstices in a ferromagnetic bcc crystal. The cubic axes and the tetragonality axes of the interstices are numbered 1,2,3.

Fig. 1a (top): Magnetic dipole moments of the ions, $\underset{\sim}{\mu}_{ion}$, parallel to [100].

Fig. 1b (bottom): Magnetic dipole moments parallel to [111].

Fig. 2: Frequencies of jumps between tetrahedral and/or octahedral interstices in a bcc crystal. Regular lattice sites are represented by hatched circles, tetrahedral (T) interstices are numbered 1,2,3, octahedral interstices (O) 4,5,6. Examples of possible diffusion paths of interstitial positive muons are indicated by arrows together with the jump frequencies $\nu_{IJ}$.

Fig. 3: The functions $F_x(\theta) = (3/4)\sin^2\theta$, $F_y(\theta) = (9/16)\sin^2\theta$, and $F(\theta) = F_x(\theta)+F_y(\theta)$ characterizing the dependence of the relaxation rates and of the muon spin precession frequency on the angle between the magnetic field $B_\mu$ in a (110) plane and the [001] direction in the case of an initial polarization $\underset{\sim}{P}(0)$ parallel to [110].

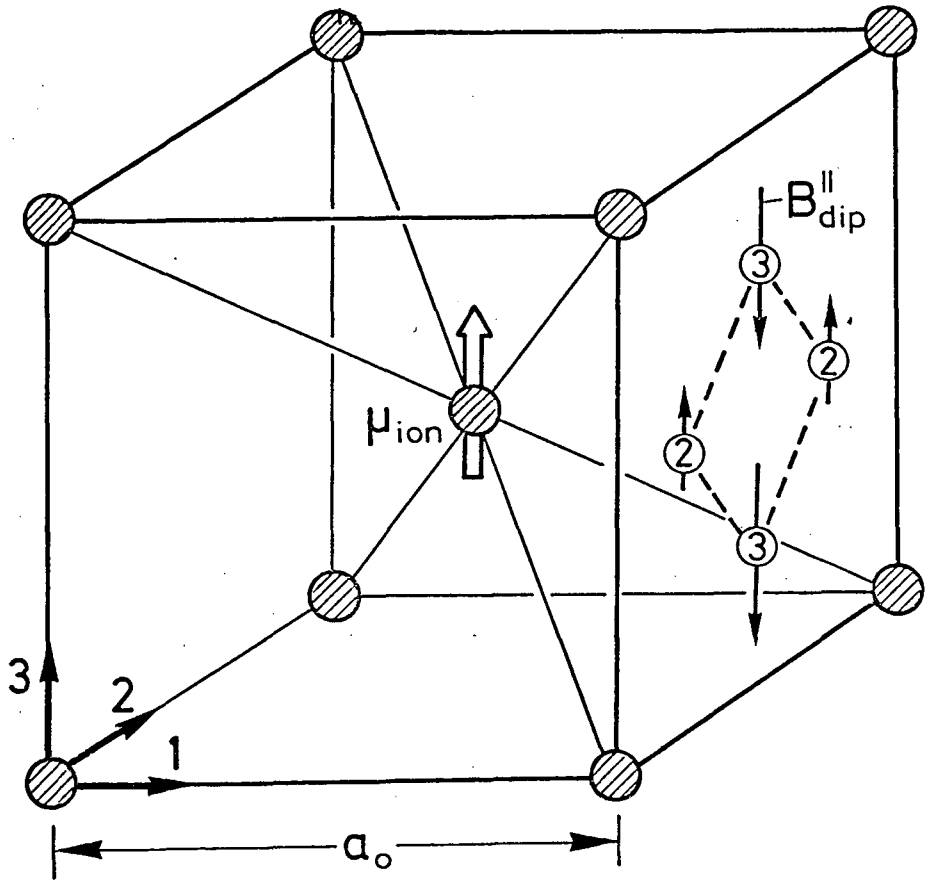


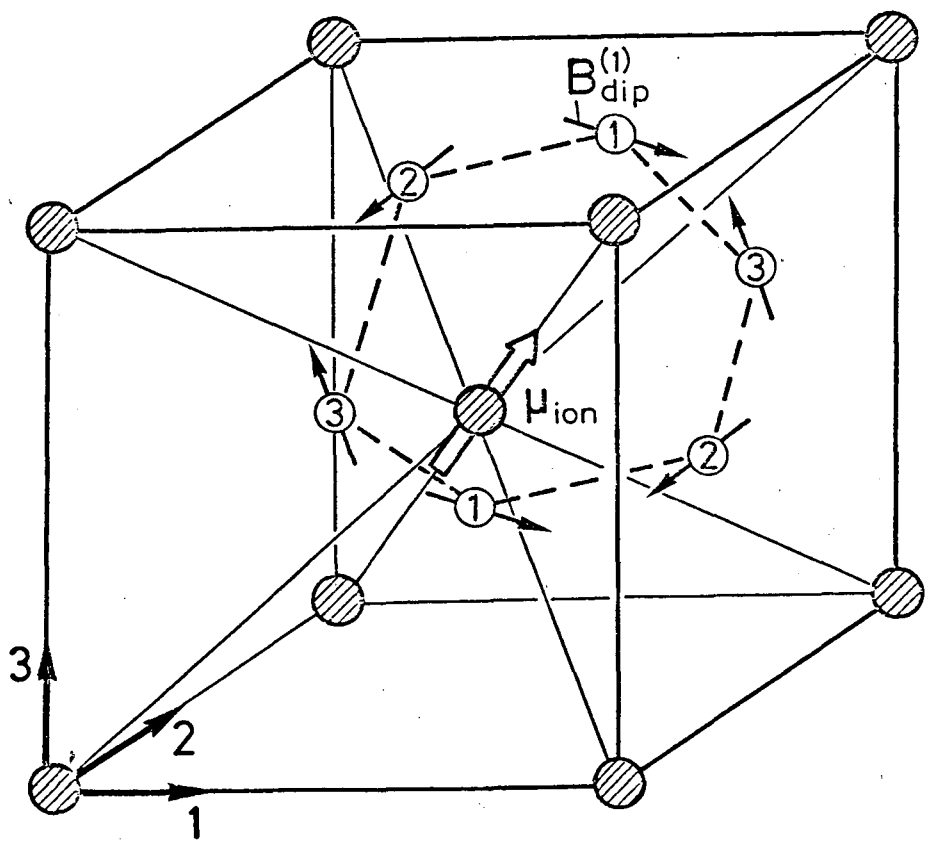


Fig. 1

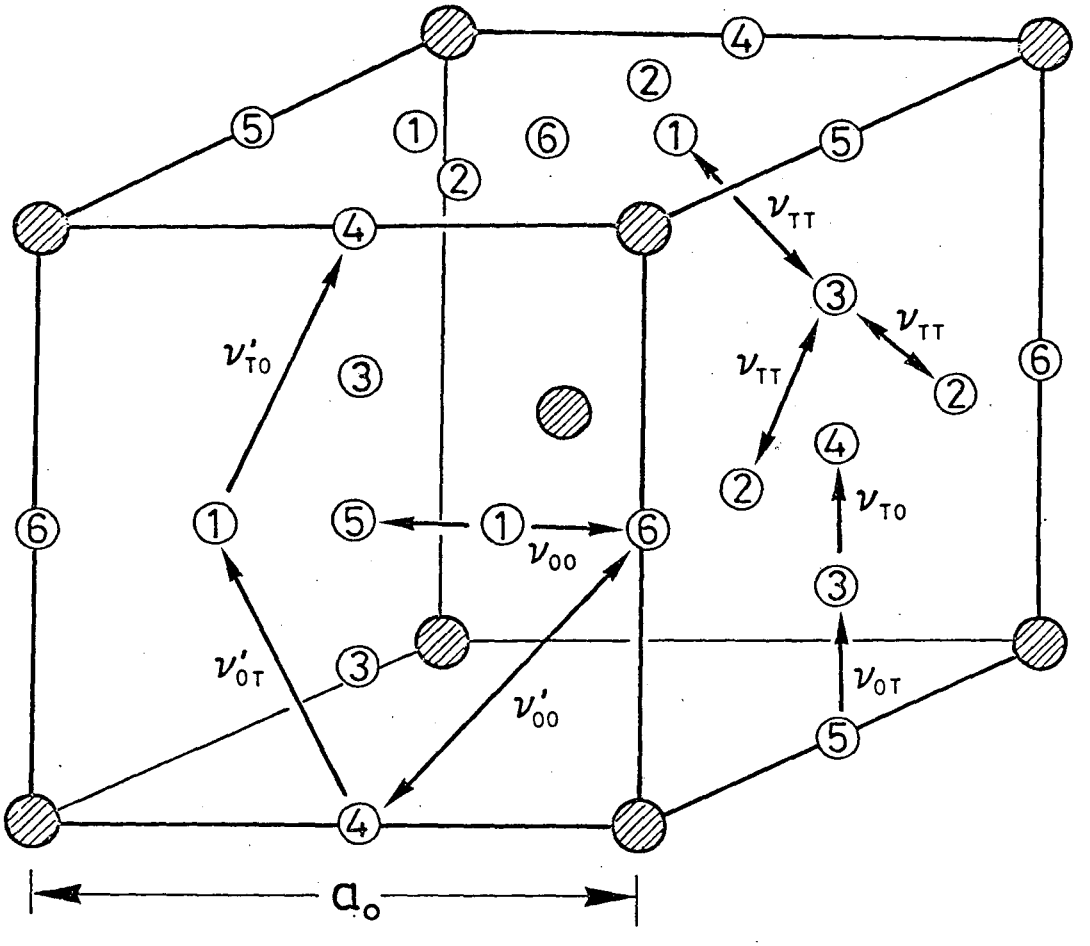


Fig. 2

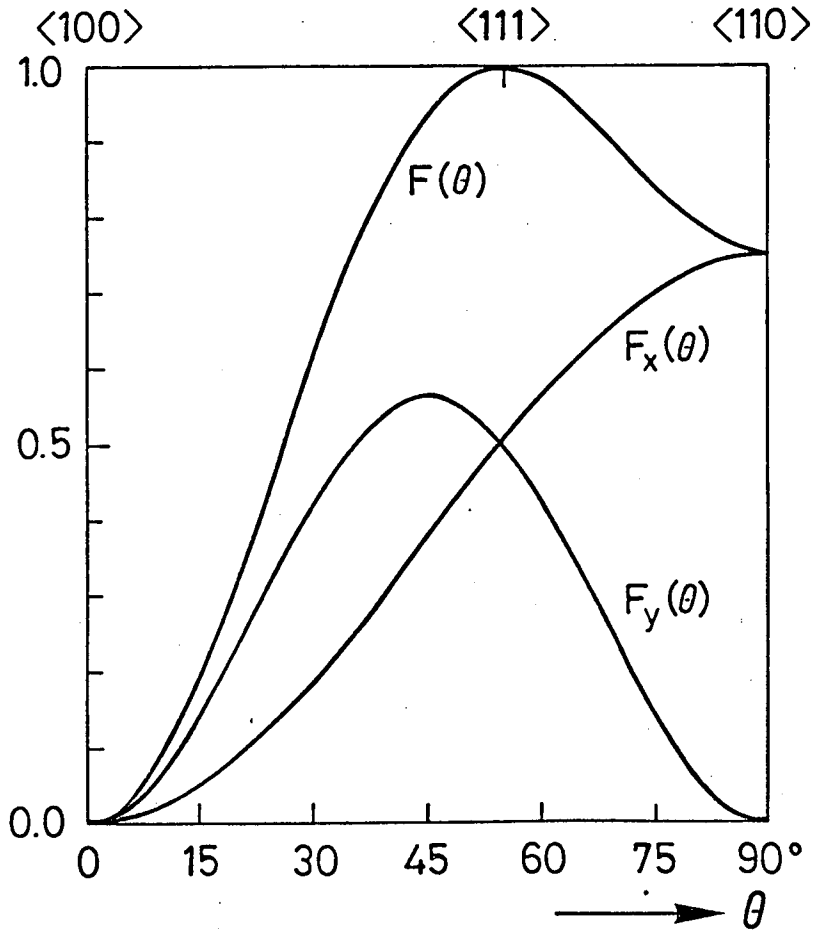


Fig. 3

# DIFFUSION AND TRAPPING OF POSITIVE MUONS IN NIOBIUM

C. Boekema, R. H. Heffner, R. L. Hutson, M. Leon, and M. E. Schillaci
Los Alamos National Laboratory, Los Alamos, NM 87545

W. J. Kossler and M. Numan
College of William and Mary, Williamsburg, VA 23185

S. A. Dodds
Rice University, Houston, TX 77001

## ABSTRACT

Using zero- and longitudinal-field μSR, the conventional interpretation of the "double-humped" behavior of the $\mu^+$-depolarization rate in Nb has been established unambiguously. Thus the $\mu^+$ mobility is shown to increase monotonically with temperature. The widths of the magnetic field distributions (due to the Nb nuclear moments) and the rates for finding or escaping from traps have been measured at several temperatures. In addition, equations are presented which govern the time-evolution of the $\mu^+$ polarization, when the muons are finding traps, escaping from traps, or both, for zero, longitudinal, and transverse external magnetic fields. A method for including the effect of more than one kind of trap acting at a particular temperature is given.

## I. INTRODUCTION

Transverse field μSR has been employed to measure the mobility of positive muons in a variety of materials. When the muon is stationary in a nonmagnetic metal, it is depolarized by the surrounding nuclear magnetic moments; when it is moving, the depolarization rate is reduced by motional narrowing.[1] Often it has been found that the depolarization rate is a complicated function of temperature, and that much of this structure is due to the effect of impurities and defects in the sample material which can trap muons in certain temperature ranges. An example of this behavior for impure Nb is shown schematically in Fig. 1.[2]

The conventional interpretation of the behavior shown in Fig. 1 is that the muon's motion is thermally activated, and that at point 1 all the muons are weakly bound to a high-concentration trap, at point 2 many are escaping these traps because of thermal agitation (hence motional narrowing), at point 3 the muons are finding a lower concentration but deeper trap, at point 4 all muons are bound to these deeper traps, and at point 5 the muons are being activated out of these deeper traps.

A drastically different interpretation has been offered for analogous behavior seen in Bi.[3] There it is suggested that muon mobility <u>increases</u> as the temperature decreases below point 4 [because of the onset of a coherent (quantum) diffusion mechanism], that the peak at point 4 is due to self-trapping in the host material, and that the peak at point 1 is due to the muons finding traps because of their greatly increased mobility.

While one cannot choose between these interpretations on the basis of transverse field measurements, Petzinger has pointed out that zero-field measurements can do so quite unambiguously.[4] This is because in zero-field a muon that is static at long times will have its polarization

recover to 1/3, while a moving muon will have a polarization approaching zero at long times. Thus the difference between finding traps and escaping from traps becomes readily measurable.

In the present paper we report on an experiment which uses zero- and longitudinal-field μSR to resolve this ambiguity for a Nb sample which exhibits the $\mu^+$ behavior shown in Fig. 1. The longitudinal field configuration, while giving results qualitatively similar to the zero field case, also provides both an additional check on the theory and the opportunity to extract more information about the trapping and escape rates.

The plan of this paper is as follows: in Sec. II we derive general expressions which give the polarization as a function of time for a trapping and/or detrapping muon, for longitudinal and transverse fields as well as for the zero-field case discussed by Petzinger. Then in Sec. III we discuss experimental details, and the methods of data analysis in Sec. IV. Our results are given and discussed in Section V. Section VI contains a brief summary.

## II. THEORY

### (a) Trapping

The effect of trapping on $\mu^+$ depolarization has already been calculated by Petzinger for zero external field.[4] Here we proceed more generally using what is, to us at least, a more physically transparent method.[cf., ref. 8] If the trapping rate is $\nu$, the probability of the muon surviving untrapped until time $t'$ and then trapping during the interval $dt'$ is $e^{-\nu t'} \nu dt'$. Assuming no release from traps, a trapped muon then contributes $\nu \int_0^t dt' \; e^{-\nu t'} P_1(t - t') P_0(t')$ to the polarization,

where $P_o(t)$ is the polarization function in the free state and $P_1(t)$ that in the trapped state. Then including the contribution of muons remaining free, we have for the polarization as a function of time (for transverse, longitudinal or zero external field)

$$P(t) = e^{-\nu t} P_o(t) + \nu \int_o^t dt' e^{-\nu t'} P_1(t-t') P_o(t'). \tag{1}$$

As long as the depolarization in the free state is slow compared to the trapping. we can substitute

$$P_o(t) = 1 \tag{2}$$

in Eq. 1 to give

$$P(t) = e^{-\nu t} + \nu \int_o^t dt' \, e^{-\nu t'} P_1(t-t'). \tag{3}$$

(The case of significant depolarization in the free state is considered in Sec. IId below.) Letting $\Delta$ be the Gaussian width of the local field distribution from the nuclear moments and $\omega$ the muon precession angular frequency in the external field, we have for the trapped state and transverse field such that $\frac{\Delta}{\omega} << 1$,

$$P_1(t) \simeq e^{-\Delta^2 t^2/2}, \qquad (H_\perp), \tag{4a}$$

while for longitudinal field[5]

$$P_1(t) = 1 - 2(\frac{\Delta}{\omega})^2 \left[1 - e^{-\Delta^2 t^2/2} \cos(\omega t)\right]$$

$$+ 2\frac{\Delta^4}{\omega^3} \int_o^t d\tau\, e^{-\Delta^2\tau^2/2} \sin(\omega\tau); \qquad (H_\parallel) \qquad (4b)$$

for zero field this reduces to the expression[5]

$$P_1(t) = \frac{1}{3} + \frac{2}{3}(1 - \Delta^2 t^2)e^{-\Delta^2 t^2/2}. \qquad (H=0) \qquad (4c)$$

Then for the transverse field polarization function we find

$$P(t) \cong e^{-\nu t}\{1 + \nu \int_o^t d\tau \exp(-\Delta^2\tau^2/2 + \nu\tau)\} \qquad (H_\perp, \text{ trapping}) \qquad (5a)$$

and for longitudinal field

$$P(t) = e^{-\nu t}\{1 + \nu \int_o^t d\tau \left\{e^{\nu\tau}\left(1-2(\frac{\Delta}{\omega})^2[1 - \exp(-\Delta^2\tau^2/2) \cos(\omega\tau)]\right)\right.$$

$$\left. + \frac{2}{\nu}\frac{\Delta^4}{\omega^3}(e^{\nu t} - e^{\nu\tau})\exp(-\Delta^2\tau^2/2) \sin(\omega t)]\right\}.(H_\parallel, \text{trapping})$$

For zero field ($\omega$=0), Eq. (5b) reduces to Petzinger's Eq. (9).[4]

For both zero and longitudinal field, it is interesting to look at the $t > 0$ <u>extrema</u> of $P(t)$. From Eq. 3, one finds

$$P(T) = P_1(T) \qquad (6)$$

where $\frac{d}{dt} P(T) = 0$.

where $P_o(t)$ is the polarization function in the free state and $P_1(t)$ that in the trapped state. Then including the contribution of muons remaining free, we have for the polarization as a function of time (for transverse, longitudinal or zero external field)

$$P(t) = e^{-\nu t} P_o(t) + \nu \int_o^t dt' e^{-\nu t'} P_1(t-t') P_o(t'). \tag{1}$$

As long as the depolarization in the free state is slow compared to the trapping. we can substitute

$$P_o(t) = 1 \tag{2}$$

in Eq. 1 to give

$$P(t) = e^{-\nu t} + \nu \int_o^t dt' \, e^{-\nu t'} P_1(t-t'). \tag{3}$$

(The case of significant depolarization in the free state is considered in Sec. IId below.) Letting $\Delta$ be the Gaussian width of the local field distribution from the nuclear moments and $\omega$ the muon precession angular frequency in the external field, we have for the trapped state and transverse field such that $\frac{\Delta}{\omega} << 1$,

$$P_1(t) \simeq e^{-\Delta^2 t^2/2}, \qquad (H_\perp), \tag{4a}$$

while for longitudinal field[5]

$$P_1(t) = 1 - 2(\frac{\Delta}{\omega})^2 \left[1 - e^{-\Delta^2 t^2/2} \cos(\omega t)\right]$$

$$+ 2\frac{\Delta^4}{\omega^3} \int_0^t d\tau\, e^{-\Delta^2\tau^2/2} \sin(\omega\tau); \qquad (H_\parallel) \qquad (4b)$$

for zero field this reduces to the expression[5]

$$P_1(t) = \frac{1}{3} + \frac{2}{3}(1 - \Delta^2 t^2)e^{-\Delta^2 t^2/2}. \qquad (H=0) \qquad (4c)$$

Then for the transverse field polarization function we find

$$P(t) \cong e^{-\nu t}\{1 + \nu \int_0^t d\tau \exp(-\Delta^2\tau^2/2 + \nu\tau)\} \qquad (H_\perp, \text{ trapping}) \qquad (5a)$$

and for longitudinal field

$$P(t) = e^{-\nu t}\{1 + \nu \int_0^t d\tau \,\{e^{\nu\tau}\left(1-2(\frac{\Delta}{\omega})^2\left[1 - \exp(-\Delta^2\tau^2/2) \cos(\omega\tau)\right]\right)$$

$$+ \frac{2}{\nu}\frac{\Delta^4}{\omega^3}(e^{\nu t} - e^{\nu\tau})\exp(-\Delta^2\tau^2/2) \sin(\omega t)]\}.(H_\parallel, \text{trapping})$$

For zero field ($\omega$=0), Eq. (5b) reduces to Petzinger's Eq. (9).[4]

For both zero and longitudinal field, it is interesting to look at the $t > 0$ <u>extrema</u> of $P(t)$. From Eq. 3, one finds

$$P(T) = P_1(T) \qquad (6)$$

where $\frac{d}{dt} P(T) = 0$.

This is the generalization (to include longitudinal field) of Petzinger's Eq. (10).[4]

(b) Escape from traps

If the muon is escaping from traps rather than finding them, we have the situation already described by Kubo and Toyabe,[6] and discussed at length in the μSR context by Hayano et al.[5] The polarization function now includes contributions from muons escaping from traps zero, one, ... times, so that the contribution from one or more escapes is given by $\varepsilon \int_0^t dt' \; P(t - t') \, e^{-\varepsilon t'} \, P_1(t')$, $\underline{\varepsilon}$ being the escape rate. Then including the "no-escape" term, we have an <u>integral equation</u> for P(t):

$$P(t) = e^{-\varepsilon t} P_1(t) + \varepsilon \int_0^t dt' \; P(t-t') e^{-\varepsilon t'} P_1(t'). \tag{7}$$

As before, Eqs. (4) are used for $P_1(t)$. An approximate solution for the transverse field case is given by the function[7,8]:

$$P(t) \simeq \exp\left[-\frac{\Delta^2}{\varepsilon^2}(e^{-\varepsilon t} - 1 + \varepsilon t)\right] \qquad (H_\perp, \text{escaping}) \tag{8}$$

(c) Trapping and escape

Equation (7) assumes that the trapping rate $\underline{\nu}$ is very much larger than either $\underline{\Delta}$ or $\underline{\varepsilon}$. If $\underline{\nu}$ is not so large, we must include the time intervals the $\mu^+$ spends in the free state [cf., ref. 8]. P(t) now includes no trapping. one trapping-no escape, one trapping-one escape,...terms, all starting from the free state; the integral equation including all these contributions is therefore

$$P(t) = e^{-\nu t}P_o(t) + \nu \int_o^t dt' \, e^{-\nu t' - \varepsilon(t-t')} \, P_1(t-t')P_o(t')$$

$$+ \varepsilon \int_o^t dt'' \cdot \nu \int_o^{t''} dt' \, e^{-\nu t' - \varepsilon(t''-t')} P(t-t'')P_1(t''-t')P_o(t'). \quad (9)$$

This equation reduces to Eq. (7) for $\nu \to \infty$, and to Eq. (1) for $\varepsilon \to 0$. Using Eq. (2), we have

$$P(t) = e^{-\nu t} + e^{-\varepsilon t} \, \nu \int_o^t dt' \, e^{-\bar{\nu} t'} P_1(t-t')$$

$$+ \varepsilon \int_o^t dt'' \, e^{-\varepsilon t''} \, P(t-t'') \cdot \nu \int_o^{t''} dt' \, e^{-\bar{\nu} t'} P_1(t''-t') \quad (10)$$

where $\bar{\nu} \equiv \nu - \varepsilon$.

Equation (10) can easily be solved numerically using the same methods as for Eq. (7). (E.g., using Laplace transforms as in [5,8], or directly by replacing the integrals by sums.)

(d) Several traps acting simultaneously: the hierarchy of integral equations

So far, we have considered only the action of a single type of trap in depolarizing the muon, but this might well be inadequate in general. For example, at temperature point (3) of Fig. 1 the muon is finding the high temperature traps (according to the conventional interpretation), but its "free state" polarization function $P_o(t)$ reflects its escape from the more common low temperature traps, and replacing $P_o(t)$ by unity (Eq. 2) may not always be an adequate approximation. Happily, the situation can be modeled in a manner which is both physically clear and computationally convenient: One first solves the integral equation expressing the effect of the low

temperature traps only; the solution is then inserted, as $P_o(t)$, in the integral equation for the high temperature trap. In this way we can generate a hierarchy of integral equations to express the effect of any number of traps, and of motion in the perfect lattice, to any desired degree of accuracy.

In all of the above except Sec. IIb, we have assumed a small enough trap concentration to allow the neglect of any muons starting out in traps.

## III. EXPERIMENTAL DETAILS

The experiment was carried out at the Stopped Muon Channel of the Clinton P. Anderson Meson Physics Facility (LAMPF) using a highly polarized ($\gtrsim$ 90%) muon beam of incident momentum 80 MeV/c. Using the standard time-differential μSR technique[1], time histograms were collected for each of two counter telescopes located upstream and downstream of the sample as shown schematically in Fig. 2. The inner counters of the electron telescopes were located inside the vacuum jacket of the dewar; this ensures that muons stopping in the jacket do not contribute to the μSR signal. The target was cooled in an Air Products Helitran refrigerator using a cold-finger sample mount; its temperature was monitored using a standard carbon-glass resistance thermometer and was controlled to within ± 0.1 K for the measurements reported here. The external magnetic field, if present, was oriented either parallel or perpendicular to the $\mu^+$ beam (and polarization) direction.

The Nb sample, one of seven slabs spark-cut from a parent crystal, was previously studied at SIN[9] and at LAMPF[10] (and is referred to as Nb-2 in these references). It is a single crystal approximately 2.5 cm in diameter by 1 cm thick, and was prepared by H. K. Birnbaum as described

earlier[10]. Mass spectrograph analysis revealed the dominant substitutional impurity to be 200 ppm at. Ta; other heavy substitutional metals were found to be present in concentrations less than 1 ppm at. Neutron activation studies on other crystals from the same parent showed interstitial impurity concentrations of C (100 ppm at.), N (44 ppm at.), and O (40 ppm at.). Resistivity measurements implied smaller C and O concentrations, however, indicating the possible existence of highly stable Nb-C-O complexes which may have precipitated along grain boundaries. No hydrogen was found at the detection limit of 50 ppm at.[12]

## IV. DATA ANALYSIS

### (a) Zero and Longitudinal Field

Here we indicate how the 11 K zero-field data are used to extract the experimental polarization data for all of the runs. At 11 K (corresponding to point (1) of Fig. 1), the muon is supposed to be stationary, so that

$$P(t) \simeq P_1(t) \tag{11}$$

(as follows from Eq. (1) with $\nu$ very large or from Eq. (7) with $\varepsilon=0$). Then for zero field, the simple expression given by Eq. (4c) can be used to determine (in addition to $\Delta$) the background, asymmetry and normalization parameters, by fitting the front and back histograms simultaneously using for the number of counts in each time bin

$$n_1(t) = n_1^{o}\left[\exp(-t/\tau_\mu)(1 + a_1P(t)) + b_1\right] \tag{12a}$$

and

$$n_2(t) = n_2^o \left[\exp(-t/\tau_\mu)(1 - a_2P(t)) + b_2\right], \tag{12b}$$

respectively, in a $\chi^2$ - minimization algorithm. The data and fit for P(t) are shown in Fig. 3a. The fact that P(t) has vanishing slope at t = 0 and is nonmonotonic results in the six parameters ($n_i^o$, $a_i$, $b_i$) being very well-determined in this way. These parameters are then used for each of the following runs (including another 11 K run at the end) to form the experimental polarization function $P_{ex}(t)$:

$$P_{ex}(t) = \frac{F(t) - \alpha B(t)}{a_2F(t) + \alpha a_1B(t)}. \tag{13}$$

Here $\alpha \equiv n_1^o/n_2^o$ and $F(t) \equiv N_1(t) - N_1^o b_1$, $B(t) \equiv N_2(t) - N_2^o b_2$, and $N_1^o$ and $N_2^o$ are estimated from the early channels for each run. The $P_{ex}(t)$ data for the final 11 K run did indeed closely reproduce the initial 11 K data, demonstrating that the six parameters needed to extract $P_{ex}(t)$ were stable from run to run.

Solutions to Eq. 7 for detrapping and Eq. (5b) for trapping were fitted to the $P_{ex}(t)$, both at zero and 15 gauss fields, giving the parameters $\Delta$ and $\varepsilon$ or $\nu$.

(b) Transverse Field

The transverse field data were fitted to

$$N(t) = N^o\{\exp(-t/\tau_\mu)\ [1 + a\ P(t)\ \cos(\omega t + \phi)] + b\} \tag{14}$$

for each histogram. For P(t) Eq. (4a) was used for the stationary muon temperature (11 K), solutions to Eq. (5a) for the trapping (24.3 and 46 K) points, and Eq. (8) for the detrapping temperatures (18.5 K and 77.3 K).

## V. RESULTS

Our results for $P_{ex}(t)$ for zero-field are shown in Fig. 3, while those for 15 Oe longitudinal field are shown in Fig. 4. These plots immediately resolve the trapping-detrapping ambiguities. That is, the 11 K results (Figs. 3a, 4a, corresponding to point 1 of Fig. 1) are completely consistent with a stationary (trapped) $\mu^+$; the 18.5 K plots (Figs. 3b, 4b, point 2), with no sign of a recovery of polarization at long times, indicate de-trapping; the 24.3 K results (Figs. 3c, 4c, point 3) show clearly the recovery of polarization at long time which demonstrates that the $\mu^+$ is finding traps; the 46 K result (Fig. 3d, point 4) is consistent with either trapping or stationary muons; finally, the 77.3 K plots (Figs. 3e, 4e, point 5) indicate release from traps.

The solid curves in Figs. 3 and 4 are fits to the data using the appropriate model. Thus for 11 K (Figs. 3a, 4a), the curves represent Eqs. (4c) and (4b), respectively; for 18.5 K and 77.3 K (Figs. 3b, 3e, 4b and 4e) solutions to Eq. 7 with Eq. 4c or 4b; 24.3 K and 46 K (Figs. 3c, 3d, and 4c) solutions to Eq. (5b). The transverse field data (not shown) were also fitted with the appropriate functions (as discussed following Eq. (14)). The parameters obtained from these fits are displayed in Table I.

The errors shown in Table I are purely statistical. The agreement among the parameters from the H=0, $H_{\parallel}$ and $H_{\perp}$ measurements is generally good; however, the amount of scatter of the values, especially for the trapping or escape rates, indicates the probable presence of systematic errors in addition to the statistical ones.

The $\Delta$ values for the 11 K and 18.5 K measurements can be combined to give a value characterizing the low temperature (LT) trap: $\Delta(LT) = .495 \pm .002\ \mu s^{-1}$. Similarly, combining the 24.3 K, 46 K and 77.3 K values gives

the high temperature (HT) trap parameters: $\Delta(HT) = .491 \pm .003\ \mu s^{-1}$. It is interesting to note that if the time needed for the muon to find the HT trap at 46 K is ignored (in effect, taking $\nu = \infty$), a significantly smaller $\Delta$ value emerges from the (zero-field, 46 K) data: $\Delta(HT, \nu=\infty) = 0.430 \pm .033\ \mu s^{-1}$. However, we see that when the finite trapping rate is included, $\Delta(LT) \approx \Delta(HT)$.

The values of $\Delta$ found here can be compared to those reported earlier [9]; this is done in Table II.

We have already made use of the fact that the same $\Delta$ values emerge from the transverse- and zero- and longitudinal-field data. It should be pointed out that if the nuclear moments were free to precess around the external field, then, because the precession is rapid, the effective $\Delta$ is reduced and we would expect

$$\Delta_\perp = \sqrt{\frac{2}{5}}\,\Delta_o. \tag{15}$$

The equality of $\Delta$'s evident in Table I arises because the interaction of the quadrupole moments of the niobium nuclei with the electric field gradients produced by the muon is much stronger than their Zeeman interaction for $H \ll 1$ kG.[13] Thus the niobium nuclei precess rapidly around the radial electric field gradient directions, so that, in a polycrystalline sample, the same time average of the nuclear magnetic moments is seen in the different field orientations. In fact, the niobium target used is a single crystal, but the anisotropy is known to be quite small in the low-field region,[11] so that $\Delta_\perp \approx \Delta_o$. The relation $\Delta_o = \Delta_\parallel$ should hold independent of this approximate isotropy. The numbers in Table I show that both relations hold for our data.

## VI. SUMMARY

By using zero- and longitudinal-field μSR, we have established unambiguously that the conventional interpretation of the "double-humped" behavior of the $\mu^+$ depolarization rate in Nb, Fig. 1, is correct, and hence that the $\mu^+$ mobility increases monotonically with increasing temperature. We have measured the widths of the distribution of fields, Δ, seen by the muons at several temperatures, as well as the rates for finding or escaping from traps, for all three field configurations.

In the present work we have not attempted to identify the trap sites, but have concentrated on verifying the conventional interpretation of trapping and detrapping and the monotonic increase of muon mobility with temperature. In fact, experiments on Nb targets with most of the substitutional Ta removed (3 ppm instead of the 200 ppm in the target of this experiment)[10] do not show the two-hump behavior of Fig. 1, so these traps may be associated with the Ta impurity atoms.

Finally, we have derived equations governing the evolution of the $\mu^+$ polarization, for transverse-, longitudinal-, and zero-fields, when the muon is finding traps, escaping from traps, or both, and have shown how the effect of more than one kind of trap acting simultaneously can be handled.

ACKNOWLEDGMENTS

We thank H. K. Birnbaum for the loan of the sample. One of us (ML) is indebted to P. F. Meier for suggesting that direct solution of the integral equations of Sec. II might be easier than using Laplace transforms. This research was supported in part by the U.S. DOE and in part by the NSF under grant DMR 800 7059.

REFERENCES

1. See, e.g., A. Schenck, in Nuclear and Particle Physics at Intermediate Energies, ed. J. B. Warren (Plenum, 1976) for a review of this technique.

2. H. K. Birnbaum et al., Phys. Rev. B17 (1978) 4143; M. Borghini et al., Phys. Rev. Lett. 40 (1978) 1723; O. Hartmann, Hyperf. Int. 6 (1979) 203; K. G. Petzinger et al., ibid., 223.

3. V. G. Grebinnik et al., JETP Lett. 25 (1977) 298.

4. K. G. Petzinger, Phys. Lett. 75A (1980) 225.

5. R. S. Hayano et al., Phys. Rev. B20 (1979) 850.

6. R. Kubo and T. Toyabe, Colloque Ampére XIV (1967) 810.

7. A. Abragam, Principles of Nuclear Magnetism (Clarendon Press, Oxford, 1970).

8. K. W. Kehr et al., Hyperf. Int. 6 (1979) 219;
   -, Z. Phys. B39 (1978) 49.

9. H. K. Birnbaum et al., Phys. Rev. B17 (1978) 4143.

10. J. A. Brown et al., Hyperf. Int. 6 (1979) 233.

11. H. Schilling et al., Hyperf. Int. 8 (1981) 675.

12. H. K. Birnbaum, private communication.

13. O. Hartmann et al., Phys. Rev. Lett. 39 (1977) 832.

TABLE I. FITTED PARAMETERS

| Region | T(K) | H(g) | Type of Fit | $\Delta$ ($\mu s^{-1}$) | $\nu$ ($\mu s^{-1}$) | $\varepsilon$ ($\mu s^{-1}$) |
|---|---|---|---|---|---|---|
| 1 | 11.0 | 0 | static | .504 ± .003 | | |
| | | 15∥ | | .495 ± .006 | | |
| | | 100⊥ | | .493 ± .010 | | |
| 2 | 18.5 | 0 | detrapping | .486 ± .003 | | .647 ± .016 |
| | | 15∥ | | .477 ± .005 | | .499 ± .034 |
| | | 100⊥ | | .493 ± .016 | | .607 ± .085 |
| 1 & 2 combined | | | | .495 ± .002 | | |
| 3 | 24.3 | 0 | trapping | .490 ± .006 | 1.743 ± .069 | |
| | | 15∥ | | .453 ± .006 | 2.23 ± .21 | |
| | | 100⊥ | | .490 ± .022 | 1.10 ± .15 | |
| 4 | 46.0 | 0 | trapping | .504 ± .005 | 3.26 ± .08 | |
| | | 100⊥ | | .499 ± .015 | 3.29 ± .13 | |
| 5 | 77.3 | 0 | detrapping | .473 ± .003 | | .925 ± .014 |
| | | 15∥ | | .484 ± .005 | | 1.12 ± .12 |
| | | 100⊥ | | .529 ± .008 | | 1.11 ± .05 |
| 3 + 4 + 5 combined | | | | .491 ± .003 | | |

TABLE II. COMPARISON WITH EARLIER WORK

| | $\Delta$ (LT) ($\mu s^{-1}$) | $\Delta$ (HT,$\nu=\infty$) ($\mu s^{-1}$) |
|---|---|---|
| This work | .495 ± .002 | .433 ± .033 |
| *Reference 9 | .454 ± .011 | .366 ± .013 |

---

*The values from [9] have been multiplied by $\sqrt{2}$ to conform with the convention of the present paper (cf. Eq. (4a)).

## FIGURE CAPTIONS

Figure 1 Schematic plot of the temperature dependence of the transverse-field depolarization rate $\Lambda$ obtained in a niobium sample containing impurities.

Figure 2 Diagram of the $\mu$SR spectrometer employed in this experiment.

Figure 3 Zero-field polarization functions for the temperature points of Fig. 1.

Figure 4 Longitudinal-field polarization functions.

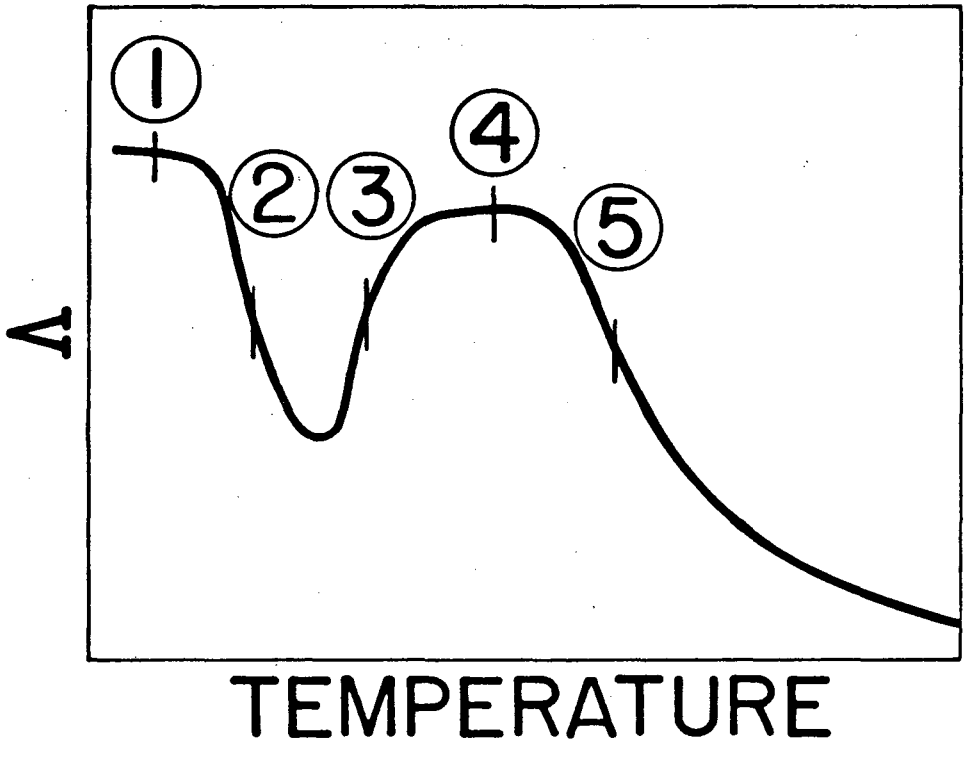


Fig. 1

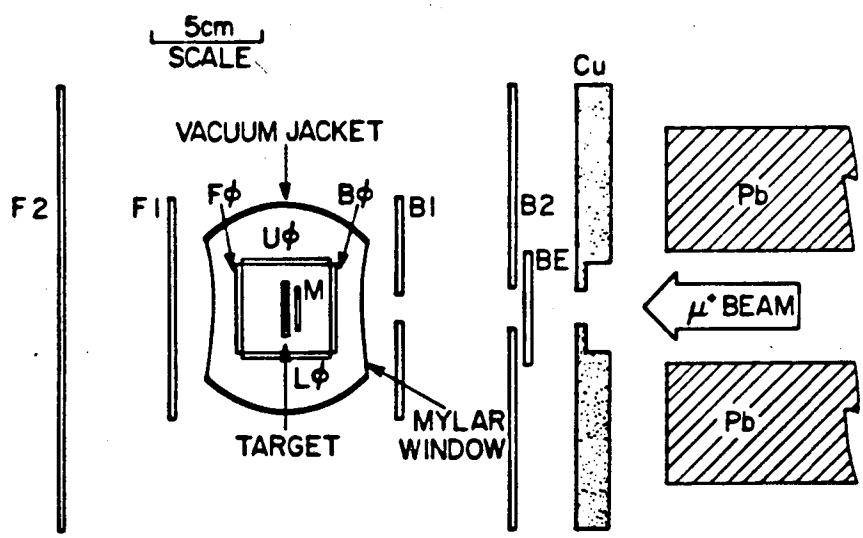


EVENT DEFINITIONS: - MUON STOP IN TARGET = $BE \cdot M \cdot \overline{F\phi} \cdot \overline{U\phi} \cdot \overline{L\phi}$

- DECAY POSITRON (FORWARD) = $F\phi \cdot F1 \cdot F2 \cdot \overline{U\phi} \cdot \overline{L\phi} \cdot \overline{B\phi} \cdot \overline{BE}$
- DECAY POSITRON (BACKWARD) = $B\phi \cdot B1 \cdot B2 \cdot \overline{U\phi} \cdot \overline{L\phi} \cdot \overline{F\phi} \cdot \overline{BE}$

Fig. 2

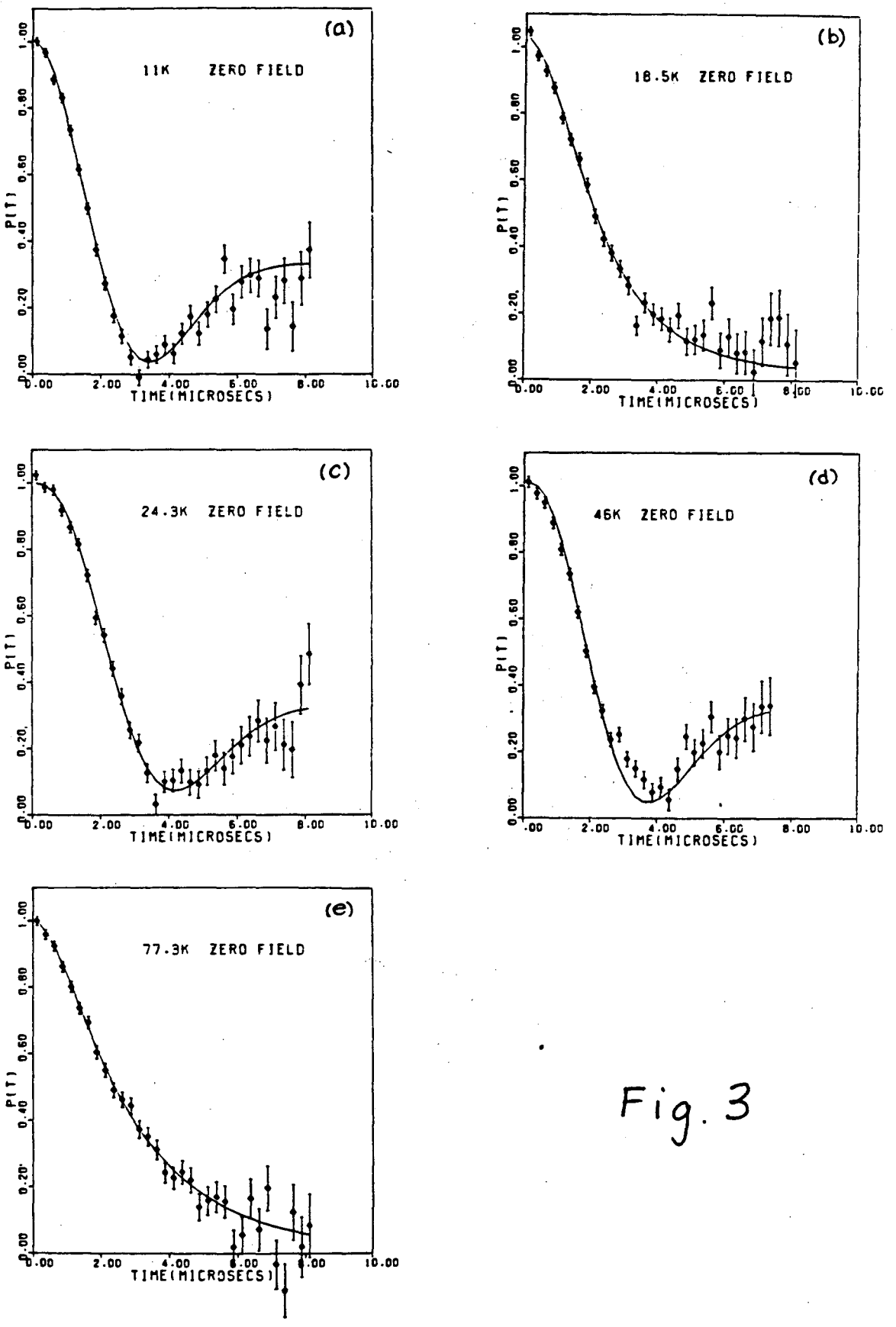
(a)
11K ZERO FIELD
(b)
18.5K ZERO FIELD
(c)
24.3K ZERO FIELD
(d)
46K ZERO FIELD
(e)
77.3K ZERO FIELD
P(T)
TIME(MICROSECS)
0.00
0.20
0.40
0.60
0.80
1.00
2.00
4.00
6.00
8.00
10.00

Fig. 3

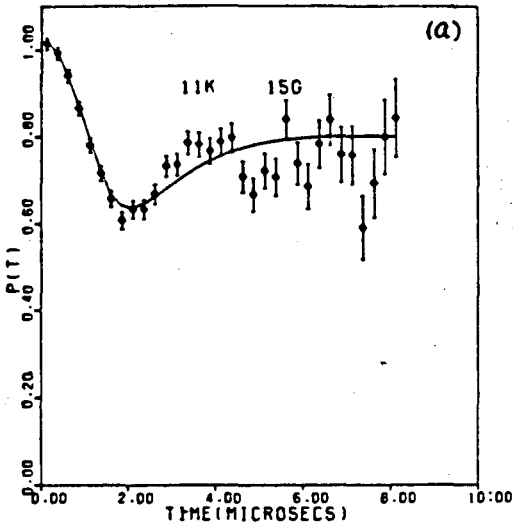
(a)
11K 15G
P(T)
TIME(MICROSECS)

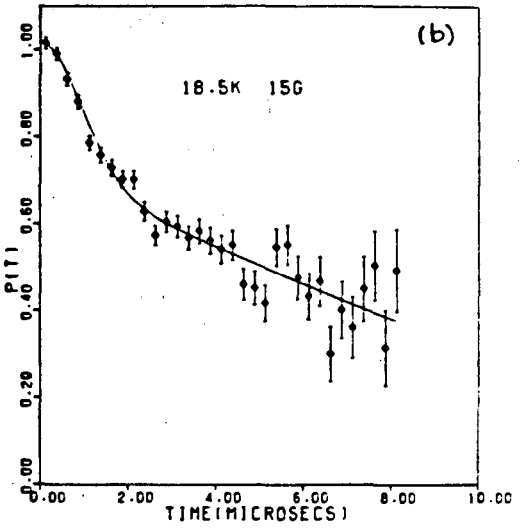
(b)
18.5K 15G
P(T)
TIME(MICROSECS)

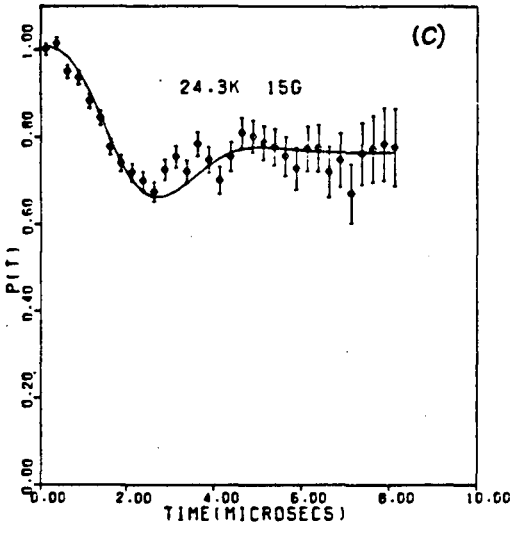
(c)
24.3K 15G
P(T)
TIME(MICROSECS)

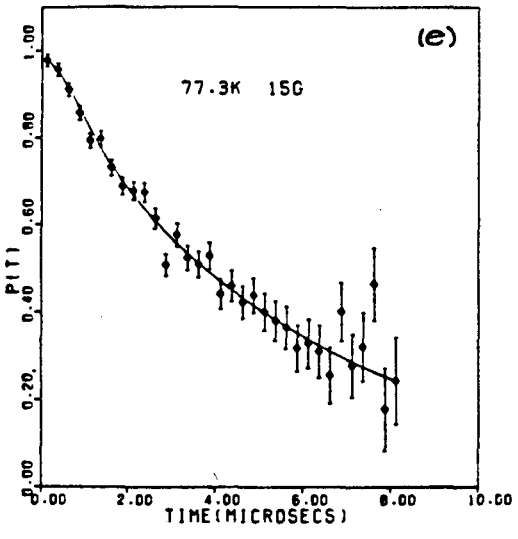
(e)
77.3K 15G
P(T)
TIME(MICROSECS)

Fig. 4

# "Self-Consistent Field Investigation of Location and Hyperfine Interaction of Muonium in Diamond"

N. Sahoo, Santosh K. Mishra, K.C. Mishra,
A. Coker*, T.P. Das, C.K. Mitra and L.C. Snyder
Departments of Physics and Chemistry, State University of New York at Albany
Albany, New York 12222
and
A. Glodeanu
Institute of Physics and Materials Science, Bucharest, Romania

## ABSTRACT

Using an unrestricted Hartree-Fock self-consistent field cluster approach, the potential experienced by a muon in diamond has been investigated. The results show conclusively that normal muonium is localized in the tetrahedral interstitial space. Using the calculated spin density and averaging it explicitly over the vibrational motion of the muon a successful explanation is obtained for the observed reduction of the hyperfine field as compared to free muonium.

*Permanent Address: Department of Physics, University of Port Harcourt, Port Harcourt, Nigeria

The recent development of the muon-spin-rotation technique[1] in solid state systems has produced a wealth of information regarding the electron spin-distributions in interstitial regions and the effect of the muonic positive charge on them. In particular, hyperfine data from such experiments in group IV semi-conductors[2,3] have provided a number of conclusions regarding the nature of the muonium and its location in these systems, three of the important ones being:

(i) The hyperfine fields associated with normal muonium in these systems[3,4] are smaller than but a significant fraction of the vacuum hyperfine field and show the irregular trend of decrease from diamond to silicon and increase from silicon to germanium.

(ii) An anomalous muonium level is observed in all three systems[4,5] with a rather weak but anisotropic hyperfine interaction, also following the same trend as in the case of the deep level.

(iii) The exact location of the normal and anomalous muonium systems has not yet been established.[4]

The earliest investigation specifically[6] devoted to the understanding of the hyperfine interaction of normal muonium in semi-conductors utilized a dielectric treatment to incorporate the influence of the surrounding atoms on the potential seen by the electron of the muonium atom. It was successful in producing a significant reduction of the hyperfine field in silicon and germanium as compared to free muonium. However, when applied[4] to diamond it led to a hyperfine field substantially smaller than silicon, in contradiction with experiment[3,4]. This situation has led to the proposition[4] in the literature that a procedure explicitly incorporating the effects of the electron distributions on the neighboring atoms was needed to understand the experimental results and explore the location of the muonium. An approximate molecular orbital calculation[7] in silicon and germanium using the self-consi-

stent charge extended Hückel procedure has also suggested the need for more first-principle investigations if one is interested in a quantitative understanding of hyperfine data.

In the present work, we have studied the electronic structures and energies associated with normal (1s-like) muonium at different positions in diamond, using an Unrestricted Hartree-Fock (UHF)[8] self-consistent field molecular orbital approach involving the muonium and a cluster of twenty-six atoms surrounding it as shown in fig. 1. The potential thus obtained for the motion of the muon shows a shallow minimum in the tetrahedral interstitial region and a maximum at the hexagonal site, demonstrating conclusively that normal muonium in diamond is trapped in the tetrahedral space but is virtually free to move in this region. Secondly, using the spin-density at the muon site from our UHF calculations and averaging over the vibrational motion of the muon, we are able to explain the reduction of the hyperfine field with respect to free muonium, the inclusion of the vibrational motion being critical in this respect. This analysis provided valuable insight into the factors that could explain the interesting trend in the hyperfine field in going from diamond to germanium.

The choice of the self-consistent field molecular orbital approach was dictated by the following considerations. This approach has the advantages that it avoids the need for a local potential seen by the unpaired spin electron of the muonium, allows one to conveniently incorporate spin-polarization effects so that the contributions to the hyperfine field from both the unpaired spin muonium-like molecular orbital as well as other paired spin orbitals can be included and lastly it can be easily applied for studying the electronic structure associated with different positions of the muon.

In the chosen cluster (fig. 1), the nearest and next nearest neighbors of muonium were taken to be tetrahedrally co-ordinated carbon atoms, the dangling bonds being saturated by hydrogen atoms. The energy and hyperfine

density at the muon were calculated for a number of points (including the tetrahedral center T) along the <111> axis in both the tetrahedral interstitial region enclosed by the carbon atoms A,E,F and G as well as the hexagonal region enclosed by the atoms EFG and HIJ in fig. 1. The choice of <111> axis for the direction of exploration was made in view of both the fact that the hyperfine tensors in the normal and anomalous states were found to be isotropic and axially symmetric[3,5], respectively, and the deuteron channeling results[9] in silicon which indicated that the deuteron is located along the <111> axis away from T. The cluster size of twenty-seven atoms was considered adequate, since a smaller cluster involving fifteen atoms yielded an energy curve within ten percent of that for the chosen larger cluster.

The electronic energy levels and wave-functions were obtained by the Gaussian 80 system[10] of programs. The STO-3G basis set used was appropriate for including the 1s state of muonium atom and the 1s, 2s and 2p states of the carbon atoms. The reliability of the basis set used was verified by performing calculations on the spin-density at the nuclei in small molecular systems with both this choice as well as more extensive basis sets.

In fig. 2, we have plotted the total energy of the chosen cluster as a function of the distance R from T. The energy at the tetrahedral site T is chosen as the zero in the energy scale. This energy curve, which represents the potential experienced by the muon as it moves along the <111> axis, was obtained by fitting the results of Hartree-Fock calculations of the total energy at six points over the range corresponding to 0.565 Å below the tetrahedral site to 0.772 Å above it along the <111> axis. The latter point corresponds to the hexagonal site while the former corresponds to a point about 0.975 Å above the carbon atom A, slightly smaller than the normal CH bond length. The portion of the potential curve in fig. 2 on the right of 0.772 Å, the hexagonal site, is exactly symmetrical with the left half.

Two major features of the potential energy curve in fig. 2 are the maximum at the center of the hexagonal region and a flat structure in the tetrahedral region exhibiting a small dip away from T towards the carbon atom A. The maximum at the hexagonal site precludes the possibility of normal muonium being trapped in the hexagonal region, the most likely place for it being the tetrahedral region. Since the minimum in the tetrahedral region is not pronounced and the potential increases rather steeply on either side, it is reasonable in obtaining the wave-functions for the muon vibrational motion, to approximate the potential in this region by a one-dimensional box[11] with infinite walls. The ground-state wave-function in such a box has a nodeless cosine-type behavior with a maximum at the center of the well. This center is seen from fig. 2 to lie to the left of the site T and is actually close to the shallow dip in the potential in this region. Thus if the average position of the muon could be observed in the diamond lattice, it would be expected to be located away from T towards the carbon atom A. Since the ground state wave-function in an infinite potential well does not depend on the mass of the particle,[11] one would expect a similar location for the proton and deuteron in diamond. No experimental data are available in diamond to verify this result, but the available channelling data for deuteron implanted in silicon agree with the direction of movement away from T expected from our results.

The spin-density $\rho(R)$ was calculated for the six different positions at which wave-functions were obtained. The relative contributions from the unpaired and paired spin orbitals varied from point to point and on an average, the latter contributed about twenty-five percent of the net spin-density, which would have been missed if the UHF procedure had not been employed. The fractional spin density $f(R)$ which is the ratio of $\rho(R)$ and $\rho_{vac} = 0.318\ a_o^{-3}$ is plotted as a function of R in fig. 3. This plot has the following features. Thus f is a maximum and larger than 100% at T. It decreases as one

moves away in either direction, the drop being more pronounced as one moves towards the carbon atom A. Since the spin-density is larger at the tetrahedral site than $\rho_{vac}$, one cannot explain the observed reduction of the hyperfine constant[4] with respect to free muonium without explicitly considering the motion of the muon into regions in fig. 3 where $\rho(R)$ is significantly smaller than $\rho_{vac}$. The decrease in $\rho(R)$ in fig. 3 as one moves away from T can be explained as a consequence of the increased bonding between the muonium atom and the carbon atoms ABC and D (particularly A). It is interesting however that when one moves sufficiently close to carbon atom A as well as those of the hexagonal region, the decrease in $\rho(R)$ (fig. 3) is accompanied by an increase in the total energy (fig. 2). This behavior can perhaps be understood by considering the fact that each carbon atom is bonded tetrahedrally to four neighbors and that as the muonium atom moves towards a carbon atom, the draining of electron density from the latter to the region between it and the muonium atom to produce bonding comes at the expense of electron density directed towards the other bonds. This would lead to a weakening of these other bonds and hence a net increase in the energy of the cluster.

The expected average spin-density for the vibrating muon in the potential shown in fig. 1 can be expressed as

$$\rho_{Av} = \int \psi_G^2(R)\, \rho(R)\, dR \tag{1}$$

where $\Psi_G(R)$ corresponds to the ground vibrational state. As discussed earlier, in view of the steep nature of the potential (fig. 2) on either side of the tetrahedral region, it is a good approximation to consider the tetrahedral region as a potential box with infinite walls. The ground state wave-function for such a potential is given by:

$$\psi_G(R) = \sqrt{\frac{2}{a}}\, \mathrm{Cos}\left(\frac{\pi R}{a}\right) \tag{2}$$

where R is now measured from the center of the potential well located on the left of T in fig. 2 and a is the width of the well. Considering the form of the potential well, a reasonable choice for a seems to lie between 1.0 Å and 0.92 Å. For a in this range, one gets using Eqs. (1) and (2), a value for $\rho_{av}$ between 0.28 and 0.29 $a_o^{-3}$ which corresponds to a fraction f equal to 0.87 to 0.91 of $\rho_{vac}$ and hyperfine constants A of 3880 MHz to 4060 MHz. These results are in good agreement with the experimental values[4] of $\rho_{av}$, f and a, respectively 0.263 $a_o^{-3}$, 0.829 and (3711 ± 21) MHz respectively. A few other points are important to note here. First, for the choices of a used, the excitation energy from the ground vibrational state to the first excited state corresponds to about 6500°K, which justifies using only the ground vibrational state in Eq. (1). Secondly, in obtaining a result for f in reasonable agreement with experiment, it was important to carry out the averaging over the motion of the muon in Eq. (1). If this averaging had not been carried out and the result for $\rho(R)$ at the tetrahedral site had been used from fig. 3, the calculated value of f would have been found to be 1.13, that is, greater than 1. Lastly, Eq. (2) shows that $\rho_{av}$ and hence f involves the variation of two factors with R, the vibrational density $\Psi_G^2(R)$ and the spin density $\rho(R)$. The nature of the results for diamond contained in figs. 2 and 3 allows one to suggest possible qualitative explanations of the irregular trend in going from diamond to silicon to germanium. Thus, in view of the larger lattice constants in silicon and germanium, one would expect $\Psi_G^2(R)$ to progressively peak at larger distances away from T. This by itself would lead to an expected decrease in $\rho_{av}$ from diamond through germanium. However, the function $\rho(R)$ depends on the strength of bonding between the muonium and host atom A and this function could well show a weaker decrease with R for germanium than in silicon, leading to a possible increase in $\rho_{av}$ from silicon to germanium. These expectations would of course have to be confirmed by actual calculations in silicon and germanium in the future.

In summary, the present investigations using a self-consistent UHF approach applied to a sizeable cluster corresponding to the muonium and its neighboring carbon atoms has provided both a definite conclusion regarding the position of the muon atom as well as a reasonable satisfactory explanation of the experimentally observed[4] hyperfine constant. It has been demonstrated that for explaining the hyperfine field it is crucial to consider explicitly the vibrational motion of the muon in the calculated potential in which it moves. The success of the present work suggests that the procedure adopted here would be appropriate to use to attempt explanations of the observed trends in the normal muonium hyperfine constants in going to the heavier semi-conductors[3,4], as well as the anomalous level hyperfine constants, which could be associated with an excited 2p-like muonium state[12]. However, both these investigations are expected to be substantially more time-consuming than the present work.

The authors are grateful to Mr. Barry D. Krawchuk for several helpful suggestions in course of this work.

REFERENCES


1. See for example: J.H. Brewer, K.M. Crowe, F.N. Gygax and A. Schenck in "Muon Physics" ed. by V.W. Hughes and C.S. Wu, Academic Press New York (1975): B.D. Patterson, Hyperfine Interactions 6, 155 (1979); W.J. Kossler, A.T. Fiory, W.F. Lankford, K.G. Lynn, R.P. Minnich and C.E. Stronach, Hyperfine Interactions 6, 93 (1979) and references therein.

2. J.H. Brewer et.al. Ref. 1.

3. E. Holzschuh, W. Kündig, P.F. Meier, B.D. Patterson, J.P.F. Sellschop, M.C. Stemmet and H. Appel, Phys. Rev. A 25, 1272 (1982); H. Brewer, K.M. Crowe, F.N. Gygax, R.F. Johnson, B.D. Patterson, D.G. Fleming and A. Schenck, Phys. Rev. Lett. 31, 143 (1973); I.I. Gurevich et.al. Sov. Phys. JETP 33, 253 (1971); E. Holzschuh, H. Graf, E. Recknagel. A. Weidinger, Th. Wichert and P.F. Meier, Phys. Rev. B 20, 4391 (1979).

4. E. Holzschuh et.al. (1982), Ref. 3.

5. B.D. Patterson, A. Hintermann, W. Kündig, P.F. Meier, F. Waldner, H. Graf, E. Recknagel, A. Weidinger, T. Wichert, Phys. Rev. Lett. 40, 1347 (1978); E. Holzschuh et.al. (1979), Ref. 3.

6. J.S. Wang and C. Kittel, Phys. Rev. B 7, 713 (1973).

7. A. Coker, T. Lee and T.P. Das, Hyperfine Interactions 4, 821 (1978).

8. R.E. Watson and A.J. Freeman in "Hyperfine Interactions" ed. A.J. Freeman and R.B. Fraenkel, Academic Press, New York (1971).

9. S.T. Picraux and F.L. Vook, Phys. Rev. B 18, 2066 (1978).

10. J.S. Brinkley, R.A. Whiteside, R. Krishnau, R. Seeger, D.J. Defrees, H.B. Schlegel, S. Topiol, L.R. Kahn and J.A. Pople Gaussian 80 - An Ab Initio Molecular Orbital Program (Unpublished). For explanation of STO-3G approximation, see W.J. Hehre, R.F. Stewart and J.A. Pople, J. Chem. Phys. 51, 2657 (1969).

11. L.I. Schiff, "Quantum Mechanics", McGraw Hill Book Company, Inc. (1955) Second Edition, page 34.

12. T.L. Estle, Hyperfine Interactions 8, 365 (1981).

Figure Captions

Fig. 1 Cluster used in present work. A through J are carbon atoms, and the rest are hydrogen atoms. Calculations are carried out for different positions of muon on dotted line along <111> through tetrahedral site T.

Fig. 2 Variation of total energy of 27-atom cluster with position of muon. Zero of energy is taken at tetrahedral site T. H is hexagonal site.

Fig. 3 Variation of fractional spin-density f with muonium position, T and H being the tetrahedral and hexagonal sites.

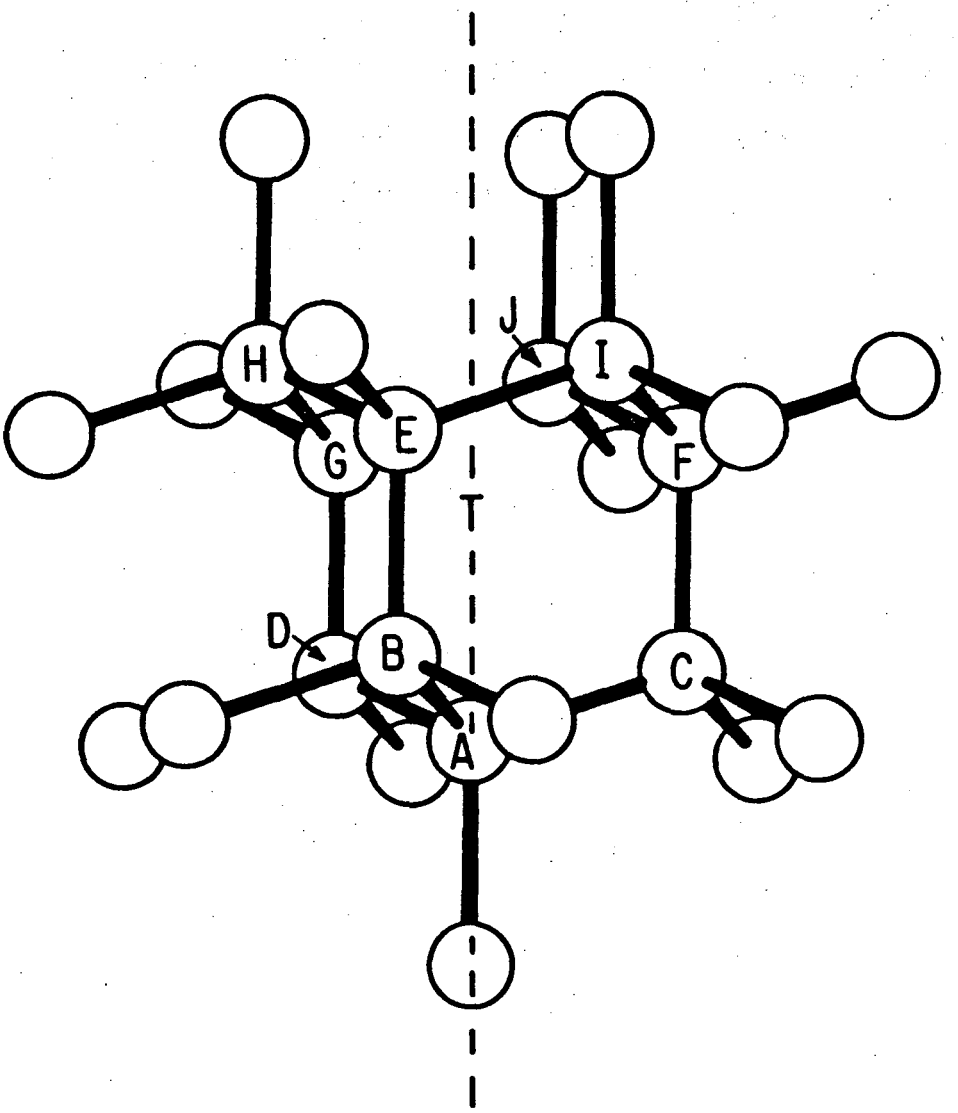


FIGURE 1

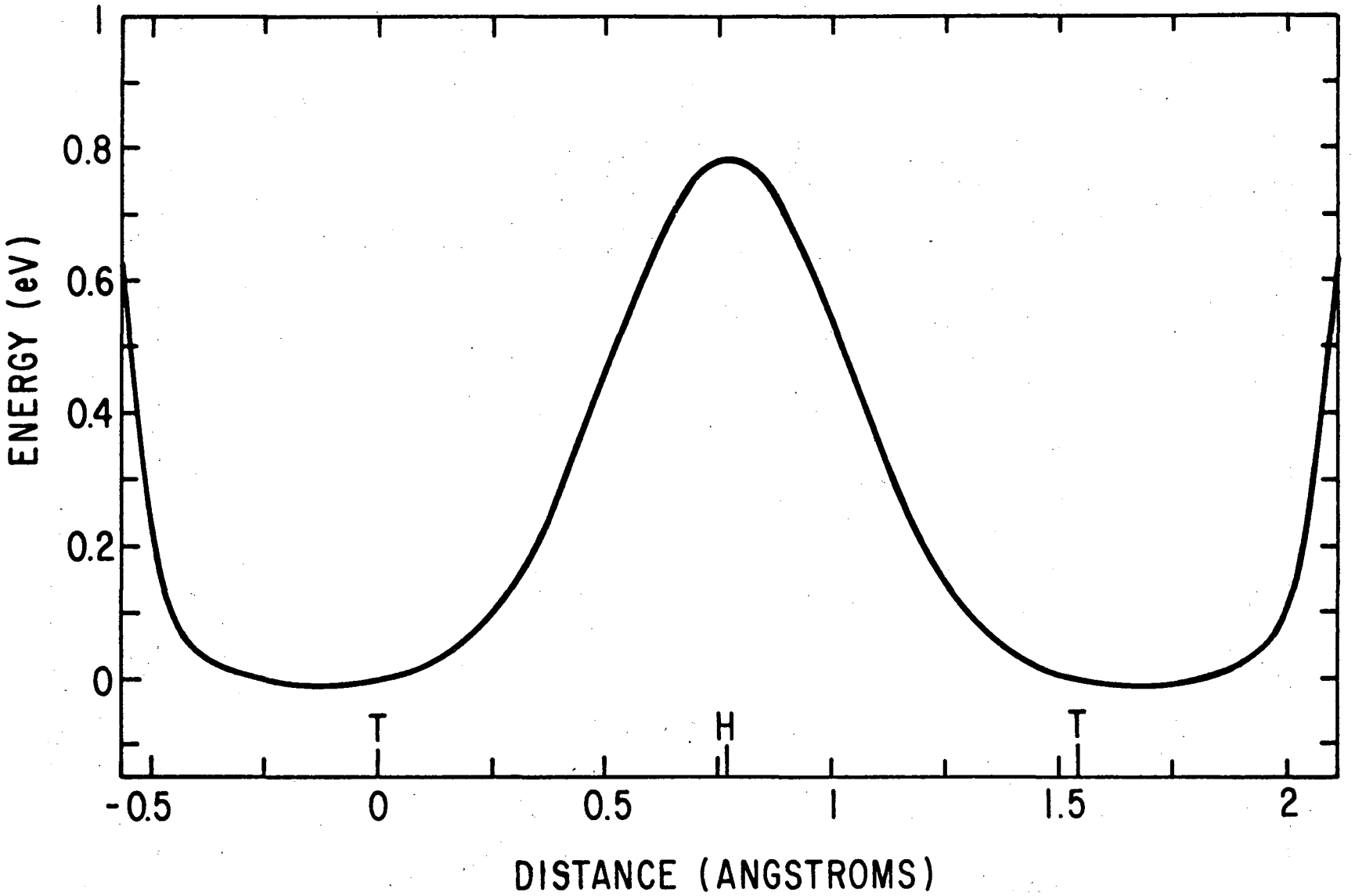


FIGURE 2

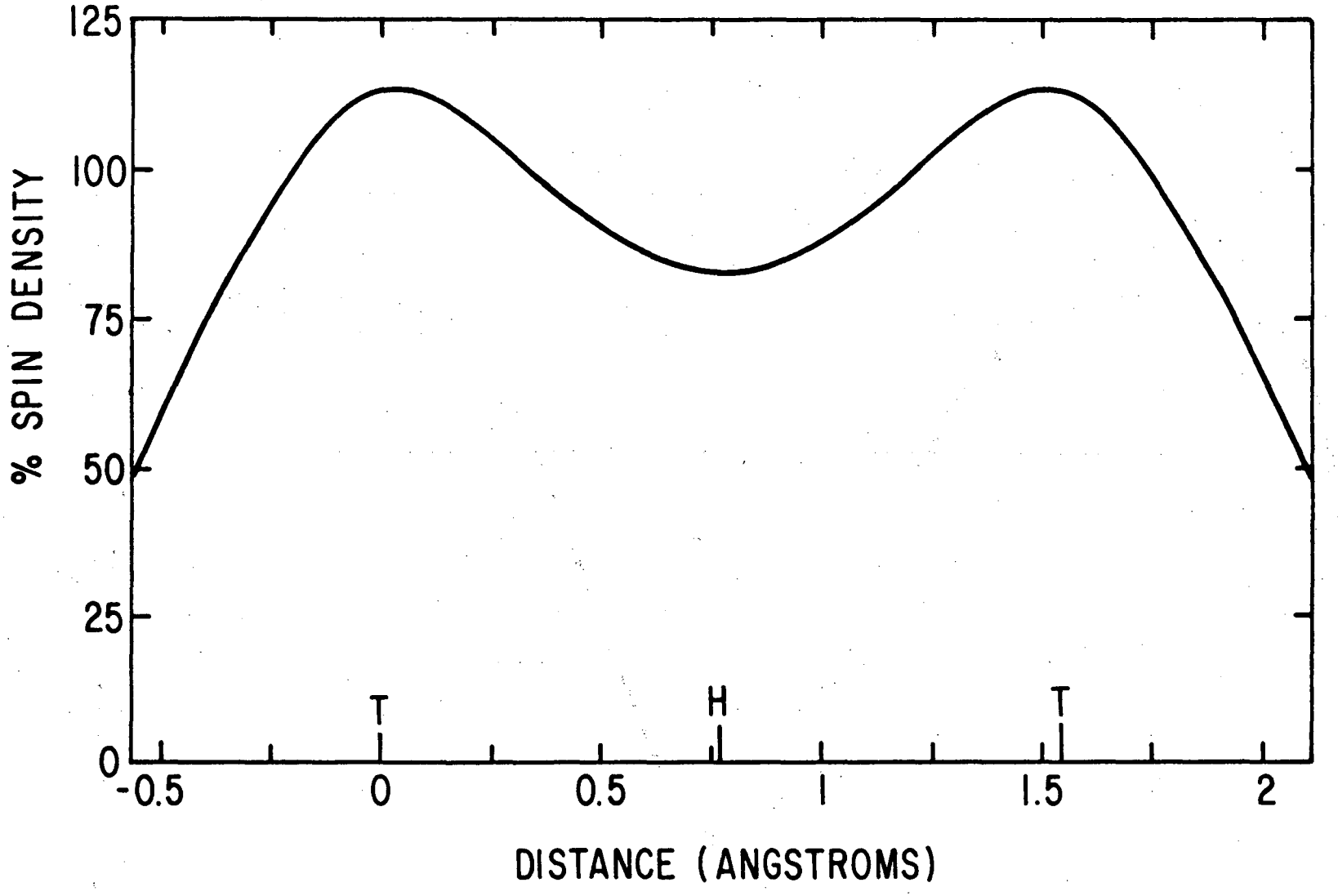
125
100
75
50
25
0
% SPIN DENSITY
T
H
T
-0.5
0
0.5
1
1.5
2
DISTANCE (ANGSTROMS)

FIGURE 3

# THE LOW-TEMPERATURE MOBILITY OF POSITIVE MUONS IN PURE COPPER

A. SEEGER

Max-Planck-Institut für Metallforschung, Institut für Physik, and Universität Stuttgart, Institut für Theoretische und Angewandte Physik, D 7000 Stuttgart, Postfach 800665, Fed. Rep. Germany

For the recently discovered mobility of positive muons in pure copper at liquid-helium temperatures a model based on transitions from metastable to stable interstitial sites is proposed and shown to be in good agreement with the observations. Several additional experimental tests of this interpretation are suggested.

In 1972, Gurevich et al. [1] demonstrated for the first time that the motional averaging effect in the relaxation of the transverse spin polarization of positive muons may be used to determine the diffusivity of muons in metals with a sufficiently large interaction between the nuclear and muon magnetic moments. The pionneering work of Gurevich et al. [1] on Cu was extended by other groups [2] and was, until recently, considered to be well understood in terms of the occupancy of octahedral interstices by positive muons in Cu and the onset of motional averaging due to muon diffusion by thermally activated hopping (incoherent tunnelling) at about 80 K [3,4]. This belief was shaken by the extension of the experiments on Cu to lower temperatures [5-7].

Hartmann et al. [4] showed that in pure Cu the transverse relaxation rate, which is virtually temperature-independent between 80 K and 5 K, decreases between 10 K and 0.5 K by about 40%, and becomes again temperature-independent from 0.5 K down to the lowest temperature so far investigated (0.03 K). During this decrease the dependence of the Gaussian rate coefficient $\Gamma_o$ on the direction and strength of the applied magnetic field $\underset{\sim}{B}$, which is characteristic for the sites occupied by the muons, changes to a moderate degree [6] (comp. Fig.1).

The decrease of $\Gamma_o$ with decreasing temperature between 10 K and 0.5 K has been confirmed quantitatively by Clawson et al. [7]. In addition, measurements of the longitudinal muon spin relaxation in zero applied field by these authors [7] strongly indicate that in this temperature interval there is some movement of the muons in times of the order of magnitude of $\tau_\mu = 2.2 \cdot 10^{-6}$s that is not present at higher or lower temperatures.

The two groups involved in the experimental work just reported have interpreted their findings differently. Chappert et al. [6] believe that in Cu below 0.5 K the muons are localized in octahedral interstices and immobile on the $\tau_\mu$ timescale. The muons are thought to move by thermally activated hopping between 0.5 K and 10 K and to become trapped at higher temperatures by residual interstitial impurities. The plateau of $\Gamma_0$ between 10 K and 80 K is attributed to impurity-trapped muons, the drop of $\Gamma_0$ above 80 K to detrapping.

Clawson et al. [7] retain the "classical" interpretation described in the introductory paragraph for temperatures above 10 K and suggest that below 10 K another diffusion mechanism sets in with a diffusion rate that <u>increases</u> with <u>decreasing</u> temperature. As an obvious candidate for such a process they suggest coherent tunnelling of positive muons.

In the judgement of the present writer neither one of the two explanations is likely to be correct. On the basis of the residual resistivity ratio of the samples (≈6400 [8]) and the available information on foreign-interstitial solubilities in Cu [9] he considers the estimate of the concentration of residual foreign interstitials by Chappert et al. [6] to be an overestimate by at least a factor of ten.[1] A realistic estimate of the possible impurity effects

[1] In the explanation proposed by Chappert et al. [6] it is the concentration of the foreign interstitials in <u>solid solution</u> that is relevant. An upper limit for this may be obtained from the residual electrical resistivity by assuming the contribution of the substitutional foreign atoms to be negligible. With the quite conservative estimate that the specific resistivity of the foreign interstitial atoms is $\Delta\rho_i = (1 - 2)\cdot 10^{-6}$ Ωm (for oxygen $\Delta\rho_O = 5.3\cdot 10^{-6}$ Ωm is quoted [9,10]) one obtains an upper limit for the concentration of dispersed foreign interstitial atoms of $(1.2 - 2.5)\cdot 10^{-6}$.

indicates that before the rise of $\Gamma_o$ attributed to trapping by these impurities a quite pronounced drop due to motional averaging should have been observed. This is not the case. In the tentative explanation of Clawson et al. [7] it is not clear how one can, without additional hypotheses, account for the behaviour observed below 0.5 K.

In this note we propose an interpretation for the low-temperature behaviour of muons in Cu that is based on the idea that, due to the short-range interaction of positive muons with neighbouring ions, in metals metastable self-localized states may exist [11]. In order to fix the ideas, we assume that in the case of Cu the stable sites are octahedral interstices with Gaussian relaxation rate $\Gamma_o^O$ and that the tetrahedral sites (Gaussian relaxation rate $\Gamma_o^T$) are the metastable sites in question.

Fig. 2 shows, in a schematized manner, the potential energy of a positive test charge along a sequence of octahedral and tetrahedral interstices in an fcc lattice. The lowering of the potential energy associated with the self-localization of a positive muon in a specific interstice is indicated by dashed lines. $H_a$ indicates the energy of the lowest self-localized state. (We disregard the fact that on account of the translational symmetry of the Hamiltonian the localized states may be combined to form Bloch states; it is assumed that on the time scale of the experiments under discussion the localized states are the more appropriate description.) In this state the muon wavefunction is confined to an octahedral interstice and fairly concentrated. The temperature-independent relaxation rate as observed between 10 K and 80 K is attributed to muons located in such a state.

Among the excited states that are mainly concentrated in tetrahedral interstices the state b has the lowest energy, $H_b$. The metastability hypothesis stated above implies that under static conditions energy barriers separating a muon in state b from the surrounding octahedral sites exist in all space directions.[2] It is assumed that during the thermalization of the implanted muons both octahedral and tetrahedral interstices are occupied (with probabilities $p_O(o)$ and $p_T(o)$ (normalized according to $p_O(o) + p_T(o) = 1$). Transitions at a rate $\nu$ from b to a are possible either by (classical) over-barrier jumps or by tunnelling. The transverse relaxation function for this model reads

$$
\begin{aligned}
R(t) &= p_O(o)\exp[-(\Gamma_o^O t)^2] + p_T(o)\exp[-(\Gamma_o^T t)^2 - 4\nu t] + \\
&\quad + 4\nu p_T(o)\int_0^t \exp[-(\Gamma_o^T t')^2 - \{\Gamma_o^O(t-t')\}^2 - 4\nu t']dt' = \\
&= p_O(o)\exp[-(\Gamma_o^O t)^2] + p_T(o)\exp[-(\Gamma_o^T t)^2 - 4\nu t] + \\
&\quad + \frac{2\pi^{1/2}\nu}{\bar{\Gamma}}\, p_T(o)\exp[-(\Gamma_o^O\,{}_o^T t/\bar{\Gamma})^2 - (\Gamma_o^O/\bar{\Gamma})^2] \times \\
&\quad \times \mathrm{erf}\left[\frac{(\Gamma_o^T)^2 t + 2\nu}{\bar{\Gamma}}\right] + \mathrm{erf}\left[\frac{(\Gamma_o^O)^2 t - 2\nu)}{\bar{\Gamma}}\right]\} \quad , \qquad (1)
\end{aligned}
$$

with

$$\bar{\Gamma}^2 \equiv (\Gamma_o^O)^2 + (\Gamma_o^T)^2 \quad .$$

In the application of the model to the specific results on Cu mentioned above the temperature dependence of the transverse

---

2) This is made plausible by Teichler's calculations based on the rigid-lattice approximation, which indicates that even in the <111> directions, where the existence of an energy barrier is most doubtful, there is a finite barrier between T and O sites.

relaxation rate between 0.5 K and 10 K is explained by the gradual emptying of the meastable states. Above 10 K the transitions from b to a are so rapid that on the time scale of the measurements only a levels are occupied and the relaxation rate becomes equal to $\Gamma_o^O$, in agreement with the "classical" interpretation referred to in the introductory paragraph.

Below 0.5 K the transition rate $\nu$ is negligibly small, hence

$$R(t) = p_O(o)\ \exp[-(\Gamma_o^O t)^2] + p_T(o)\ \exp[-(\Gamma_c^T t)^2] \quad . \qquad (2)$$

If there is equipartition between O and T sites, we have $p_O(o)=1/3$, $p_T(o)=2/3$. The muon wavefunction of the excited state b is considerably more extended than that of the ground state a. At low magnetic fields B, at which the dependence on the crystallographic direction of $\underset{\sim}{B}$ is suppressed [12], this implies [13]

$$(\Gamma_o^T)^2 \ll (\Gamma_o^O)^2 \quad , \qquad (3)$$

so that the reduction of the relaxation rate observed at low temperatures is as expected. At high magnetic fields the orientation dependence of the relaxation rate is strong for both types of site but of opposite sense. As a consequence (3) continues to hold for the <100> orientation, whereas for the <111> orientation $\Gamma_o^T$ and $\Gamma_o^O$ may become comparable. This explains the experimental result (Fig. 1) that for $\underset{\sim}{B}$ ||<100> the temperature dependence of the relaxation rate is B-independent, whereas for B ||<111> it decreases strongly with increasing B.

Theoretical estimates of the temperature dependence of $\nu$ require a specific model for the transitions from b to a. The most likely model is that phonon-assisted tunnelling occurs via an excited state c that is mainly located in an octahedral interstice and that happens to have an energy $H_c$ close to $H_b$. Thermal

fluctuations (phonons) may bring the levels b and c to the same energy, so that tunnelling transitions may take place. Since T and O sites are not transitionally equivalent, the dominant processes should be one-phonon processes (for further discussions see [8,14]), whose rate is proportional to $[\exp(H_{bc}/kT)-1]^{-1}$ with $H_{bc} \equiv |H_b - H_c|$. Simple estimates based on three-dimensional square-well or harmonic-oscillator potentials indicate that $H_a$ should lie about 0.3 eV above the bottom of an O well and that the density of c-type energy levels with $H_c \approx H_b$ should be of the order of magnitude of $10^2$ $eV^{-1}$. This means that we expect $H_{bc}$ to be of the order of magnitude of $10^{-3}$ eV. This is indeed what is needed in order to account for the observed temperature dependence of R(t). The temperature range in which the variation of $\Gamma_0$ is observed is thus roughly as predicted by the present model.

As we have seen, the present model accounts rather well for the observations on the low-temperature mobility of positive muons in Cu. We propose the following additional tests:

(i) Introduce, say by electron or neutron irradiation, a sufficently high concentration of vacancies. Muon trapping [15] should be observed according to the proposal of Chappert et al. [6] above about 2 K, according to that of Clawson et al. [7] below that temperature. The present model predicts that up to quite high temperatures trapping will not be observed.

(ii) Compare the time dependence (1) quantitatively with the experimental data on R(t) and deduce $\nu(T)$.

(iii) Investigate on Cu $\pi^+/\mu^+$ lattice steering [16,17] at low temperatures. Positive pions are expected to behave similarly to

positive muons. The occupation of T sites at low temperatures should show up in the channelling and blocking patterns. Owing to the mass dependence of the tunnelling matrix element and the shorter pion lifetime the transition to O-type occupation should occur somewhat above liquid-helium temperatures.

Finally we discuss the influence of solute additions to Cu. Chappert et al. [ 6] report that the addition of 200 ppm Ni to Cu reduces both the height and the width of the step in the temperature dependence of $\Gamma_o$ at liquid-helium temperatures. Within the present picture these results may be understood in terms of muon—foreign-atom interactions during the slowing-down of the muons, a process suggested earlier by Stoneham [18]. We have to make the plausible assumption that such interactions reduce considerably the probability for muons to come to rest in the metastable b states (e.g., because near the impurities the energy barrier between T and O is removed in some of the <111> directions), so that at low temperatures the distribution of muons between a and b states is shifted in favour of the former.

Acknowledgement.

The author is grateful to Dr. O. Hartmann and Professor K.M. Crowe for the permission to refer to the results [6,7] of their groups before publication.

Legends.

Fig.1: Gaussian relaxation rate $\Gamma_o$ of Cu (residual resistivity ratio $6.4 \cdot 10^3$) at low temperatures as a function of the magnetic field [6]. Open symbols: Magnetic field $\underset{\sim}{B}$ parallel to [100] direction. Full symbols: Magnetic field $\underset{\sim}{B}$ parallel to [111] direction. Squares: Measurements at 0.1 K. Circles: Measurements at 2 K.

Fig.2: Schematized picture of the potential energy of a positive point charge along a sequence of octahedral (O) and tetrahedral (T) interstices in a face-centred cubic metal. The dashed curve indicates the lowering of the potential energy due to self-trapping.

References:

1) I.I. Gurevich, E.A. Mel'eshko, I.A. Muratova, B.A. Nikol'skii, V.S. Roganov, V.I. Selivanov, B.V. Sokolov, Phys. Letters 40 A, (1972) 146

2) M. Camani, F.N. Gygax, W. Rüegg, A. Schenck, H. Schilling, Phys.Rev.Letters 39, (1977)

3) H. Teichler, Phys.Letters 64 A (1977) 78

4) H. Teichler, Phys.Letters 67 A (1978) 313

5) O. Hartmann, E. Karlsson, L.-O. Norlin, T.O. Niinikoski, K.W. Kehr, D. Richter, J.-M. Welter, A. Yaouanc, and J. LeHericy, Phys.Rev.Letters 44 (1980) 337

6) J. Chappert, O. Hartmann, E. Karlsson, T.O. Niinikoski, L.-O. Norlin, A. Yaouanc, submitted to Solid State Communications

7) C.W. Clawson, K.M. Crowe, S.E. Kohn, S.S. Rosenblum, C.Y. Huang, J.L. Smith, J.H. Brewer, Physica, to be published

8) A. Yaouanc, Thèse, Université Scientifique et Médicale de Grenoble, 1982

9) E. Fromm and E. Gebhardt, Gase und Kohlenstoff in Metallen, Springer, Berlin-Heidelberg-New York, 1976

10) E.G. Hess, and F. Pawlek, Z.Metallkde. 50 (1959) 57

11) A. Seeger, Appl. Phys. 7 (1975) 85

12) O. Hartmann, Phys.Rev.Letters 39 (1977) 832

13) T. McMullen and E. Zaremba, Phys.Rev. 18 (1978) 3026

14) H. Teichler and A. Seeger, Phys. Letters 82A (1981) 91

15) A. Seeger, Phys. Letters 53A (1975) 324

16) K. Maier, G. Flik, D. Herlach, G. Jünemann, H. Rempp, A. Seeger, H.-D. Carstanjen, Phys. Letters 83A (1981) 341

17) K. Maier, G. Flik, A. Seeger, D. Herlach, H. Rempp, G. Jünemann, H.-D. Carstanjen, Nucl.Instr.Methods 194 (1982) 159

18) A.M. Stoneham, Hyperfine Interact. 6 (1979) 227

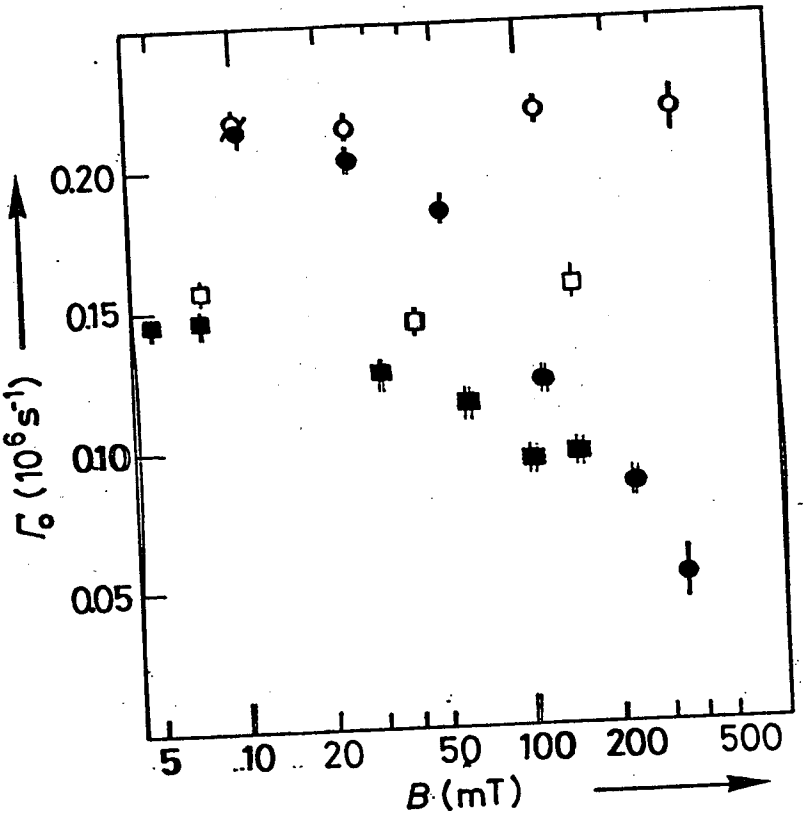
0.20
0.15
0.10
0.05
$\Gamma_0$ ($10^6 s^{-1}$)
5
10
20
50
100
200
500
B (mT)

Fig. 1

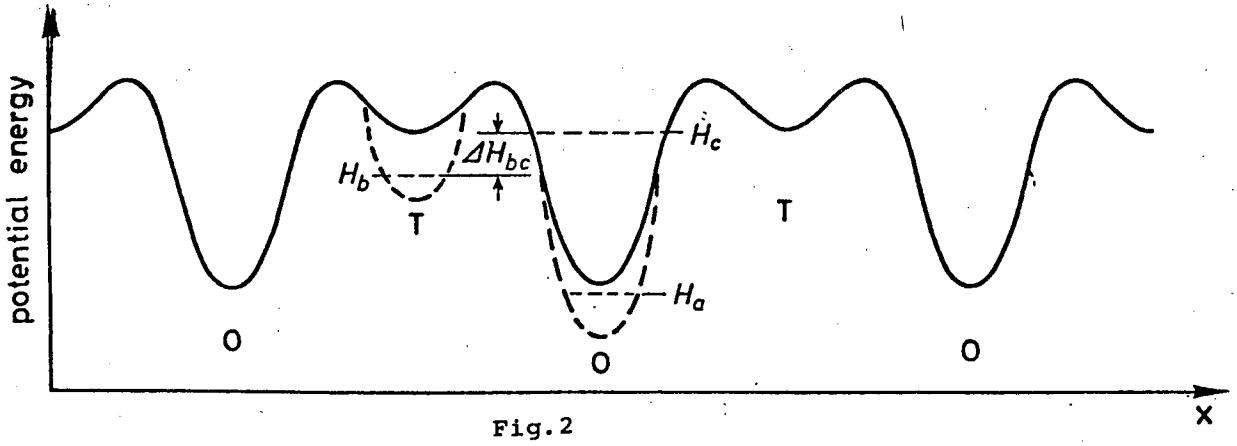
potential energy
$H_b$
$\Delta H_{bc}$
$H_c$
$H_a$
T
T
O
O
O
x

Fig.2